Two Sphere Immunoassay on a Microfluidic Device

K. Pieter Roos

A Thesis

In

The Department

Of

Chemistry and Biochemistry

Presented in Partial Fulfillment of the Requirements
For the Degree of Doctor of Philosophy
Concordia University
Montreal, Quebec, Canada

July, 2005

Your file Votre référence
ISBN: 0-494-09952-6
Our file Notre référence
ISBN: 0-494-09952-6

Abstract

Two sphere Immunoassay on a Microfluidic Device

K. Pieter Roos, Ph.D
Concordia University, 2005

Clinical measurements of biologically important proteins and peptides are routinely carried out in the laboratory setting using immunoassays. However, the most recent trend in medicine is the advance of personalized medicine. The goal is to tailor the diagnosis, care and the drugs to the individual. To make this a reality, fast and inexpensive, analytical tools need to be developed that are capable of measuring multiple biological markers at one time in small volumes. When an assay can use very small volumes less invasive methods for obtaining samples such as blood can be used (finger prick).

The measurement of more than one biomarker from the same sample using the traditional ELISA method requires a separate immunoassay for each analyte. This is expensive, requires large amount of sample and is time consuming. A faster and more economical way is by developing a multiplexing assay where not one but several analytes are measured at one time.

The immunoassay we developed uses microspheres (capture spheres) conjugated with monoclonal antibodies specific to the targeted analyte. These microspheres capture the antigen and form a microsphere-antibody-antigen complex, which are then bound by a secondary monoclonal antibody, recognizing a different exposed epitope on the antigen. This secondary antibody is conjugated to a second microsphere (detection sphere). The

capture and detection spheres are loaded with fluorescent dyes, each with a different wavelength, allowing for easy differentiation.

Detection of the capture sphere-antigen-detection sphere complexes can be accomplished by three different formats, 96 well plate, Flow cytometer and Microfluidic devices. In this Thesis we will discuss the development of this fast and sensitive aminoassay using these three formats. We will show that the assay can be performed in less then 15 minutes with sensitivity comparable to, or better than that obtained with the gold standard ELISA assay. Also we will calculate the theoretical limits of this assay and compare them to a commercial single bead assay.

This thesis is dedicated to my wife Lori and my children, Riley and Thomas

Without your love and support this thesis would never have been written.

Acknowledgements

I would like to thank my research supervisor, Dr. Cameron Skinner, for taking me on as a graduate student, for the useful and enlightening discussions about science and for the guidance which led to the completion of this thesis. I wish to thank my committee members, Dr. Joanne Turnbull and Dr. Marcus Lawrence, for the interest, guidance and support that they have shown throughout my studies.

I enjoyed working in the Skinner lab and I am grateful to my colleagues (Michael Harvey, Donald Paquette, Vincent Lau, Dirk Bandilla, Zackarias Papachristou and Jean-Louis Cabral) for technical and moral support.

Finally I wish to thank Lori, without her years of support and encouragement I would never have finished this Thesis.

Table of Contents

List of Figures

List of Tables

List of Equations

List of Abbreviations

A2FCS	ASCII to FCS
BSA	bovine serum albumin
CCD	charge-coupled device
CDRs	complementary-determining regions
CE	capillary electrophoresis
CK-MM	creatin kinase MM
DAPEO	Diamino terminated Poly(ethylene oxide)
DAPI	4',6-diamidino-2-phenylindole, dihydrochloride
DMP	dimethylpimelimidate
DNA	deoxyribonucleic acid
EOF	electroosmotic flow
5-FAM, SE	5-carboxyfluorescein, succinimidyl ester
FITC	fluorescein-5-isothiocyanate
HIV	human immunodeficiency virus
HPLC	high-performance liquid chromatography
Ig	immunoglobulins
IgG	immunoglobulin G
IHP	inner Helmholz plane
IL-6	interleukin 6
IRT	immunoreactive trypsin
ks/s	kilo samples per second
LAT	latex agglutination test
LIF	laser induced fluorescence
NA	numerical aperture
Nd:YAG	neodymium:yttrium-aluminum garnet
17 OHP	17-α-hydroxyprogesterone
OHP	outer Helmholz plane
PBS	phosphate buffered saline
PDMA,	poly(N,N-dimethylacrylamide)
PMT	photomultiplier tube
QDs	quantum dots

RF	rheumatoid factors
RMS	root mean square
RNA	ribonucleic acid
rpm	revolutionsotations per minute
RSD	relative standard deviation
TNF-α	tumor necrosis factor alpha
TSH	human thyroid-stimulating hormone
μTAS	micro-Total Analytical Systems
UV	ultraviolet

CHAPTER 1

Introduction to a Two Sphere Immunoassay in a Microfluidic device

"Nothing tends so much to the advancement of knowledge as the application of a new instrument. The native intellectual powers of men in different times are not so much the causes of the different success of their labours, as the peculiar nature of the means and artificial resources in their possession."

Thomas Hager, Force of Nature, Simon and Schuster, New York, 1995, p 86.

1.1 Introduction to Immunoassays

Immunoassays were introduced in the 1960s by Berson and Yalow[1] for insulin and by Ekins for thyroxine.[2] Since then many immunoassays have been developed using the natural ability of an antibody to recognize a specific antigen. In this thesis we are discussing the development of a two bead immunoassay on a chip that can detect multiple antigens simultaneously at very low levels. The assay can be divided into a biological section; antibody attachment and recognition of antigen, and an instrumentation section; manipulation and detection of the complexes. This chapter will introduce these two elements.

1.1.1. Immunoassays Overview

The immunoassay is the fastest-growing analytical technology in use for the detection and quantification of biomolecules in the diagnosis and management of diseases.[3] In addition to the immunoassay, other techniques such as gel electrophoresis, HPLC, and more recently mass spectrometry are routinely employed for the analysis of biomolecules. However, while the latter techniques detect and quantify a family of components, an immunoassay is intended for the quantification of a single molecular species.

In an immunoassay, antibodies are used for the detection of molecules of interest (antigens). The antibody recognizes, on the antigen, a complementary epitope to its binding site, the paratope. The antigen, depending on its size, can have several epitopes available for binding of antibodies.

Antibodies, or immunoglobulins (Ig), are heterodimers consisting of four polypeptide chains linked by disulfide bridges. Two of the peptides form identical large or heavy (H) chains and two form identical small light (L) chains (Figure 1-1). Both the H and L chains contain a variable (V_H and V_L) and a constant region (C_H and C_L). Within the variable region there are three hyper-variable areas or complementary-determining regions (CDRs) of the antibodies. The CDRs, three from each L and H chain, form loops that come together in a three-dimensional structure creating the binding regions of the antibody. Polyclonal antibodies recognize the same antigen, but target several epitopes on this antigen. Conversely, monoclonal antibodies are specific for only one particular epitope, all of which have the same CDR regions. The Fc portion of the antibody is the non-binding part of the two heavy chains and is more hydrophobic in nature than the antigen binding section.[4]

The enzyme-linked immunosorbent assay (ELISA) is probably the most commonly used method for affinity analysis of antigen-antibody interactions. There are three classes of immunoassays: the antibody capture assay, the antigen capture assay and the two-antibody sandwich assay. With the two-antibody immunoassay the analyte is first captured by the immobilized antibody and then is detected by using a second labelled antibody. In the antigen capture assay, the antigen is attached to the solid phase, and the antibodies bound are then quantified by using a labelled anti-immunoglobulin.

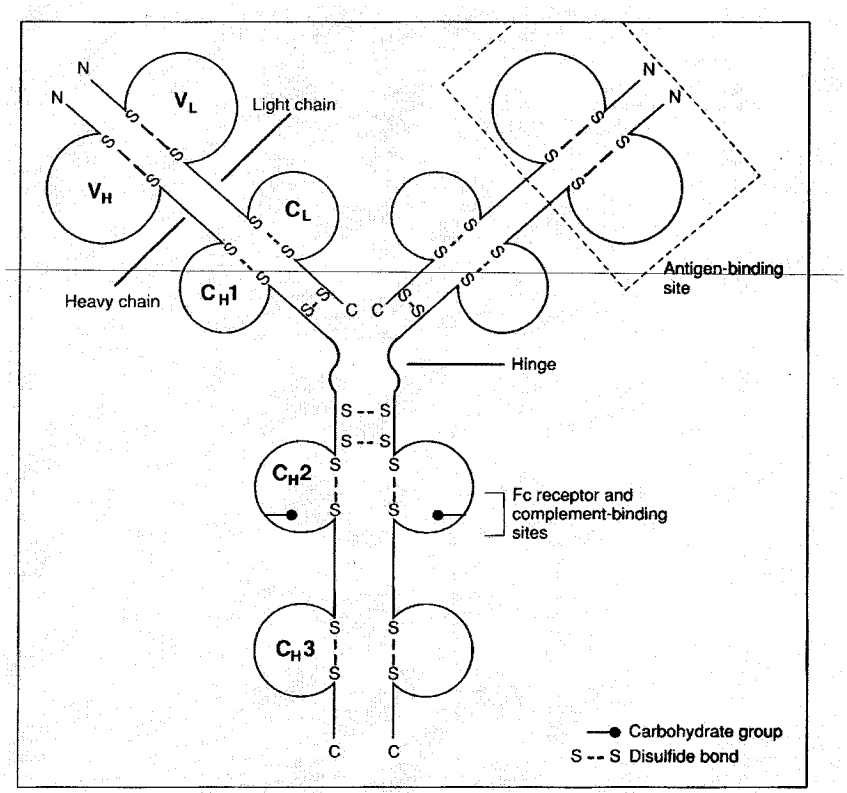

Figure 1-1: Schematic of an immunoglobin molecule.[4]

An antibody capture assay allows for the determination of a class of antibodies. Here, a class of immunoglobulins are captured by anti-class antibodies. Then the antigen is added and binds only to specific antibodies of the class. The bound antigens are quantitated using a labelled secondary antibody. Of these three methods, the antibody capture and the two-antibody sandwich assays can be used for ELISA. The two-antibody assay is the most useful for the detection and quantification of antigens.[5]

In the two-antibody assay, a fixed concentration of monoclonal antibody is bound to the walls of a microtitre plate (Figure 1-2, panel 1). Samples with variable concentrations of antigen are incubated with the attached antibodies and after binding equilibrium is reached, the plate is washed (Figure 1-2, panel 2). A second monoclonal antibody, labelled with a biotin on the Fc portion, against a different epitope is subsequently allowed to bind (Figure 1-2, panel 3). Detection of the antibody-antigen-antibody sandwich is accomplished using an enzyme that binds to the second antibody through a biotin-Streptavidin interaction (Figure 1-2, panel 4). In this particular example, Streptavidin is attached to a substrate-converting enzyme via a fusion protein. The substrate is added to the sample and is converted from a non-absorbent or non-fluorescent species, into an absorbing or fluorescent product by the enzyme. This assay allows very low detection limits due to the multitude of products formed by each enzyme.[5]

1.1.2. Multianalyte Immunoassays

Immunoassays are typically performed for measuring single analytes.

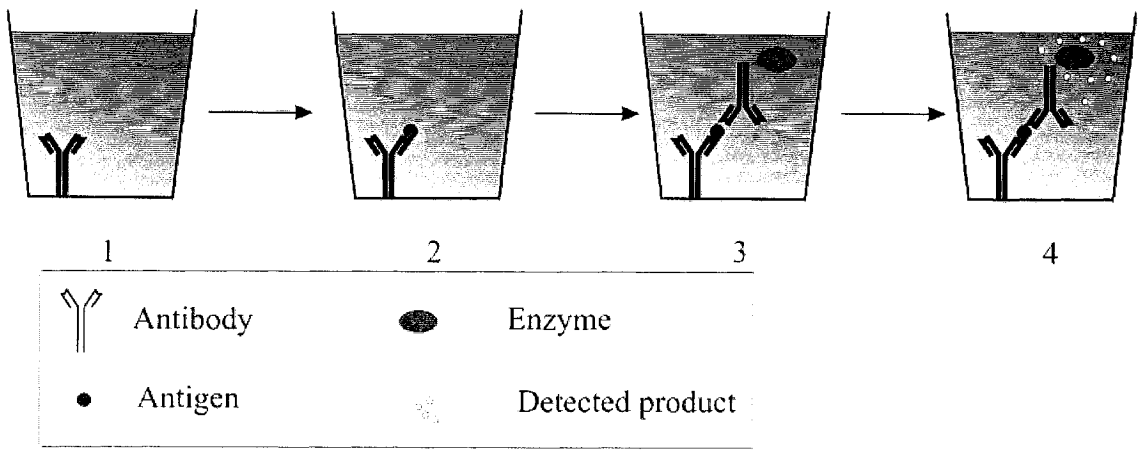

Figure 1-2: Microplate immunoassay; first the antibody is attached to microplate wall, then the antigen is captured from the sample followed by the secondary antibody containing an enzyme. Finally, the conversion of a substrate into detectable product by the enzyme.

Measuring multiple analytes in a sample can have several advantages such as: increasing the number of assays that can be run per day, reducing the cost per test, and decreasing the amount of sample needed to perform all tests. Multiplexing an assay is very attractive for analytes that are grouped, such as the cytokine allergen test, thyroid test, triple test for Down's syndrome, testing for antigens against HIV and hepatitis.[6]

There are two basic formats for simultaneous multianalyte testing; assays based on spatially separated test zones with the same label, and assays using multiple labels all mixed together. When using separate test zones one can use discrete solid phases, for example separate beads, one for each antibody or discrete zones on a single solid phase. These assays typically use a sandwich immunoassay strategy where antigens or antibodies are immobilized on solid phases. One of the earliest assays used colour-coded beads coated with different antibodies.[7] Instead of using discrete surfaces, detection using multiple labels has been achieved using four different fluorescent lanthanide labels in the simultaneous immunoassay for human thyroid-stimulating hormone (TSH), 17-α-hydroxyprogesterone (17 OHP), immunoreactive trypsin (IRT) and creatin kinase MM (CK-MM).[8] This assay was performed in a single microtiter well where all four antigens were detected in a single assay.

Of course a combination of these approaches is possible by using discrete surfaces and multiple labelling. The number of multiplex assays that are used in routine clinical laboratories is limited; a few important examples are HIV antibody, drugs of abuse, and allergen testing.[5]

1.1.3. Microsphere Assays

Polystyrene or latex microspheres are micron sized beads that have been used as a solid support for several different assays, including tests for pregnancy, as well as those detecting bacterial, viral and fungal infections. These tests are usually fast and easy to perform, requiring only a few drops of blood or a few milliliters of urine, and give a clear answer regarding the presence of a specific antigen.[9] The first test developed using microspheres, was in 1956 as a rheumatoid microsphere agglutination test,[10] and followed by a pregnancy test in 1957.[11] Commercial microsphere tests have since been developed for; infectious diseases, chemical analyses, plant health, veterinary medicine, food and the environment. These tests are simple to perform, fast (2 minutes analysis time), portable and relatively inexpensive. Initially these tests measured agglutination of latex microspheres in a liquid. Latex agglutination tests are relatively sensitive and can detect down to 600 ng/ml of antigen. The clumping occurs due to the use of polyclonal antibodies against the antigen of interest. When the antigen is present several sites are available for antibody binding. Therefore not only one sphere, but many spheres can potentially bind to one antigen. The other way is also true; one microsphere can bind many antigens. The result of both these binding events is the creation of large aggregates. Light scatter from the complexes in an agglutination test can be used to develop immunoassays. The intensity of the scatter is dependent on the wavelength of the incident light, the size and number of particles and the angle of the detector relative to the incident beam. When the assay starts, single particles form doublets that accrete additional particles. This results in a dramatic increase in the scatter intensity as light scatter is highly dependent on particle size. In an assay small (<0.1 μm) microspheres

that are poor scatterers are exposed to an antigen. As the particles clump together they start to scatter light much better. Thus this change in light scatter intensity with concentration of the analyte can be used in an end-point or rate method immunoassay. The agglutination can be measured directly, in a nephelometer by measuring the scatter light, or indirectly, in a spectrophotometer by measuring the absorbance of signal (turbidimetry). Sensitivity using these methods is very good, with a detection limit for proteins of 100 pg/ml. Complete microtiter plates can be read in two seconds, allowing fast determination of a variety of antigens.[11]

A more recent agglutination test uses dried coloured microspheres on a suitable carrier to increase the contrast and improve sensitivity. Wetting of the carrier with the sample allows the microspheres to clump together creating visible spots or lines on the carrier material. Multiplexing is possible using different coloured spheres; a test for Salmonella employs this to differentiate between three different antigen groups.[12]

It is also possible to perform an immunoassay using particles and carrier without looking at agglutination. The particle capture immunoassay uses a strip of nitrocellulose that has on one part dyed microspheres coated with antibodies against the antigen of interest (Figure 1-3), and on the strip a second immobilized antibody directed against an alternate epitope of the same antigen. The end of the strip, containing the microspheres is dipped into the sample containing urine or blood. From the migration of the fluid along the paper, due to capillary action, the microspheres are swept to the section containing the second antibody. If the antigen is present in the sample, it will be retained between the microsphere and the second antibody, resulting in a visible line on the test strip, the colour of which is dependent on the dye used in the microsphere. The sensitivity

(Signal/[antigen]) of this test is dependent on molecular weight of the antigen (i.e. size and thus number of binding sites for the antibodies), and affinity of the antibodies for the antigen. Concentrations as low as 67 pg/ml can, in some tests, give a positive test result.[5]

Microspheres can also be used as a solid phase due to the unique properties they exhibit; small enough to be suspended in solution for several hours but easily separated from suspension using centrifugation, magnetic extraction or filtration. These characteristics can be used to extract proteins, DNA or even cells out of solution, and allows the performance of an assay on these molecules without interference from the sample matrix. A practical example is the purification of RNA or DNA samples with silica microspheres for use in PCR reactions.[13] In another assay, IgG antibodies are isolated from the serum using microspheres coated with mouse antibodies raised against the Fc portion of the human IgG antibodies. Once a representative sample is attached to the beads a competitive assay is performed to determine the concentration of a specific antibody in the serum. A standard immunoassay is also possible where the microsphere is used as the solid phase instead of the bottom of a microtiter plate well. When using paramagnetic microparticles, washing steps can be performed easily and quickly. When these particles are brought in close contact with a magnetic field, the particles are pulled out of the solution against the wall of the container. While applying the magnetic field the solution without the spheres can be removed and a washing solution can be added to the beads. This process can be repeated several times to wash away any contaminating species. Several assays have been developed using paramagnetic microspheres and luminescence detection.[14]

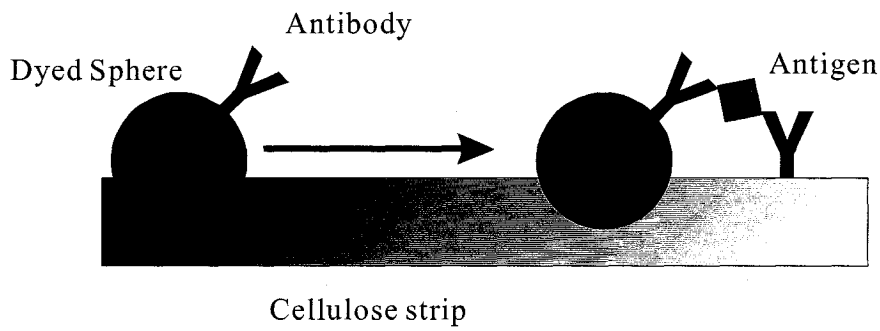

Figure 1-3: Strip immunoassay; the spheres are dragged by capillary action along the strip until they reach an area where antibodies are immobilized on the strip. If the antibodies on both the spheres and the cellulose strip can bind the antigen, then the beads are retained at this location and a line becomes visible on the cellulose strip.

Capture spheres with a diameter of 4-10 μm are used instead of the well of a microtiter plate in a flow cytometer based assay. These capture spheres are internally labelled to allow the use of several different antibodies each associated with a specific bead colour. Antibodies attached to these spheres capture antigens in the solution, to which fluorescently labelled secondary antibodies form a sandwiched complex. The fluorescence signals from the labelled antibodies and capture sphere is measured to quantify and identify the antigen. By using a unique fluorescent signal (intensity and/or wavelength) in the capture spheres, many antigens can be measured simultaneously. This type of multiplex assay can be developed using the Luminex 100 xMAP system (Luminex Inc., Riverside, CA) that works with a flow cytometer for detection. The Luminex 100 flow cytometer employs two lasers, a 635 nm diode laser and a 523 nm frequency doubled Nd-YAG laser. The first laser excites the fluorphore in the capture spheres while the second laser excites the reporter dye on the secondary antibodies. By using a specific ratio between a red and an infrared dye inside each bead, 100 labels can be differentiated. In theory, with this bead set, 100 different analytes can be detected at one time.[12]

1.2 Working with Microspheres

1.2.1. Labelling of Microspheres with Organic Dyes

Labelling of microspheres with organic dyes can be accomplished by one of two methods. The first relies on entrapment of the dye or fluorophore in the microsphere. In this method the microspheres are first swollen in an organic solvent, allowing the dyes to

diffuse into the polymer matrix. Subsequently, the dye becomes trapped in the microspheres as the solvent is removed. This internal labelling leaves the surface available for coupling reactions and at the same time yields a very high dye load. The second method requires attachment through reactive groups of the dye to the surface of the microspheres (i.e. external labelling). Organic dyes suitable for internal versus external labelling of microspheres are listed in Table 1-1.[15]

1.2.2. Labelling of Microspheres with Molecular Dots

Alternatively, microspheres can be labelled using molecular dots, which are semiconductor nanocrystals that absorb light and release this energy through emission of a photon.

Quantum dots (QD) are strongly luminescent with a 35 to 50% quantum yield at room temperature and are more than 20 times brighter than organic dyes such as rhodamine.[16] The emission wavelength can be tuned from blue to red by changing the diameter of the CdSe inner core from 18 Å (~200 atoms) to 70 Å (~10,000 atoms). All QDs can be excited with a single wavelength resulting in many emission colours that can be detected simultaneously. Quantum dots are highly resistant to photobleaching, being up to 100 times more stable than rhodamine.

The use of polystyrene beads embedded with a combination of different sizes and numbers of quantum dots creates a variety of labels. Thus the intensity and colour of each bead is dependent on the size and the number of QDs present.

Table 1-1: Fluophores used for internal or external labelling of microspheres.[11]

Fluorophore	Excitation Maximum (nm)	Emission Maximum (nm)	Labelling Method
Acridine Orange	500	526	internal
Cy-5	649	666	external
Dansyl Chloride	334	465	internal
DAPI	350	470	internal
FITC	490	525	external
Fura-2	340-380	512	internal
Hoechst	346	375,390	internal
Indo-1	350	405-482	internal
Phycoerythrin	480-565	578	external
Propidium Iodide	536	617	internal
Rhodamine 123	522	534	internal
Starfire Red	488	685	internal
Rhodamine B	540	625	internal
Tetramethyl Rhodamine	557	576	internal

Using five sizes of QDs will create very little spectral overlap and allows the use of six fluorescence intensity levels, yielding 10,000 codes.[17]

1.2.3. Immobilization of Antibodies onto Microspheres

Attachment of antibodies to the polystyrene beads can be accomplished using several methods, the simplest of which is passive adsorption onto the surface of the bead. The mechanism of attachment is mainly through hydrophobic interaction with the Fc portion (i.e. hydrophobic region) of the antibody. These antibodies are often not very active (<20% of activity) and thus have a negative effect on the assay sensitivity and even on the amount of nonspecific binding.[18] The latter occurs because the partially denatured inactive antibodies might allow nonspecific interactions with newly exposed sites. Low activity of the physisorbed antibodies is thought to be due to unfolding of the antibody on the hydrophobic surface in order to increase the number of interfacial contacts between antibody and surface.[19] Binding can be improved by introducing ionic interactions between the bead surface and the antibody. The most common way is to use a bead copolymer of styrene and acrylic acid, resulting in carboxyl groups on the surface of the bead. For complete coverage of the beads with antibodies, a 3-10 fold excess of the calculated concentration for a monolayer of these antibodies is needed. The monolayer concentration can be calculated using:

$$S = \left(\frac{6}{\rho D}\right) C \qquad \text{Equation 1-1}$$

where S is the amount of representative protein (i.e. antibody) needed to achieve surface saturation (mg protein/g of microsphere), C is the capacity of microsphere surface for a given protein (mg protein/m^2 of polymer surface), ρ is the density of the microsphere and D is the diameter of the microsphere (μm). For a polystyrene microsphere the capacity factor C has been determined experimentally for IgG and is approximately 2.5 mg/m^2.[20]

A second method to attach antibodies to the surface of a microsphere is by covalent coupling. Many chemistries exist that can be used to form the covalent bond between the microsphere and the antibody. A well-described method uses carboxylated microspheres and a water-soluble carbodiimide as a linker (Figure 1-4, A).[20] In the reaction, performed at acidic pH (4.5), the carbodiimide reacts with the carboxyl group of the bead to form an O-acylisourea intermediate. In the second step, performed at a basic pH (8.5), the O-acylisourea intermediate reacts with a primary amine from the antibody to form an amide bond.

Problems associated with this reaction are; the cleaning procedure needed after completion of the reaction, the time needed to optimize the reaction and difficulties with obtaining the proper orientation of the antibody on the surface so that the binding epitope is accessible for binding of antigen. The binding region can be sterically blocked if the recognition site is facing the bead surface, or chemically blocked if reaction of NH_2 groups in the binding region occurs with the O-acylisourea intermediate.

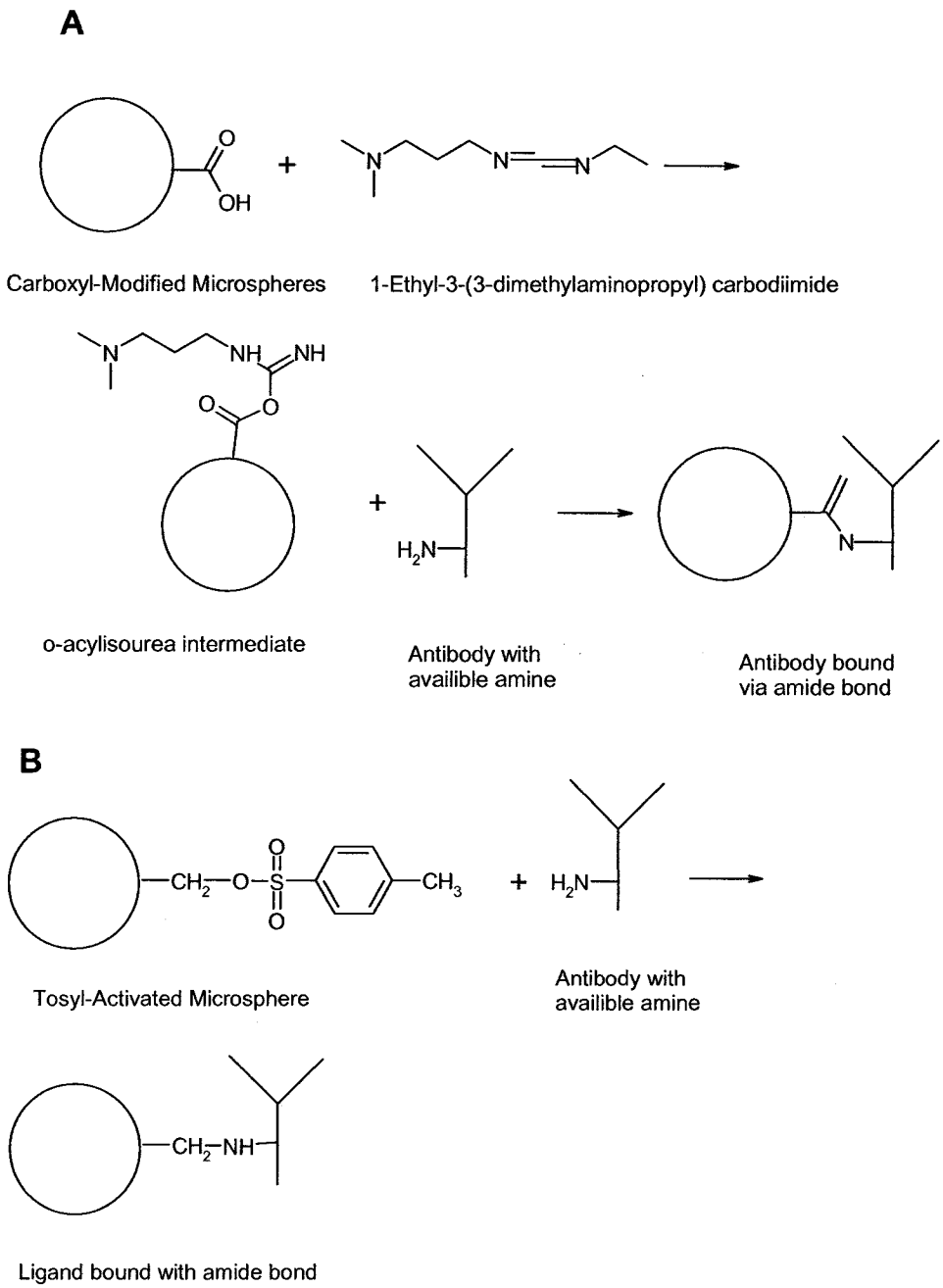

Figure 1-4: Covalent attachment of antibodies to microspheres. (A) Carbodiimide linker chemistry for attachment of antibody and (B) direct coupling of antibody with tosyl modified microspheres.

An alternative covalent coupling method uses tosyl groups (p-toluenesulfonic acid) for attachment of antibodies. With this scheme, the tosyl group reacts through a nucleophilic attack on the primary amine group of the antibody (Figure 1-4, B). The reaction involves mixing of antibodies with tosylated beads followed by incubation at an elevated temperature, typically 37 °C for 24 hours. Since removal of non reacted chemicals is not needed the reaction needs fewer steps, simplifying the linking procedure. Improper orientation of the antibody is still possible but can be minimized with the use of more hydrophobic surfaces, increasing the probability that the more hydrophobic Fc portion of the antibody reacts with the tosyl group.

A third method uses microspheres pre-conjugated to a desired binding protein (i.e. protein A, streptavidin or a secondary antibody (Figure 1-5). A biotinylated antibody forms strong noncovalent bonds ($K_a=10^{15}$ M^{-1}) with streptavidin-coated microspheres through the biotin streptavidin interaction. Biotinylated antibodies can be purchased or they can be made through a one step chemical reaction. Protein A is a 42 kD polypeptide from the cell wall of Staphylococcus aureus that is capable of tightly binding to the Fc portion of IgG ($K_a=10^9$ M^{-1}).[21] The binding is pH dependent and reversible at low pH, however this can be overcome by cross-linking the antibody to Protein A with dimethylpimelimidate (DMP).[22]

One of the easiest methods to attach antibodies to the microspheres is with the use of pre-attached secondary antibodies. Typically the secondary antibody is goat anti-mouse IgG raised against the Fc portion of the antigen-binding mouse primary antibody.

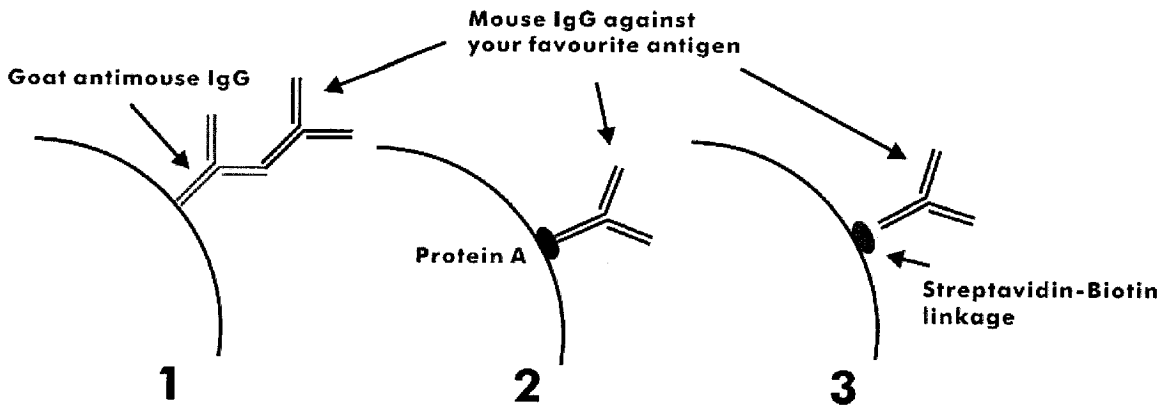

Figure 1-5: Three types of pre-conjugated microspheres: 1 antibodies, 2 Protein A and 3 streptavidin.

In addition to easy attachment, it allows proper orientation of the primary antibodies binding sites towards the solution, making them more accessible to the antigens. A disadvantage is competition with other antibodies present in a sample and potential cross reactivity.[23]

1.2.4. Manipulation and Transport of Microspheres using Pressure

Flow cytometers were initially designed to quantitate and sort eukaryotic cells. The instrument consists of: a sample inlet, a sheath system and a detector area (Figure 1-6). The cells enter the sheath system by pressurization of the sample tube, here the cells are focused and transported to the detection region after which they exit the system. Focusing of the cells is accomplished by the force of the sheath liquid flowing around the sample tube in combination with the shape of the cuvette and results in a narrow stream of particles, all with the same velocity. When the cells exit the cuvette into the sensing region they are illuminated by a laser and the resulting scatter and/or fluorescence signals are used to determine the size and, in some cases, the type of cells.

With the introduction of fluorescently labelled antibodies and more recently, green fluorescent protein, the instruments were adapted to detect the signals from these analytes. It is now possible, on the most advanced flow cytometers, to detect up to 8 different wavelengths simultaneously using 3 separate lasers.[24]

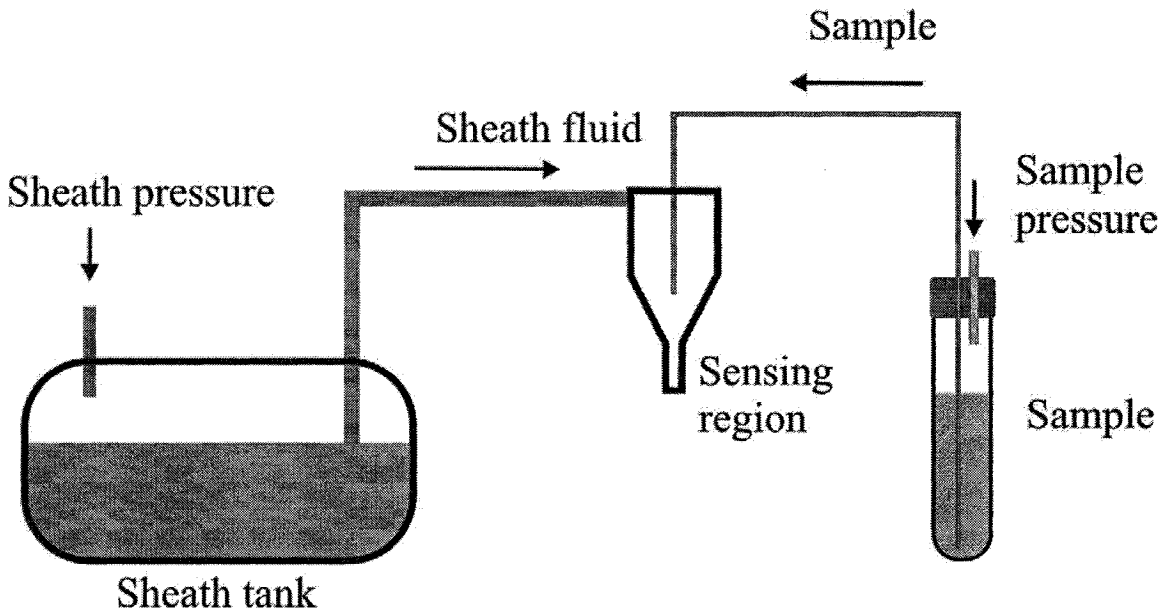

Figure 1-6: Schematic of a flow cytometer sheath system. Sample is introduced into the system by pressurizing the sample tube. The sample is moved to the sheath flow cuvette where the sheath fluid focuses the particles into a narrow stream. The particles are detected in the sensing region.[24]

1.2.5. Manipulation of Microspheres using Electrophoretic Mobilization.

Another way, other than pressure, of moving fluids and thus particles is the use of an electric field. It is much easier to manipulate an electric field than it is to make small changes with a pressure system. This is especially advantageous in a multichannel system such as a microfluidic device where flow rates in individual channels must be regulated. Capillary electrophoresis (CE) is a good example of a technique that uses electrophoretic force to mobilize the solution in the capillary. This technique uses silica capillaries with typical lengths of 20-100 cm and with inner diameters of 25 to 75 μm. Figure 1-7 is a schematic illustration of a typical CE instrument. The basic components for all CE instruments include a high voltage supply, a capillary, two buffer reservoirs and a detector connected to a data collection and storage system. To perform a separation, the capillary is filled with buffer and each end is placed in a separate buffer vial. A sample is introduced into the inlet end of the capillary and a voltage is applied between the inlet and outlet, creating an electric field in the capillary that causes movement of all analyte species. This flow inside the capillary under the influence of an electric field is referred to as electroosmotic flow or EOF. At the outlet end, the components are detected as they pass through the detection window.

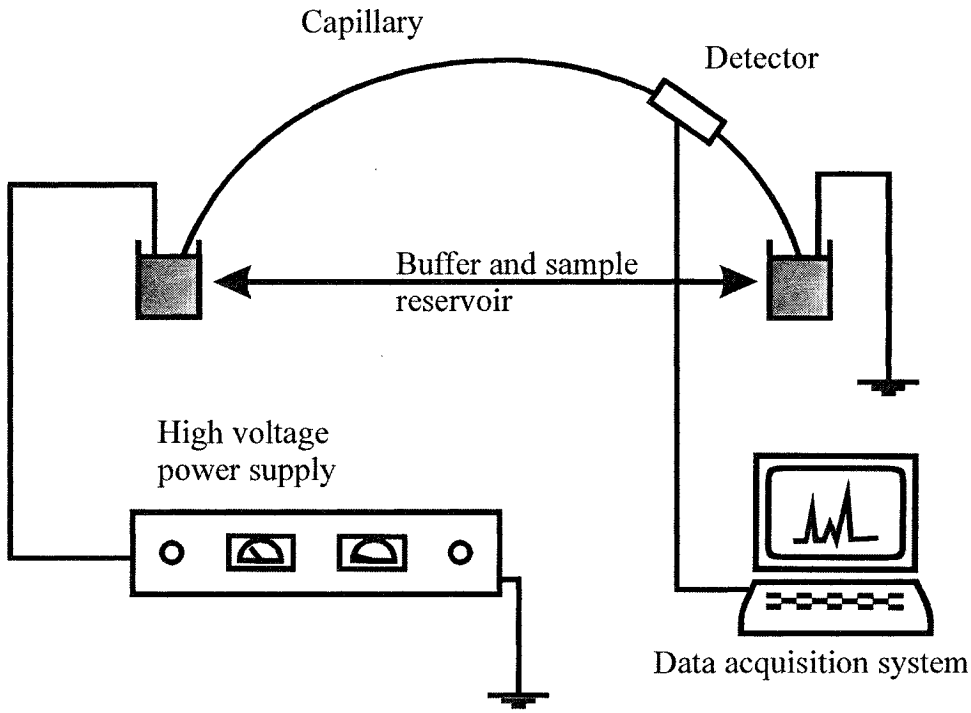

Figure 1-7: A simple capillary electrophoresis system. Indicated is the capillary in between the two reservoirs. A high voltage power supply is used to establish an electric field in the buffer filled capillary. A detector connected to a data acquisition system allows for recording of detection events.

The basis behind the EOF is the presence of excess anionic charges at the capillary wall from the internal silanol groups in the capillary. These charges attract cations as counter ions and form an electric double layer, of which the outer part, under the influence of an electric field, migrates to the cathode (Figure 1-8). Since these ions are solvated, they will drag the bulk solution with them through H-bonding and ionic interactions with the buffer ions. The double layer consists of an immobile tightly bound adsorbed layer of cations stripped of their solvation sphere where the edge is called the inner Helmholtz plane (IHP). The ions in the compact layer or Stern layer are solvated or partly solvated and are mobile with substantial cation character. The point where all the ions are completely solvated is called the outer Helmholtz plane (OHP). Past the OHP the diffuse layer or Gouy-Chapman layer extends into the bulk solution. The zeta potential drop in the Stern layer is linear with the distance from the wall, while in the diffuse layer the potential drops exponentially.[25] Under standard CE conditions, the EOF generated flow of the bulk solution will be larger than the movement of most analyte anions (that move contrary to the EOF) to the anode. Cations move in the same direction as the EOF and the vector sum of the velocities imply that they will elute early in the separation. The large EOF ensures that all ions end up passing the detector (cathode). The EOF, as defined by von Smoluchowski is expressed as:

$$v_{eo} = \frac{\varepsilon\zeta}{\eta} \times E \qquad \text{Equation 1-2}$$

where v_{eo} is the electroosmotic velocity of a solvent in an electric field, ε is the dielectric constant, η is the viscosity of the buffer, ζ is the zeta potential of the liquid-solid

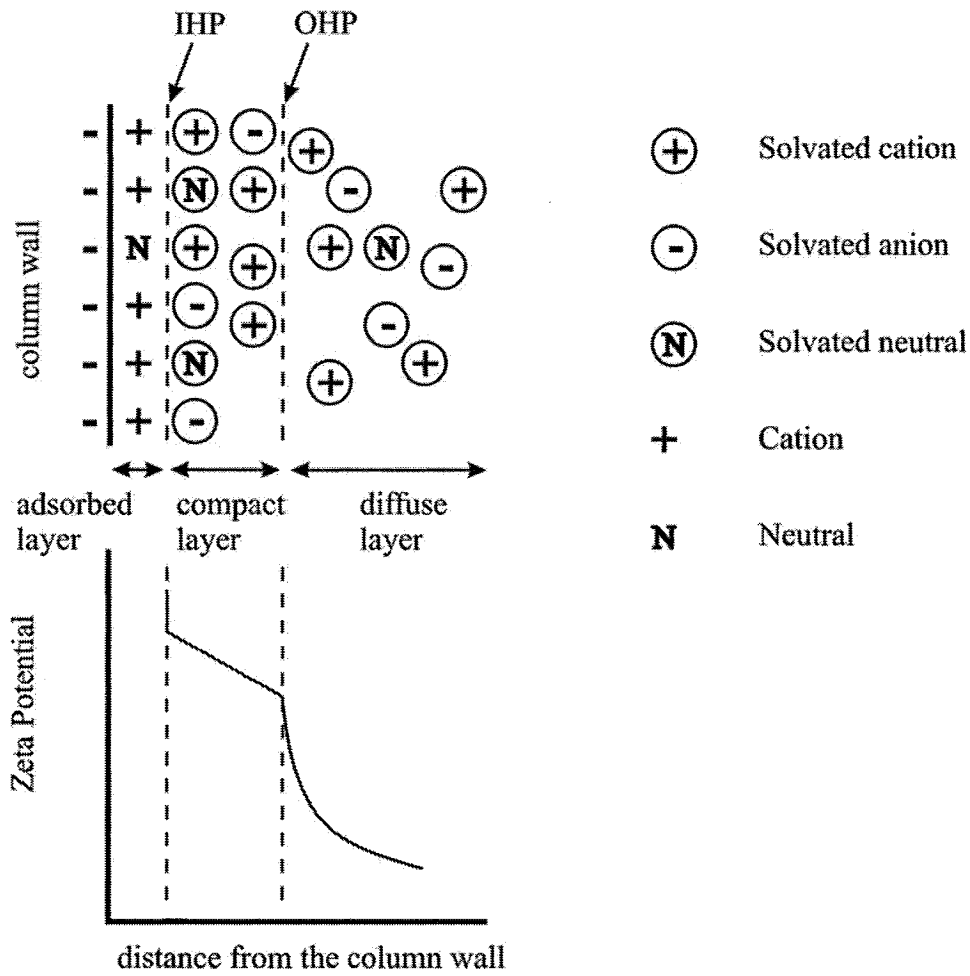

Figure 1-8: Electric double layer versus distance from the capillary wall. Indicated are the inner and outer Helmholtz planes dividing either the adsorbed from the compact layer or the compact from the diffuse layer

interface and E is the electric field. The EOF is dependent on the number of ionized groups on the capillary surface and thus the pH of the buffer solution. Data by Bello *et al*[26] suggest that the pK value of the silanol groups on the capillary wall is 6.3 which is consistent with very low EOF at pH 2.3 and an EOF plateau at pH 9.

1.3 Instrumental Considerations

The instrument we designed needed to be more compact than the current flow cytometer type detectors, but still capable of focusing the spheres used in the assay into a narrow stream, to allow efficient excitation and detection. A compact design would allow for the future development of a portable device where not only the measurements are made but also all of the incubation and washing steps. The requirements and the basic concepts of the elements involved in this instrument are described in the following sections. First we will discuss the microfluidic device, how they are made and how fluids and thus particles are moved around and focused. We will also discuss some of theory of the optics used and how they affect the measurement of the spheres.

1.3.1. Planar Glass Chips for Biomolecular Analysis

Planar glass chips are devices made up of two glass plates; one plate contains etched channels (50μm wide by 15μm deep) while the second plate is sandwiched on top of the first one. In this way closed channels are created that behave in a similar way as a silica capillary (e.g. capillary electrophoresis). One major difference is the versatility of the chip layout in terms of channel layout as compared with a capillary. Such versatility

allows the integration of particle focusing, mixing and incubation chambers in one microfluidic device. Moving liquids in the microfluidic device can be done in a similar fashion as with the capillary, using pressure or an electric field. The manufacturing process of a glass chip is a three step procedure.[27-31] First, the design of the layout on the chip is made on a computer. Secondly, the master mask is fabricated by standard electron beam techniques borrowed from the semiconductor industry. The third step consists of fabrication of the chip itself (Figure 1-9): on a glass substrate, a layer of chromium and gold are deposited, followed by a layer of photoresist (Figure 1-9, panel a). The mask is placed on top of this final layer and the complex is exposed to a light source (Figure 1-9, panel b). After exposure, the photoresist layer is developed, removing the photoresist in the irradiated areas (Figure 1-9, panel c). Exposed metal is etched away using aqua regia (Figure 1-9, panel d), leaving bare glass available for etching with a mixture of 20% hydrofluoric acid (49% solution) and 14% nitric acid (70% solution) in water (Figure 1-9, panel e). The remaining photoresist and metal layer are removed from the etched plate and together with a cover plate with access holes drilled into it are washed in H_2SO_4–H_2O_2 to remove traces of organics. Bonding of the etched plate to the cover plate is achieved by heating the sandwich to 650 $^{\circ}$C for 6 hours.

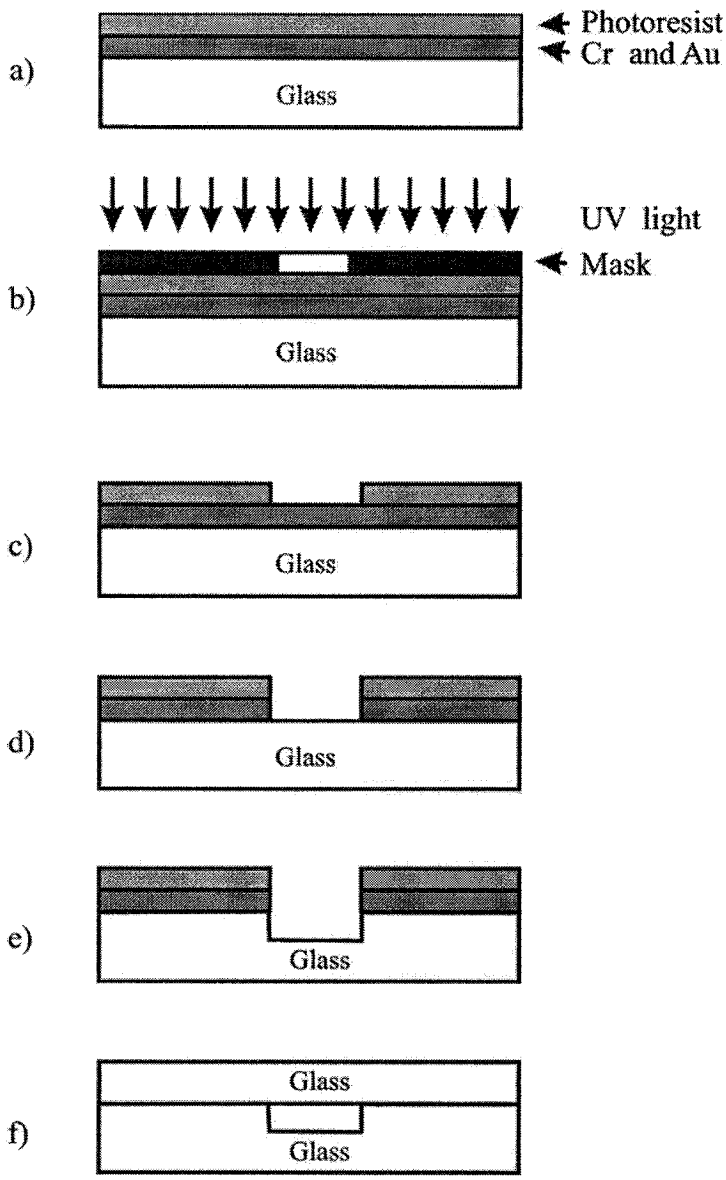

Figure 1-9: Photolithographic fabrication of a chip.[30] Indicated are the different steps involved in creating the structures in the glass.

1.3.2. Hydrodynamic Focusing.

Focusing is the reduction in the stream diameter of the particles. Focusing reduces signal variations due to the Gaussian intensity distribution of the excitation laser and variations due to velocity differences between particles.

Kachel *et al* used potential flow theory[32] to explain the hydrodynamic properties of conventional flow cytometry instruments. An area A in a reservoir that is located at a distance (*s*) from the inlet of a tube with a radius (R) (Figure 1-10). Assuming that fluid passes through with the same velocity at each cross section, conservation of mass assures that the following is true:

$$V_A 2 \cdot \pi \cdot s^2 = \nu \cdot \pi R^2 \qquad \text{Equation 1-3}$$

$$\frac{V_A}{\nu} = \frac{R^2}{2s^2} \qquad \text{Equation 1-4}$$

where V_A and ν are the velocities at point A and at the inlet of the tube, respectively. These equations are the principle behind hydrodynamic focusing as used in flow cytometer sheath flow cells. In our particular case the area (A) represents the main microfluidic channel in which the particles are moved to the focussing point where the particles are focused into a narrow stream (a) to allow detection (Figure 1-11). At the cross intersection of the chip the flow of the main channel is reduced to a narrow stream by the flow from the focusing channels.

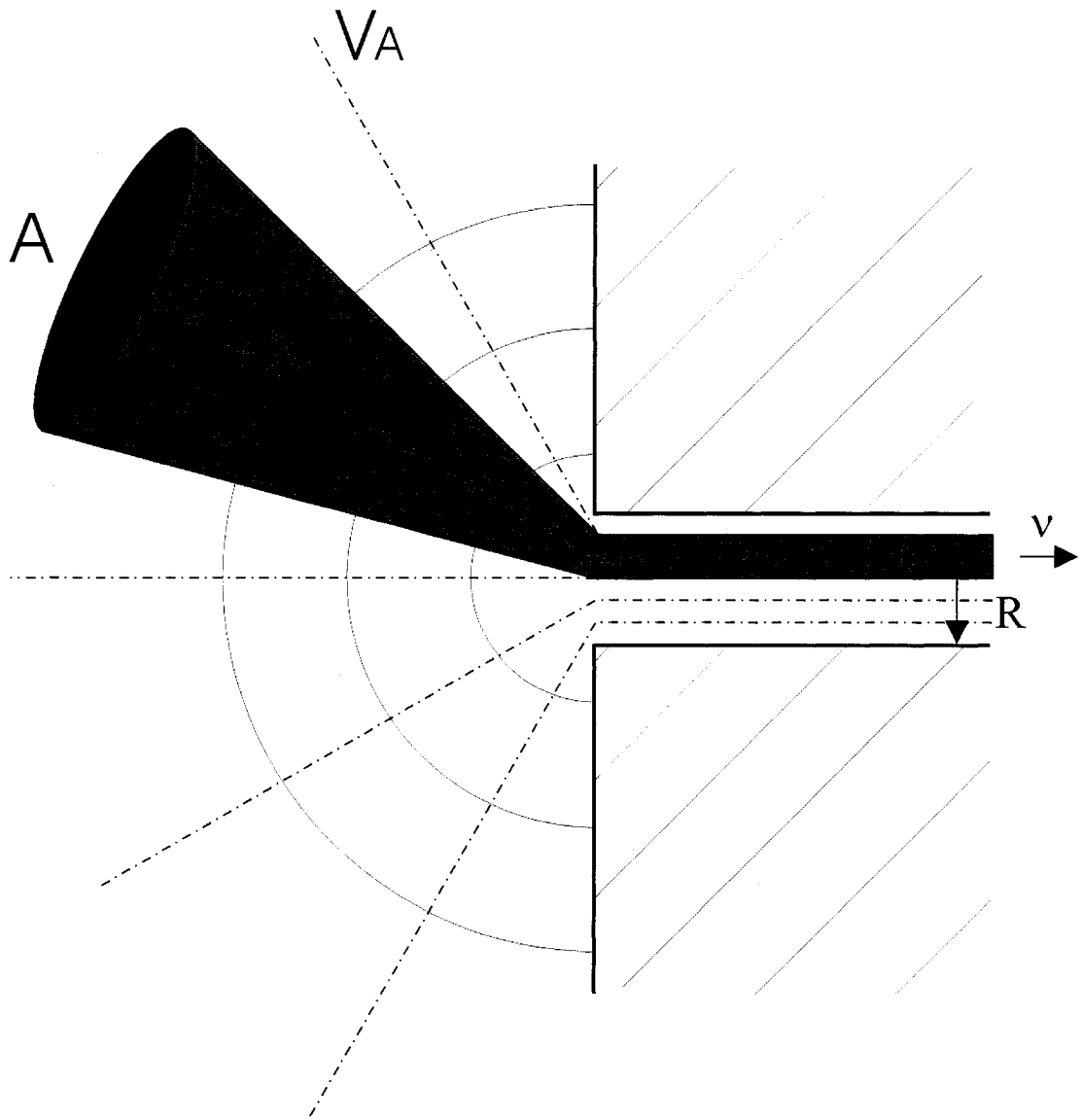

Figure 1-10: Flow conversion of liquid passing through the cross section (A) in distance (s) is focused into a smaller cross section (a) inside the tube.[32]

Conservation of mass requires that the amount of fluid crossing the main channel must be equal to the amount of fluid crossing the focused stream. It follows that

$$v_2 \cdot D_2 = v_c \cdot d \qquad \text{Equation 1-5}$$

$$d = \frac{v_2}{v_c} \cdot D_2 \qquad \text{Equation 1-6}$$

where D_2, d, v_2, v_c are the width of the center channel before focusing, the width of the focused stream, the velocities inside center channel and the focused stream, respectively. (Figure 1-11)

When we consider the flow inside the chip to be laminar, and diffusion and mixing between focused stream and sheath stream to be negligible, conservation of mass assures the following equations.

$$m_{in} = \rho_1 v_1 \cdot D_1 + \rho_2 v_2 \cdot D_2 + \rho_3 v_3 \cdot D_3 \qquad \text{Equation 1-7}$$

$$m_{out} = \rho_a v_a \cdot D_a \qquad \text{Equation 1-8}$$

$$\overline{v_a} = \frac{\rho_1 v_1 \cdot D_1 + \rho_2 v_2 \cdot D_2 + \rho_3 v_3 \cdot D_3}{\rho_a D_a} \qquad \text{Equation 1-9}$$

where m_{in} and m_{out} are mass flow rates of the inlet and outlet flows, D_1 and D_3 are the width of the inlet channels 1 and 3, respectively, ρ_1 ρ_2 ρ_3 *and* ρ_a are the density of the fluids, v_1, v_2, v_a and v_3 are velocities in channels 1, 2, and 3. $\overline{v_a}$ is average velocity (mm/sec) inside the outlet channel section D_a.[33]

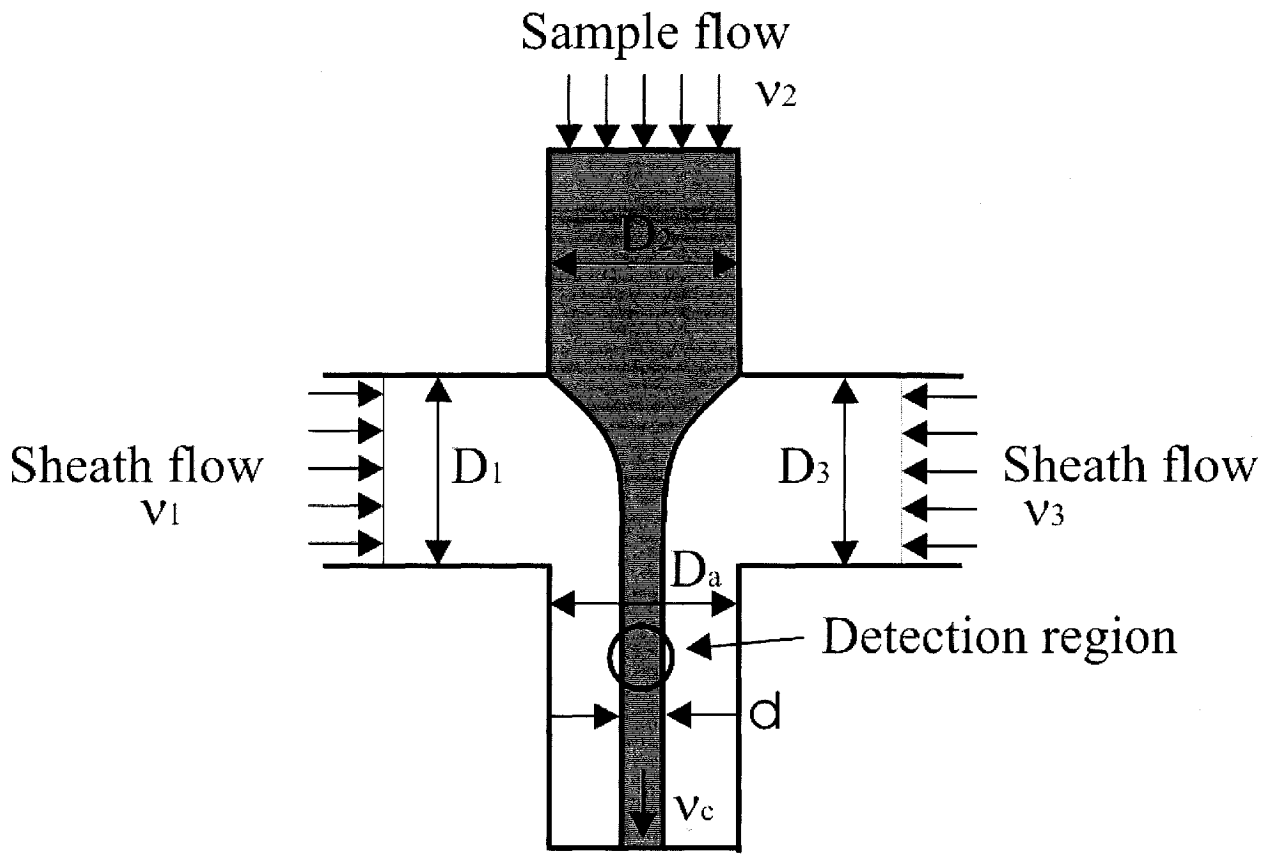

Figure 1-11: Electrokinetic focusing; the main flow (v_2) containing fluorescence dye is focused by flow from side channels (v_1,v_3). The fluorescence is measured in the detection region.

1.3.3. Focusing in an Electrophoretic Driven System

The use of a sheath flow cuvette in capillary electrophoresis systems enables the focussing of particles. Similar to a flow cytometer, the particles are hydrodynamically focused in the cuvette once they exit the capillary. When focussed, the spatially separated particles or cells flow past the detector allowing measurements of the spectral properties. Sensitivity of only a few fluorescent labelled molecules has been obtained in a capillary sheath flow system, using high numerical aperture optics and sensitive detectors.[34] It is also possible to detect small cellular components/particles that have been fluorescently labelled, such as nuclei, and mitochondria using capillary sheath flow system.[35-37] Particles have also been focused and detected in microfluidic devices. Here the focussing is accomplished by manipulating electrokinetic flow from two intersecting channels with the main channel. Much like a sheath flow cuvette, the particles are accelerated by the flow from the intercepting channels forcing them into a thin stream of individual particles.[38] These particles are then excited and detected in the sensing region. The drawback of this design is the two dimensional rather than the three dimensional focusing that occurs in a sheath flow cell. The extent of this problem is minimized by the reduced height of the flow channel (15 μm).

1.3.4. Detection of Microspheres using Fluorescence

The most sensitive method of detection in capillary and microfluidic devices is laser induced fluorescence (LIF). Concentrations into the picomolar range are obtainable and for the most sensitive instruments, less than 10 molecules can be detected.[34] In dilute

solutions and with laser intensities below the saturation limit, the fluorescence signal is proportional to the power of the excitation source according to:

$$\Phi_F = 2.3\phi_P \varepsilon c l P \qquad \text{Equation 1-10}$$

where Φ_F is the fluorescent radiant intensity, ϕ_p is the quantum yield, ε is the molar absorptivity, c is the analyte concentration, l is the optical path length and P is the radiant power of the excitation source.[39] Since a high power laser (tens of milliwatts) can be focused into a diffraction limited spot (≈10-25 μm), efficient excitation of fluorescent molecules can be achieved (10 mW/πr^2). Figure 1-12 shows a typical CE-LIF detection system consisting of an excitation source, focusing objectives, collection objectives (including the proper band pass filters) and the photomultiplier tube (PMT) detector. Microspheres are fairly easily detectable since they contain an equivalent of several hundreds to thousands of fluorescent molecules per bead. Therefore, the requirements for the detection system are not as stringent as they are for typical CE applications.

1.3.5. Detection of Microspheres using Scatter

The scattered light from microspheres can be used to detect them when passing through the detection zone. Light scatter eliminates the need for fluorescently labelling the particles and thus reduces the cost of the assay. Light scatter from particles is dependent on many parameters such as: size of particle, refractive index difference between medium and particle, shape and orientation in the laser beam.[24] How much of this light is collected from scatter on a detector is dependent on the orientation of the

detector relative to the incident laser beam. In flow cytometers scatter light is routinely used to determine cell size, cell types and cellular structural properties.

When light waves strike a particle, oscillating electric dipoles are created at the particle with a magnitude proportional to the incident field. How much light is scattered depends on the bulk property of the material through which the wave is passing. The refractive index (bulk property) is proportional to the square root of the polarizability. These oscillating electric dipoles radiate light waves in all directions at the same frequency as the incident wave. When two dipoles on the surface that lie on a line are illuminated by light parallel to this line, both dipoles will scatter light in all directions. Only in the forward direction are the scattered waves in phase while in other directions the waves might not be in phase and interfere destructively, reducing the scattered intensity. A cell, or other particles, can be thought of as a large collection of dipoles with each dipole having a different refractive index. The intensity of the scattered light from these particles increases as the sixth power of the particle radius, while the intensity changes as the fourth power of the wavelength. For homogeneous spheres and regular shaped particles the exact scattered intensity angular distribution can be calculated using Lorentz-Mie theory. Scatter from particles much smaller than the wavelength is called Rayleigh scattering.[40]

Problems associated with the collection of scatter in microfluidic devices are high background signals due to the small dimensions of the focusing chamber. The walls of the chip create a large background signal that is difficult to eliminate.

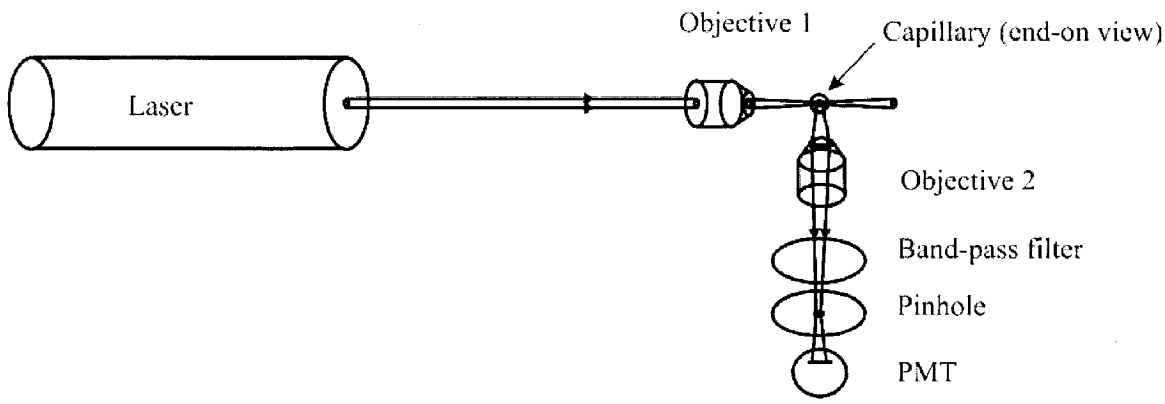

Figure 1-12: Schematic of a laser induced fluorescence capillary detection system. Indicated are the laser as excitation source, objective 1 used for focusing the laser, objective 2 used for collection of fluorescence signal at 90° angle from excitation source, band-pass filter and pinhole for wavelength selection and scatter light elimination, respectively, and finally the PMT for signal collection.

1.3.6. Optics used in Instrumentation

Fluorescent and scatter light from particles in the sample must be collected with high efficiency while rejecting interfering background signals. This is especially important when collecting scatter signals from small (< 3μm) particles since the intensity of the scatter signal decreases with the particle size. In an optical system, consisting of several components such as filters lenses and mirrors, the light deviates from its predicted path due to diffraction, an elementary property of light, and by aberrations in the optical components. The diffraction is dependent on the diameter of the lens system used and can be defined as:[41]

$$\sin\theta(1) = 1.22(\lambda / \mathrm{d}) \qquad \text{Equation 1-11}$$

where $\theta(1)$ is the angular position of the first order diffraction minima, λ is the wavelength of the incident light, d is the diameter of the aperture, and 1.22 is a geometric constant. When an optical system is free of any aberrations, its performance is completely limited by diffraction, and is referred to as diffraction limited.

Aberrations are defined as, deviations from an ideal image as defined by Snell's law for all the optical surfaces in an optical system. Snell's law is expressed as:

$$\eta_1 \sin\theta_1 = \eta_2 \sin\theta_2 \qquad \text{Equation 1-12}$$

where θ_1 is the angle of incidence, θ_2 is the angle of refraction and η is the refraction index of the media.[41] Several classes of aberration are prevalent in an optical system; in monochromatic light they are spherical aberration, astigmatism, field curvature, coma and distortion. With polychromatic light two more types of aberrations are possible, chromatic aberrations and lateral colour. The presence of these classes does not mean that only one or few types will be present in an optical system, rather all these aberrations occur in combination. A discussion of all types of aberrations is beyond the scope of this introduction; however a short overview of the basics involving chromatic aberrations will be discussed since we will collect light of different wavelengths.

According to Snell's law, light rays of different wavelength are refracted at different angles by a lens, since the index of refraction is a function of the wavelength. The index of refraction is higher for shorter wavelengths resulting in a focal point closer to the lens than with the longer wavelengths. Thus red light will focus further away from a lens than blue light does. Lenses that correct for this aberration are achromatic doublets which are two-element systems. The lens consists of a positive low index element cemented to a negative meniscus high-index element. Still not all rays will go through the paraxial focal point however the differences in the focal point are in the micrometers rather than in the millimeters.

The efficiency of the light collection is dependent on the numerical aperture, N.A., and the refractive index of the surrounding medium, η, and can be defined as

$$\text{Collection Efficiency} = \sin^2\left[\frac{\arcsin\left(\frac{\text{N.A.}}{\eta}\right)}{2}\right] \qquad \text{Equation 1-13}$$

A collection efficiency of 1 implies that all the photons emitted by a molecule are collected by the collection objective. The refractive index surrounding a lens is typically air and is thus η=1.0. A lens with a N.A. of 1 will collect half of the emitted light. Collection efficiency can also be expressed as f-number which is equal to 1/(2N.A.).[41] Microscope objectives are designed for high collection efficiencies (N.A. = 0.5 with a collection efficiency = 6.7%) and therefore well suited for use in on-chip detection systems. The working distance of the objective has to be greater than one half the thickness of the chip, about 1 mm.

1.3.7. Gaussian Beam Optics

The intensity profile from lasers can be approximated by that of an ideal Gaussian shape, when plotted along any line passing through the axis of the beam. However the output of a real laser is not completely Gaussian, and can be due to lateral beam jitter and pulsation in beam width.[42] These variations from the ideal Gaussian shape are defined by the quality factor M^2. For a theoretical Gaussian beam, M^2 =1; for a real laser beam M^2 >1. For an ion laser the M^2 factor is typically between 1.1 and 1.3 which is good compared to other type of lasers. The diameter of the Gaussian beam can be defined as where the beam irradiance has fallen to $1/e^2$ (13.5 %) of its peak value.

When a laser beam is focused through a convex lens the diameter of the spot in the focal point of the lens can be calculated using diffraction theory. Geometric optics would predict that a beam of perfectly parallel rays entering a convex lens would be focused into a spot of infinitesimal dimensions at one focal length from the lens. However, diffraction of the rays will form a finite spot size that can be defined as:

$$d \cong \left(\frac{4}{\pi}\right)\left(\frac{\lambda F}{D}\right) \cong 1.27\left(\frac{\lambda F}{D}\right) \qquad \text{Equation 1-14}$$

where F is the focal length of a convex lens, D is the beam diameter of the laser, d is the spot size at one focal length, and λ is the laser emission wavelength. This formula does not take optical aberrations into account and the real spot is usually slightly larger than the diffraction limited spot size provided that the lens is of high quality.[43] The effect of the Gaussian illumination profile on the fluorescence intensities measured from beads as they fall through the laser spot is illustrated in the following example. Assume a stream of particles with a width of 10 μm running down the centre of a laser beam with a Gaussian intensity profile and a width of 50 μm. From a Gaussian distribution the $1/e^2$ point represents a distance of 2.83 standard deviations away from the beam maximum. A particle at the edge of the 10 μm stream will be 1.13 standard deviations from the maximum and will experience an irradiance that is only 83.5 percent of the maximum beam irradiance. Since the fluorescence from the particle is dependent on the irradiance by laser beam, the intensity of the fluorescence will be dependent on the position of the particle in the laser beam. This means that the precision of the measurement will be very poor considering the 16.5 % difference in irradiance. In addition, as particles fall through

the center of the laser spot, the move from the edge where the laser intensity is low to the middle of the spot where the intensity is the highest and again to the edge of the spot. This results in a modulation of the fluorescence intensity for the particle.

Photon saturation and dye bleaching conditions using high power lasers can accomplish uniform excitation of fluorescent particles even when the intensity profile of this laser is Gaussian distributed. To achieve these conditions, laser power output of hundreds of milliwatts needs to be used for excitation. In a typical commercial instrument, 10 to 20 mW lasers are used and thus other methods have to be used to obtain uniform intensities across the particle stream to eliminate fluorescence variability. Simply, increasing the laser spot size and/or decreasing the stream width can reduce the effect of uneven irradiation. However the width of the stream is limited by the size of the particles in it and must not be narrower than the size of these particles. By increasing the diameter of the focal spot size of the laser, the variance in irradiance can be minimized. Statistically it can be determined that the central 8 % of a laser spot has less than 1 % variation in the irradiance. Thus with a 15 μm stream width, a spot size of at least 187.5 μm is needed to maintain an irradiance that is >99 % of the peak value. Of course with such a large spot size the residence time of a particle will be significant, limiting the throughput of particles. In flow cytometers, this problem is solved by reducing the height of the spot using cylindrical lenses, (focussing perpendicular to the flow direction) since this does not affect the measurement precision. The reduced spot height can also be used to measure the size and even the shape and structure of the particles passing through the detector. A technique called slit-scan uses a spot height (~ 2μm) that is smaller than the size of the particle (i.e. cells, bacteria, etc.).[24]

1.3.8. Spectral Filtering

For isolation of the appropriate fluorescent wavelength(s) and to differentiate between different fluorescent colours, Raman and Raleigh scatter, a monochromator or a filter-based detector can be used. Due to its simplicity and high transmittance at the selected wavelengths, the spectral filter is frequently preferred in fluorescence measurements. The interference filters used are made with six interfering cavities creating a nearly rectangular bandpass. Bandpass at half-heights from 10 to 100 nm are available allowing detection of low signals within 10 nm of a strong background.[41]

1.3.9. Epi-Fluorescence Confocal Microscope Systems

Reflected light fluorescence or epi-fluorescence, is a technique in which light in a certain band of wavelengths is allowed to strike the sample. The sample absorbs this light energy and emits light of a longer wavelength. Epi-fluorescence was made possible with the development of dichroic mirrors that reflect certain wavelengths while allowing longer wavelengths to pass through. In an epi-fluorescence confocal system, light from a laser is expanded to fill the aperture of a microscope objective lens. The objective lens focuses the light into a diffraction limited spot at the focal point where the sample is. Fluorescence light emitted back from the illuminated spot is collected by the same objective and directed to a pinhole placed in front of the detector via a dichroic mirror and focusing lens. This confocal pinhole is what gives the system its confocal property, by rejecting light that did not originate from the focal plane of the microscope objective

(Figure 1-13). Light rays from below the focal plane come to a focus before reaching the detector pinhole (Figure 1-13, Plane 2), and then they expand out so that most of the rays are physically blocked from reaching the detector by the detector pinhole. In the same way, light from above the focal plane (Figure 1-13, Plane 1) focuses behind the detector pinhole, so that most of that light also hits the edges of the pinhole and is not detected. However, all the light from the focal plane is focused at the detector pinhole and so passes through to the detector. When using an infinity-corrected optical configuration, the incoming laser beam is collimated and focused to a diffraction-limited spot on the specimen by an infinity-corrected microscope objective. The collected light is focused by a detector lens on the confocal pinhole. This detector lens is placed at one focal length away from the pinhole (Figure 1-13). The magnification of the imaged spot is dependent on the ratio of microscope and detection lens focal lengths. Infinity corrected optical systems allow more flexibility in the system design since the distance from the collection objective to the focusing lens is not fixed. Also, collimated beams are less affected by addition or removal of optical components in the light path such as filters, reducing the spherical aberrations in the focused spots.[44]

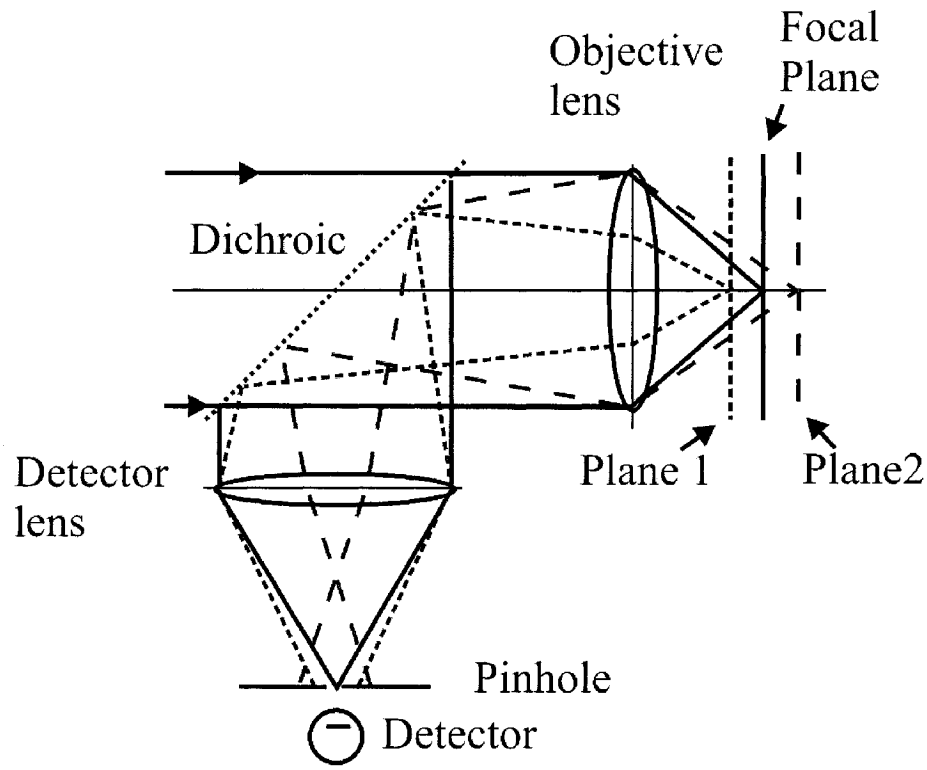

Figure 1-13: Infinity-corrected confocal microscope configuration. Rays from the focal plane are passed through the pinhole while rays from plane 1 or 2 are out of focus and are discriminated by the pinhole.

CHAPTER 2

Theoretical Model for the Assay

"All that non-fiction can do is answer questions. It's fiction's business to ask them."

Richard Hughes

2.1 Introduction

Obtaining low detection limits is an objective sought after by many analytical techniques. The quest for low detection limits is driven by a few factors; the most obvious is to measure concentrations of low abundant analytes with precision. Other reasons are, the need of analyzing smaller volumes, and the ability to dilute the sample and in this way reduce non-specific interactions.

The detection limit in an immunoassay is determined by many factors including the fundamental chemical basis of the technique as well as the size and source of experimental errors. In this chapter, we will only discuss the more sensitive two-antibody sandwich immunoassay performed with the two-bead assay or with the single bead assay that uses a fluorescently labelled antibody (as used in the Luminex system).

First, let us explore the major constraints on the detection limit in an ELISA. If we assume that the signal measurement error is insignificant, then the detection limit of an immunoassay is limited by the relative error in the non-specific signal (fraction of the labelled antibody) and the magnitude of the binding affinity of the antibody according to the following equation

$$\sigma_p = \frac{K_3.CV_{nsb}}{K_2}$$

Equation 2-1

where σ_p is the standard deviation in the measurement of the analyte, K_3 represents the percentage non-specific binding signal, CV_{nsb} represents the relative error in the response at zero dose and K_2 the affinity of the labelled antibody. If we use a labelled antibody with an affinity of $K_2 = 10^{12}$ L/mol) with a 1% CV_{nsb} and a 1% non-specific signal, the predicted potential detection limit is 10^{-16} M.[45] Thus, the detection limit is fundamentally constrained by a linear function of the fraction of non-specific binding of the labelled antibody, the precision of the separation procedure and the affinity of the antibody.

In the following sections we will describe the noise sources in the one bead (Luminex) and two bead assay, and determine the limiting noise sources and how they affect the detection limit in these techniques.

2.2 Two Bead Assay

One of the main aspects of this assay is the use of microspheres for both the capture and the detection. Since the presence of antigens (analyte) is necessary for the formation of the complexes between capture and detection spheres, the number of antigens is determined by counting. This type of detection can be classified in the counting statistic regime since the analyte can only be either present or not. On the other hand, other bead-based assays rely on the integration of the fluorescence signal of labelled secondary reporter antibodies, and are examples of an analog measurement. The statistical differences between these two types of measurements will be explored, especially the effect on the detection limit of the measurement.

With the use of signal-to-noise theory, it is possible with this assay to predict the analytical signal as the number of complexes formed with the presence of analyte. This can only be done if the antibody affinity for both antibodies used is known. Using some of the microsphere immunoassay results we can estimate the total affinity of the antibodies. Then with the equations describing the uncertainties encountered in counting statistics, it is possible to predict the uncertainty or noise in the measured signal.

2.2.1. Signal Analysis

The total number of two-colour complexes counted as they pass through the detection zone during the measurement has three components: $S_{analyte}$, S_{coin} and $S_{n\text{-}s}$. $S_{analyte}$ is the number of complexes formed via the analyte linkage. S_{coin} is the number of "false" complexes measured since there is some probability that the two different coloured beads expected in complex will be in the detector zone at the same time, *by coincidence*, even if they are not complexed. $S_{n\text{-}s}$ is the number of two-coloured complexes formed by non-specific binding rather than through an antigen.

2.2.1.1. Analytical Signal

$S_{analyte}$ is the number of analyte molecules contained in the measured volume. Since not all the analyte molecules will form a two bead complex thus the model requires a correction based on experimental results obtained with the two bead assay. This correction will also allow us to evaluate the actual complexation efficiency. This percentage of analytes complexed is dependent on the finite affinity of the antibodies,

finite probability of the two microspheres approaching each other with the correct orientation for bonding and break–up of the complex due to shear forces experienced in the flow cell and due to Brownian motion.

2.2.1.2. Coincidence Signal

S_{coin} is the Poisson's probability distribution of detecting the two beads in a measurement interval multiplied by the probability that those two beads are the "correct" colour combination to be counted as an analyte multiplied by the number of time intervals for the complete measurement.[46]

$$S_{coin} = \frac{(rt)^n e^{-rt}}{n!} \times P_{corr} \times t_{Total}\,(s) / t\,(s) \qquad \text{Equation 2-2}$$

where r = rate that beads pass the detector, t = measurement interval = the time it takes for the particles to transit the detection zone, n = number of beads measured together = 2. In this assay there are 2 sets of capture beads and 2 types of detection beads. All two bead combinations (capture-capture, detection-detection and capture-detection) are possible by coincidence but only the "correct" capture-detection combination would be mis-counted as the analyte for this assay. The total number of combinations possible are 16 but 2 of these combinations would be mis-counted as a complex of the analyte, so the probability (P_{corr}) of counting an analyte pair is 2/16. The total measurement time t_{Total} is the time required to measure the sample.

2.2.1.3. Non-specific Binding Signal

$S_{n\text{-}s}$ is the number of beads counted as an analyte that are bound by non-specific interactions and depends on experimental conditions. These conditions depend on the presence of blocking solution, concentration of protein in the matrix and cross reactivity of the antibodies.

$$S_{n\text{-}s} = 1/2 \times P_{n\text{-}s} \times \text{total number of beads measured} \qquad \text{Equation 2-3}$$

$$S_{n\text{-}s} = 1/2 \times P_{n\text{-}s} \times (\text{beads/mL}) \times Vol_{assay}\ (\text{mL}) \qquad \text{Equation 2-4}$$

$$S_{n\text{-}s} = 1/2 \times P_{n\text{-}s} \times (\text{beads/ml}) \times t_{Total}\ (\text{s}) \times \text{flow rate (mL/s)} \qquad \text{Equation 2-5}$$

where $P_{n\text{-}s}$ is the probability that any two beads will bind when brought together and depends on the surface chemistry, this factor is estimated from experimental data. Clearly, the concentration of the beads is also an important factor and in a multiplexed assay the concentration of beads is higher than it would need to be in a single analyte assay. Here the concentration of the capture beads and detection microspheres is 2 times higher than the single assay level. Thus the probability of forming a non-specifically bound complex is 4 times larger than if the assay were performed alone. This is a completely non-specific process so all possible combinations are allowed resulting in 16 combinations, but only 2 would have the correct colour combination to be counted as an analyte. We introduce a factor of 8/16 to accommodate for this concentration and colour combination effect. Vol_{assay} is the volume assayed and therefore the volume where non-specific binding events can be detected. Vol_{assay} is calculated from the volumetric flow rate and the total analysis time.

2.2.2. Noise Analysis

If we assume that the two-coloured complexes formed by the antigen near the detection limit are rare then the uncertainty in this signal is governed by the Poisson's distribution. It can be readily shown that the standard deviation in this signal is

$$\sigma_{analyte} = \sqrt{S_{analyte}} \qquad \text{Equation 2-6}$$

The same argument applies to the two-coloured signals that we measure from the random chance, or coincidence, that the correctly coloured two-bead combination is present in the detection zone simultaneously.

$$\sigma_{coin} = \sqrt{S_{coin}} \qquad \text{Equation 2-7}$$

The standard deviation in the signal due to the non-specific binding must be calculated in order to predict the detection limit. If we assume that the majority of the non-specifically bound beads are stable and that their number is significantly larger that the number of antigen bound complexes ($S_{analyte}$), then there are two potential sources of uncertainty in $S_{n\text{-}s}$. This assumption holds true near the detection limit where there are few analyte molecules around to form complexes.[39]

Source 1: Poisson distributed random fluctuations in $S_{n\text{-}s}$ where

$$\sigma_{n\text{-}s\_random} = \sqrt{S_{n-s}} \qquad \text{Equation 2-8}$$

Source 2: Non-random fluctuations where

$\sigma_{n\text{-}s\_non\text{-}random} = \varsigma S_{n\text{-}s}$ Equation 2-9

where ς is a proportionality factor. In this case we are assuming that if we were measuring the blank multiple times we would see 100ς percent standard deviation in the blank measurement. With the micro-sphere immunoassay we have found that our blank standard deviation is < 5% and is mostly due to non-specific binding.

2.2.3. Detection Limits

How many analyte molecules are needed for detection? In general the detection limit can be defined when the total signal is:

$S_{total} = S_{blank} + 3\ \sigma_{blank}$ Equation 2-10

But $S_{total} = S_{analyte} + S_{coin} + S_{n\text{-}s}$ and $S_{blank} = S_{coin} + S_{n\text{-}s}$ Equation 2-11

Rearranging for a blank subtracted regime the detection limit signal occurs when:

$S_{analyte} = 3\ \sigma_{blank}$ (This is equivalent to stating the D.L. occurs at a S/N = 3) Equation 2-12

$S_{analyte} = S/N_{DL}\ \sigma_{blank}$ or $S^2_{analyte} = (S/N)^2_{DL}\ \sigma^2_{blank}$ Equation 2-13

The 3 has been replaced with the more general value of the S/N at the detection limit S/N_{DL}

The blank error has multiple sources as noted above:

$$\sigma_{blank} = \sqrt{\sigma^2_{analyte} + \sigma^2_{coin} + \sigma^2_{n-s\_random} + \sigma^2_{n-s\_non-rand}} \quad \text{Equation 2-14}$$

$$S^2_{analyte} = (S/N)^2_{DL} \times (\sigma^2_{analyte} + \sigma^2_{coin} + \sigma^2_{n-s\_random} + \sigma^2_{n-s\_non-rand}) \quad \text{Equation 2-15}$$

Inserting the equations for the noise (Equations 2-6 to 2-9)

$$S^2_{analyte} = (S/N)^2_{DL} \times (S_{analyte} + S_{coin} + S_{n-s\_random} + (\varsigma S_{n-s})^2) \quad \text{Equation 2-16}$$

Rearranging and collecting some terms yields a quadratic equation for $S_{analyte}$

$$S^2_{analyte} - (S/N)^2_{DL} S_{analyte} - (S/N)^2_{DL}\left[S_{coin} + S_{n-s\_random} + (\varsigma S_{n-s})^2\right] = 0 \quad \text{Equation 2-17}$$

When solved for the valid root and equating it to $S_{analyte}$ = the number of two-colour complexes $\approx$ the number of analyte molecules (in the assayed volume) required to achieve sufficient signal to be detected, assuming that the affinity of the antibody is 100%.

$$S_{analyte} = \frac{1}{2}\left[(S/N)^2_{DL} \times (1 + \sqrt{(S/N)^2_{DL} + 4(S_{coin} + S_{n-s\_random} + (\varsigma S_{n-s})^2)}\right] \quad \text{Equation 2-18}$$

$\cong$ *the number of analyte molecules*

A typical experiment:

Concentration of beads that are involved with each assay = 1 x 10^6 beads/mL. Using the full multiplex for the analysis of 2 analytes implies a total bead concentration of 2 x 10^6 beads/mL. (2 sets of capture beads and 2 sets of detection beads for each set of capture beads).

Analysis time = 180s

Volumetric flow rate: flow rate = 1 nL/s = 10^{-6} mL/s

Transit time for particle across detection zone = 0.5 x 10^{-3} s

Arrival rate for particles = flow rate x bead conc. = 10^{-6} x 2 x 10^{6} = 2 beads/s

At the detection limit, the S/N = 3

The number of two-colour signals (n = 2) that will be measured due to the coincidence of two correctly coloured beads being present in the detection zone during the analysis time is:

$$S_{coin} = \frac{(rt)^n e^{-rt}}{n!} \text{ x } P_{corr} \text{ x } t_{Total}\text{ (s)} / \text{t (s)} = \frac{(20 \times 0.5 \times 10^{-3})^2 e^{-20 \times 0.5 \times 10^{-3}}}{2} \text{ x 2/81x 180 / 0.5 x } 10^{-3} = 0.4$$

If we make the assumption that 2.5% of all of the beads will form non-specific complexes, which is similar to what was encountered in the microsphere immunoassay, then the number of non-specifically bound two-colour complexes that will be observed is:

$S_{n\text{-}s}$ = 40/81 x 0.025 x 20 x 10^{6} x 180 x 10^{-6} = 44

The only remaining variable is ς. If we make the estimate that the number of non-specifically bound complexes that are measured from assay to assay would vary by 5% (i.e. 44 ± 0.05x(44)) then ς = 0.05. This is equivalent to the blank variation.

$$S_{analyte} = \frac{1}{2}\left[(S/N)^2_{DL} \times \left(1 + \sqrt{(S/N)^2_{DL} + 4(S_{coin} + S_{n-s\_random} + (\varsigma S_{n-s})^2)}\right)\right]$$

$\cong$ *the number of analyte molecules*

$$S_{analyte} = \frac{1}{2}\left[(3)^2_{DL} \times (1 + \sqrt{(3)^2_{DL} + 4(0.4 + 44 + (0.05x44)^2)} \right] = 69 \; analyte \; molecules$$

When we take into account that at this time only about 0.4% of the analyte molecules in the sample forms a complex (data not shown) resulting in a detection limit that is

$$S_{analyte} = \frac{12 \times 100}{0.4} = 1.65 \times 10^4$$

Dividing out by Avogadros Number and the volume of 180s x 1 nL/s gives the concentration D.L.

$[analyte]_{DL} = 1.5 \times 10^{-14} M$

Note that in theory the dominant term in the determination of the detection limit are the fluctuation in the non-specific binding or blank noise. This agrees with experimental observations. The affinities of the antibodies were experimentally determined and could be optimized. For each antibody about 6% binding was observed giving a 0.4% combined affinity.

2.3 Single Bead Assay

2.3.1. Analyte Signal

$S_{analyte}$ is proportional to the number of analyte molecules contained in the measured volume. The number of analyte molecules binding to the surface of a bead is dependent on both the concentration of beads and analyte molecules. Of course the formation of antibody-antigen-secondary antibody is dependent on the binding constant of the antibodies used.

The number of counted photons, and hence the signal, is dependent on the number of fluorochrome molecules (F). The background can also be expressed as an equivalent number of fluorochrome molecules to produce the background light (B). The light collection efficiency (Q) is influenced by the numerical aperture of the optics, the optical filters, and the quantum efficiency of the detector. The gain (G) is the conversion factor that includes all aspects of the signal processing (including PMT and amplifier).[40]

$$S_{analytical} = G(QF + QB) \qquad \text{Equation 2-19}$$

2.3.2. Non-Specific Binding Signal

S_{n-s} is the number of labelled reporter antibodies counted as analyte but that are actually bound by non-specific interactions, which depends on experimental conditions.

$$S_{n-s} = GQBP_{n-s} \qquad \text{Equation 2-20}$$

The non-specific binding signal is dependent on the probability ($P_{n\text{-}s}$) that a labelled secondary antibody binds to the spheres.

2.3.3. Noise Analysis

The detection limit when measuring the fluorescence intensity of the reporter antibodies on the surface of the single particles in a flow cytometer is limited by photon noise which falls into the counting statistic regime. This noise arises because of the stochastic nature of the emitted light, which implies that all emission of light exhibits a certain temporal fluctuation resulting in variations in the intensity. Other potential sources of noise such as fluctuations in the excitation intensity and sample flow are trivial and can easily be ignored.

In a flow cytometer the data processing is performed in photon counting mode. Therefore, the signal at the photocathode follows a Poisson distribution, with n as the average number of photons counted in a measured period. The standard deviation of the measured signal can then be expressed as

$$\sigma_{analyte} = \sqrt{S_{analyte}} \qquad \text{Equation 2-21}$$

Not only fluorescence photons from the particles are collected but also those from the background, caused mainly by fluorescence and scattered light from the flow cell and from filters and lenses in the optical path. Since the excitation light source has a constant intensity, then n_b is the number of photons reaching the detector within a time period that the detector integrates. The background has two potential sources of uncertainty

Source 1: Poisson distributed random fluctuations in $S_{background}$ where

$$\sigma_{background_{shot}} = \sqrt{S_{background}} \qquad \text{Equation 2-22}$$

Source 2: Non-random fluctuations where

$$\sigma_{background_{prop}} = \chi S_{background} \qquad \text{Equation 2-23}$$

Where χ is a proportionality factor.

Beside the background signal another source of error is the signal due to non-specific binding. Again two potential sources of uncertainty are possible with this signal

Source 1: Poisson distributed random fluctuations

$$\sigma_{n-s_{shot}} = \sqrt{S_{n-s}} \qquad \text{Equation 2-24}$$

Source 2: Non-random fluctuations where

$$\sigma_{n-sprop} = \delta S_{n-s} \qquad \text{Equation 2-25}$$

Where δ is a proportionality factor. Not included in this variation are errors introduced while performing the assay, such as pipetting errors.

2.3.4. Detection Limits

Again the detection limit is defined for when the signals is:

$S_{total} = S_{blank} + 3\,\sigma_{blank}$ Equation 2-26

But $S_{total} = S_{analyte} + S_{s\text{-}n} + S_{background}$ and $S_{blank} = S_{s\text{-}n} + S_{background}$ Equation 2-27

Rearranging for a blank subtracted regime:

$S_{analyte@DL} = 3\,\sigma_{blank}$ (This is equivalent to stating the D.L. occurs at a S/N = 3) Equation 2-28

$S_{analyte@DL} = S_{total@DL} - S_{blank}$ Equation 2-29

The blank error has multiple sources as noted above:

$S_{analyte@DL} = (3\,\sigma_{blank} + S_{s\text{-}n} + S_{background}) - (S_{s\text{-}n} + S_{background})$ Equation 2-30

Thus the signal at the detection limit is equal to

$$S^2_{analyte} = (S/N)^2_{DL} \times (\sigma^2_{n-s} + \sigma^2_{background})$$ Equation 2-31

$$S^2_{analyte} = (S/N)^2_{DL} \times (\sigma^2_{n-s_{shot}} + \sigma^2_{n-s_{prop}} + \sigma^2_{background_{shot}} + \sigma^2_{background_{prop}})$$ Equation 2-32

Inserting the equations for the noise (Equations 2-21 to 2-25)

$$S^2_{analyte} = (S/N)^2_{DL} \times ((GQF_{n-s}P_{n-s})_{random} + (\chi GQF_{n-s}P_{n-s})^2_{non-ran} + (GQF_{background})_{random} + (\delta GQF_{background})^2_{non-ran})$$ Equation 2-33

Now if we assume that typically $S_{n\text{-}s} >> S_{background}$ then the formula will simplify to

$$S_{analyte} = (S/N)_{DL} \times \left[(GQF_{n-s}P_{n-s})_{random} + (\chi GQF_{n-s}P_{n-s})^2_{non-ran} \right]^{\frac{1}{2}}$$ Equation 2-34

Typically the proportional noise χ is in the order of 5 %, when $GQF_{n\text{-}s}P_{n\text{-}s} >> 400$ then $0.0025(GQF_{n\text{-}s}P_{n\text{-}s})^2$ dominates the equation. Then proportional noise on the non-specific binding dominates the detection limits. However, when $GQF_{n\text{-}s}P_{n\text{-}s} < 400$, then shot noise on the non-specific term dominates and consequently the assay is shot noise limited.

From this we can conclude that only when the non-specific binding is very low does the Luminex assay become shot noise limited and is equivalent to the two bead assay. We do not have the data to verify this, but it is reasonable to predict that the Luminex system is most likely limited by the proportional noise of the non-specific signal. In this case counting beads provides a superior detection over measuring the number of ligands bound to a bead.

2.4 Conclusions

Direct comparison of detection limits is not very useful at this point since the two bead assay has not yet fully been optimized. Also antibodies can have a large range of binding affinities for its analyte and thus, only if the same set of antibodies is used for both assays can proper comparisons be made. More useful is the theoretical noise comparison as shown in this chapter for identifying limiting noise sources in each assay. By performing the analysis we show that it is only when the non-specific binding is low that the Luminex is shot noise limited, and becomes equivalent to the two bead assay.

Another distinct advantage of the two bead assay over the single bead assay is the type of instrumentation needed. For the single bead assay, instrumentation is needed capable of accurately measuring very low signal levels (200 fluorescent molecules/bead). To accomplish this, relatively expensive instruments must be used. In contrast, the two bead assay uses amplification of the binding signal with the use of a highly fluorescent detection bead. This bead is easily exited and detected using a relatively simple optical setup.

CHAPTER 3

A Two Bead Immunoassay in a Microfluidic Device Using a Flat Laser Intensity Profile for Illumination

K. Pieter Roos and Cameron Skinner

The Analyst 2003 Jun; 128(6): 527-31.

This chapter is an expansion of this paper.

To suppose that the eye with all its inimitable contrivances for adjusting the focus to different distances, for admitting different amounts of light, and for the correction of spherical and chromatic aberration, could have been formed by natural selection, seems, I confess, absurd in the highest degree.

Charles Darwin, *The Origin of Species,* John Murray, London, 1859.

3.1 Abstract

Recently it was demonstrated that a collimated Gaussian beam can be converted to a flattop beam using a Keplerian beam reshaper consisting of two aspheric lenses.[1] Here, using the same optical system, we demonstrate that this Fermi-Dirac, or flattop profile, can be maintained when used in a confocal detection system that focuses the laser beam into a diameter of only 33 μm. The intensity profile of the reshaped beam was determined by imaging the excitation of a constant stream of fluorescein inside a microfluidic device. The resulting shape had a 6.38 % RSD intensity across the flat profile when imaged with a CCD camera. This flat illumination profile was then used in a two bead multiplex immunoassay where the colour combination and/or the intensities can be used to determine the presence of an antigen. Detection limits of TNF-α and IL-6 were comparable with standard ELISA immunoassays.

3.2 Introduction

3.2.1. Gaussian Intensity Profile.

The emission intensities from gas lasers, such as an argon ion laser, have a Gaussian intensity profile proportional to $e^{-2(r/a)^2}$, where the beam waist parameter ($a = I_o e^{-2}$) determines the size of the beam.[47] This distribution is often undesirable for applications such as flow cytometry and some chip based applications where uniform

illumination, of fluorescent particles for example, is essential for accurate measurements of optical properties.

The method most often used to obtain a uniform illumination from a Gaussian beam is to expand the beam to a diameter much larger than the probe area and only the axial portion of the beam is used where the intensity varies slightly.[24] With this method a large portion of the laser beam output is wasted and therefore more laser power is required to compensate for this. Other techniques have been used to create uniform illumination (flat intensity profiles) using, filters with radially varying absorption profiles, refractive or reflective anamorphic optical systems and diffractive elements such as holograms. All these systems have their specific problems but more often are limited by the extreme difficulty to produce these optics.[48] Hoffnagle *et al.*[48] developed a refractive optical system with two aspheric lenses to efficiently convert a Gaussian laser beam to an 8-mm-diameter flattop beam with only a 5% RMS power variation. The advantages of this system are independence from the wavelength used e.g. deep UV to near infrared (limited by the bandpass of the optics) and the need for only a single prescription of aspheric lenses to enable the beam transformation. Using this type of optical system is most useful in instruments that depend on even illumination of the sample, such as a flow cytometer. The even illumination allows the correlation of scatter/fluorescence signal to size of cells, organelles or nuclei.[35-37,49]

3.2.2. A New Immunoassay.

Recently a new method has been described in the literature that uses coloured fluorescent spheres for direct, or indirect, immunoassays.[50-52] This type of immunoassay system is capable of detecting multiple antigens concurrently by using a separate colour for each antibody-antigen combination. A positive result is obtained when a fluorescently labelled antigen, or antibody, is bound to these spheres. This technique however, is less sensitive than immunoassays that use enzymatic amplification to obtain an analytical signal because of the limited signal obtained from the labelled antigen (only one or few fluorescent labels per antigen).

A modification to the microsphere assay is presented here. In our assay, the antigen of interest is captured using microspheres (micrometer sized latex beads of a defined emission wavelength) conjugated with specific monoclonal antibodies. The microsphere-antibody-antigen complex is subsequently bound by a second monoclonal antibody, recognizing a different exposed epitope on the antigen, that was conjugated to a second microsphere (detection microsphere) of an alternate emission wavelength. The reaction mixture is passed through a dual-channel detector that can differentiate between single- (unbound fluospheres) and doubly fluorescent (microsphere-antigen-microsphere) complexes. Only when a complex is formed, will a signal appear simultaneously in both fluorescence detector channels, thus indicating the presence of an antigen (Figure 3-1). Simultaneous detection of multiple antigens can be accomplished by using combinations of different emission wavelengths for the capture and detection spheres.

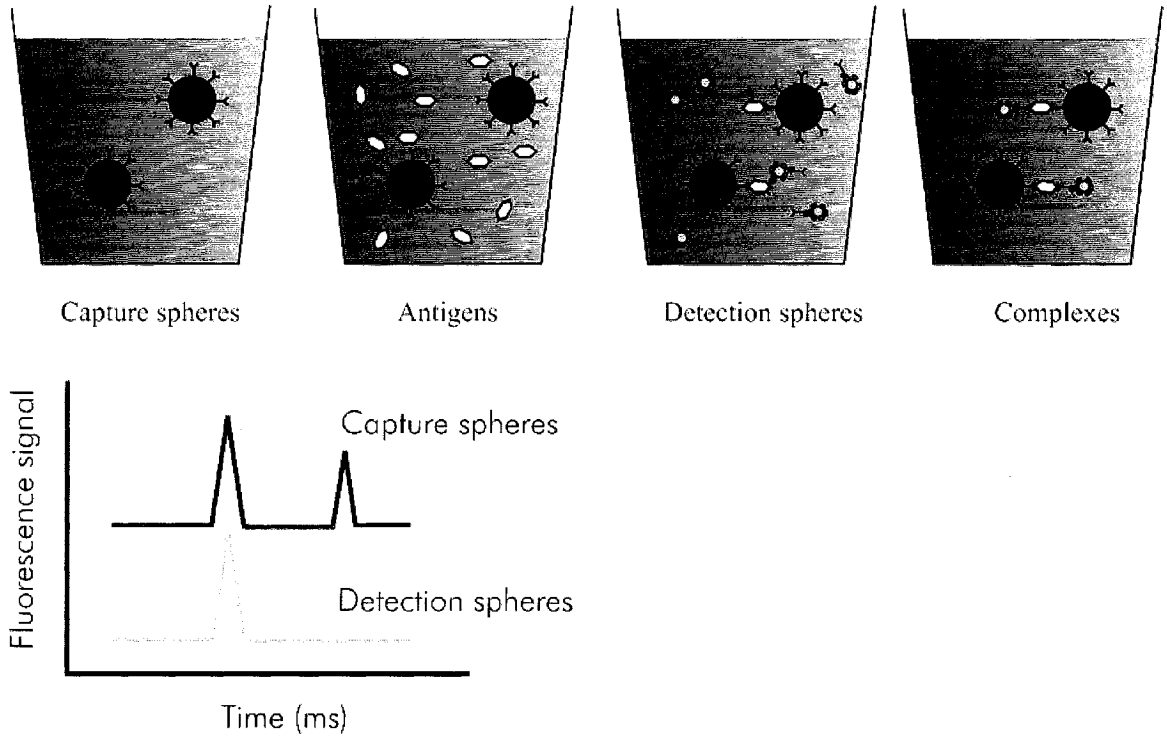

Figure 3-1: Two microsphere assay, antibodies on the capture spheres bind the antigen after which the antibodies on the smaller detection spheres bind the antigen using a different epitope to form a complex. The graph shows the signal vs. time. When a complex passes the detector a pair of signals is observed at the same time but when only a capture sphere passes the detector a single signal is observed.

Each microsphere has the equivalent of several thousand fluorescein molecules, readily allowing detection of the complexes in a way that is less demanding on the instrumentation yet allows the sensitivity of an ELISA.[53] In effect, detection is based on counting rather than the signal intensity, and as discussed this has significant implications on the S/N ratio. This assay also has the advantage of being significantly faster than traditional assays since it is effectively a "mix and measure" type of assay. Conventional immunoassays require several laborious incubation and washing steps before measurements can be taken.

Several types of instruments can be used for the detection of the formed complexes. A fluorescent plate reader can be used to quantitate the concentration of complexes formed provided that the excess unbound detection microspheres are washed away, however multiplexing is not possible. Multiplexing is possible with a flow cytometer where the individual complexes are detected as they pass through the detector zone. Differentiation of the multiple colours can be accomplished with the use of several detection channels, each of which looks at discrete colours.

Microchip based instruments offer many potential advantages over traditional instrumentation (size, cost etc.), but working with particles in these devices is relatively new. Manipulation and confinement of particles in a microfluidic chip has been described using hydrodynamic, electroosmotic[54] and dielectropheretic[55] forces. These methods can be used to manipulate and focus the particle complexes through the centre of the optical probe region to facilitate detection.[38,55,56]

3.3 Experimental

3.3.1. Apparatus

The instrument must be able to detect the complexes containing more than one wavelength simultaneously at very high scan rates (number of data points collected in a given time). How many wavelengths and the speed of collection are dependent on the number of analytes and the velocity of the complexes as they pass the detector. An in-house built detection system was built capable of simultaneously detecting three wavelengths (Figure 3-2) at a scan rate of 60 KHz per channel allowing a minimum residence time of 0.2 msec. In this detection system a laser beam is first expanded and then converted into a flat beam. The flat beam is imaged into the chip where it excites the fluorescence. The fluorescence signal is collected the by the objective, and focussed onto the pinhole by the focussing lens. Band pass and dichroic filters are used to select the desired wavelengths before collection by one of the three PMT's

3.3.2. Flat Beam Profile

As discussed, a flat beam reduces the variations in intensities from the individual spheres as they pass through the detection zone. To create a flat profile an argon ion laser with a 0.69 mm, 488nm emission line (Model 2214-10SL, JDS Uniphase, CA) was first spatially filtered (Model 910, Newport, CA) using two 5 X microscope objectives and a 25 μm pinhole. The beam was then expanded using a variable-magnification beam expander (Model 07 HBZ 001, Melles Griot, CA) to a collimated beam diameter of about

8 mm. This increase is important since the optical component for creating a flat profile, the Keplerian beam reshaper (on loan from Dr. Hoffnagle IBM), requires an input beam size of this dimension. The beam exiting the reshaper will have a flat intensity profile but is no longer collimated. Therefore the output of the Keplerian reshaper is imaged on to the chip through a 20X, 0.45 NA infinity corrected focusing objective (Model 556015, Leica, CA). The spot size in the chip is dependent on the magnification determined by the ratio between objective focal distance and the distance from the reshaper to the objective ($M = f_2 / f_1$). Therefore to achieve a 40 μm flat beam laser spot the objective was placed about 127 cm from the Keplerian beam reshaper and 6 mm from the chip.

3.3.3. Detection

A confocal epi-fluorescence system collects the fluorescence signal using the same optical path as that used for excitation. By sharing the optical path, fewer optics are needed, making alignment of the optics simpler. A 488 nm excitation laser beam was introduced onto the optical axis by reflecting it off a dichroic mirror and focusing it onto the chip by a microscope objective (20X, 0.45 NA infinity corrected focusing objective, Model 556015, Leica, CA). The fluorescence light was collected and collimated by the same objective. This radiation has a longer wavelength than that of the laser and is passed through the dichroic mirror. Typically this filter reflects more than 95% of the shorter wavelengths while passing 80-90% of the longer ones. The collected collimated fluorescence light is directed by some mirrors to a lens (f= 19.5 cm) which focuses it onto a 100 μm pinhole.

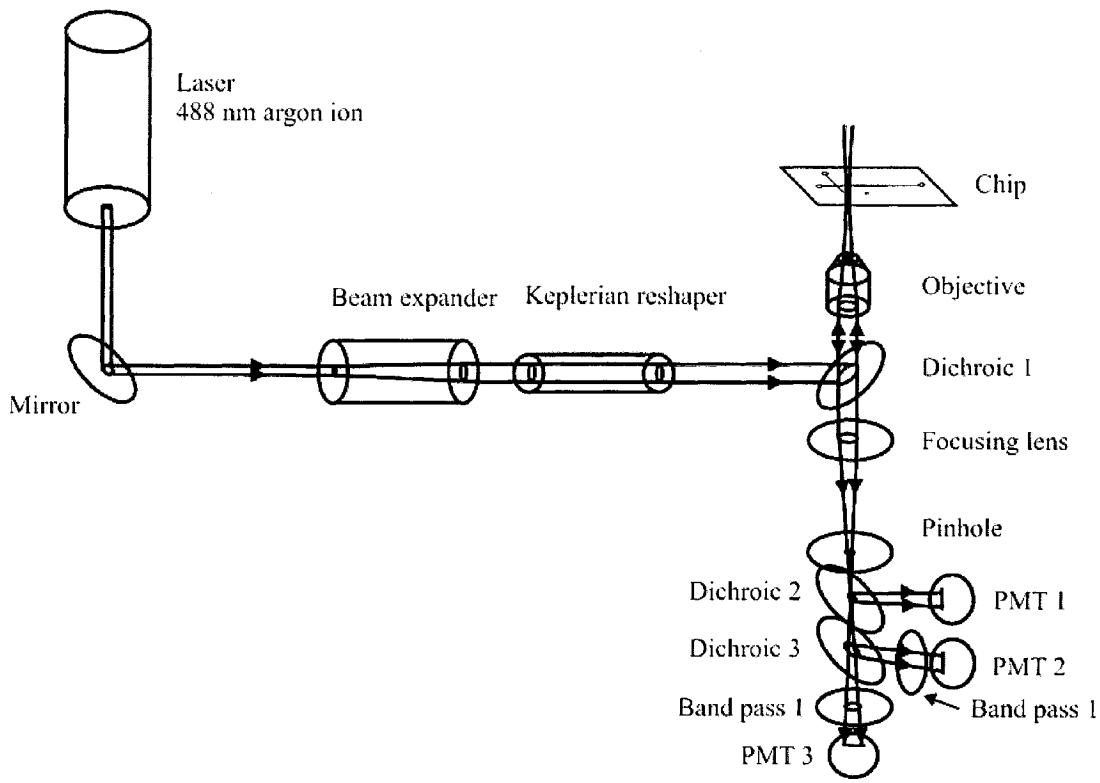

Figure 3-2: Schematic representation of the optical path used in the confocal detection system. The laser beam is first expanded and then converted into a flat beam. The flat beam is imaged into the chip where it excites the fluorescence. The fluorescence signal is collected the by the objective, and focussed onto the pinhole by the focussing lens. Band pass and dichroic filters are used to select the desired wavelengths before collection by one of the three PMT's.

The spatial discrimination from the pinhole allows for rejection of scatter and reflection light from the wall and surfaces of the chip while collecting the fluorescence light. Wavelength separation in the detection area is accomplished with the help of carefully chosen dichroic and bandpass filters. (Figure 3-2).

First, scattered light from the particles that passes through the 505 DFLP dichroic mirror (Figure 3-2, Dichroic 1) and was detected by reflecting these short wavelengths off a second dichroic mirror (Figure 3-2, Dichroic 2; 515 DFLP; Omega Optical, VT) set at 45° to the first PMT. The transmitted light is discriminated by a third dichroic mirror (Figure 3-2, Dichroic 3; 600 ALP) also set at 45° to the incident beam. Light with wavelengths shorter than 600 nm are reflected towards the second PMT, where a bandpass filter with 535 nm center λ and a 35 nm bandpass (Figure 3-2, Bandpass 1; 535DF35, Omega Optics, VT) determines the range of light detected. The light transmitted by the 600 ALP dichroic arrives at the third PMT where a 655DF35 band pass filter, Omega Optical, VT (Figure 3-2, Bandpass 2) selects the wavelength of interest. Signals from the PMT's were digitized at 16 bit resolution with a maximum collection rate of 200 ks/s (kilo samples per second) (PCI-6023E National Instruments, TX).

3.3.4. Data Analysis

To identify complexes, the raw data was processed using an algorithm written in Igor Pro (Version 3.15, Wavemetrics, OR). This program looks for a signal in the scatter channel (PMT1) above a certain threshold to identify a capture bead. This scatter signal

is compared with signals from both fluorescence channels (PMT 2 and 3) and tabulates them. The stored table, in ASCII format, was converted into standard flow cytometer data format (FCS) using A2FCS (ASCII to FCS) (Joseph Trotter, Scripps Research Institute), and analyzed with WinMDI flow cytometer software (Joseph Trotter, Scripps Research Institute). Data analysis was performed using standard cytometer methods. First, on a scatter plot of scatter signal vs. fluorescence, a blank region is determined by gating the signal region occupied by the blank. Second, the same gate was applied to a scatter profile of a sample containing the analyte. Points outside the blank gated area and inside the "sample" area are considered to be complexed.

3.3.5. Imaging the Fermi-Dirac Profile

For determining the profile of the laser beam, the flattop laser beam was focused inside the microfluidic device through which fluorescein (10^{-6} M) was pumped by applying a vacuum at the waste reservoir. This fluorescein stream size was the same width as that of the channel width. The laser beam was modulated at 0.5 Hz with a 50% duty cycle to allow the fluorescein to flush through the detection zone without excitation. This was done to avoid any issues with photo bleaching of the dye reducing the fluorescence intensity at the down-stream side of the spot. Visualization of the spot was performed using a similar setup as shown in Figure 3-2 but instead of the PMT's and pinhole, a lens and camera was used as a detector. The fluorescence image was taken using a 12-bit monochrome CCD camera (Model 1312M, DVC, TX) equipped with a Nikon lens (Micro-Nikkor 105mm f/2.8D). The data from the camera was acquired with an IMAQ PCI 1422 image acquisition board (National Instruments, TX) using IMAQ

vision builder 6.0 software (National Instruments, TX). Six consecutive images were taken during the exposure to the laser light. The images were analysed with Matlab (The MathWorks, MA) using a custom written routine to determine the RSD of the flat-top portion of the laser spot (Appendix B).

3.3.6. Microfluidic Device

A microfluidic device (Model PC-SC, Micralyne, Canada) with a simple cross layout was used for all experiments. For mobilization of the particles, an electric field was applied using a custom built power supply capable of applying a different potential to each well on the chip. For hydrodynamic mobilization, vacuum from a water aspirator was applied to the waste reservoir.

3.3.7. Other Equipment

During assay development, a fluorescence plate reader (Wallac Victor2 1420 multilabel counter, PerkinElmer Life Sciences, Finland) and a flow cytometer (FACScan, Becton-Dickinson, MI) were also used. The FACScan has one laser at 488 nm and can collect 3 fluorescence and 2 scatter signals simultaneously.

3.3.8. Reagents

Stock solutions of PBS (phosphate buffered saline, 0.88 g sodium chloride in 0.01 M sodium phosphate pH 7.4) with 4% (w/v) BSA (bovine serum albumin) were prepared by diluting a 10% (w/v) BSA PBS solution (Pierce, WI) with PBS. The 0.2 μm

neutravidin-labelled yellow-green (F-8774, excitation/emission: 505/515 nm Molecular Probes,) fluospheres were diluted in PBS 4% BSA.

3.3.9. Antibody Attachment

Dynabeads, tosylated superparamagnetic polystyrene capture beads (2.8 μm diameter) with a polyurethane coating layer (Dynal, Norway), were vortexed for approximately 1 minute. The required amount of beads (at a concentration of 2 x 10^9 beads/mL) were directly pipetted into a separate centrifuge tube and placed near a rare-earth magnet (Catalog #99k32.13, LeeValley Tools, Canada) for 1 min to pull the beads to the wall of the 0.5 ml tube. All the liquid was removed using a pipette and the beads were resuspended in ample volume (≈200 μl) of 0.1M sodium phosphate buffer at pH 7.4. After mixing for 2 minutes the washing process was repeated. After the second wash the beads were resuspended in the original volume and an equal volume of antibodies at a concentration of 1 mg/ml was added (approximately 5 μg antibody/10^7 beads). The mixture was incubated for 24 hours at 37° C with slow tumbling to prevent settling of the beads. After incubation with the antibodies, the beads were washed twice in PBS, pH 7.4, with 0.1% BSA (w/v) and once in 0.2 M Tris, pH 8.5, with 0.1 % BSA (w/v). To deactivate any un-reacted tosyl sites the beads were incubated for 12 hours at 37°C in Tris buffer. After this last incubation, the beads were washed twice in PBS (pH 7.4) with 4% BSA (w/v) and stored at 4° C for a maximum of two weeks.

3.3.10. Performing the Assay

The assays were performed in flat-bottom 96 well plates (model 3591, Costar, NY) that were blocked overnight with PBS (pH 7.4) and with 4% BSA (w/v). Into each well, 50 μL containing 10^6 capture beads and 50 μL of the appropriate concentration of antigen, both in PBS (pH 7.4) with 4% BSA (w/v), were added. After 30 minutes of incubation on a slow mixing vortex, the beads were pulled to the bottom of the plate using a magnetic separator plate. The separator plate contained 24 0.5 inch rare-earth magnets, one per four wells (Catalog #99k31.03, LeeValley Tools, Canada). The wells were washed by vortexing the beads for 5 minutes in the washing solution (PBS, pH 7.4, with 4% BSA (w/v)). The plate was removed from the magnetic separator and 100 μL containing 250 ng/mL biotinalated antibody in PBS (pH 7.4) with 4% BSA (w/v) was added. Again, the plate was incubated for 30-minutes with slow mixing on the vortex to promote binding of the second antibody. After the incubation, a second wash was performed to remove most of the excess of antibody. The detection beads (0.2 μm fluospheres) were added to the sample and binding was allowed to occur for 30 min. Finally, three washing steps were performed to remove excess detection spheres. A final buffer exchange into 10 mM phosphate buffer was performed when electrokinetic focusing was used.

3.4 Results and Discussion

The objective of this work was to perform an immunoassay by measuring antibody interactions visualized by large fluorescently labelled spheres in a microfluidic device that functioned as a flow cell. The excitation of these fluorescently labelled spheres was performed using a flat intensity profile laser beam allowing even excitation and thus illumination of the spheres. Before the immunoassay could be performed the flat intensity profile and the chip had to be verified. To that end the output of the laser beam reshaper was measured, and the flow pattern of beads in the microfluidic device was imaged. In the following sections the performance of both the reshaper and the microfluidic device will be discussed before finally the results of the actual immunoassay are finally reviewed.

3.4.1. Output Profile from the Keplerian Reshaper

To verify that the output of the reshaper was indeed flat the image was recorded with the CCD camera. Initially a neutral density filter was placed after the reshaper and the image was taken with the camera. Unfortunately the neutral density filter did not reduce the intensity of the laser beam uniformly due to imperfections in the filters used. Therefore, to obtain a profile of the intensity distribution the output of the Keplerian reshaper was imaged on to a Plexiglas disc, spun at 1100 rpm (rotations per minute). The high velocity of the disk permits averaging of imperfections in the Plexiglas. It was

possible with this setup to record an image of the back reflection from the Plexiglas without saturating the CCD array.

3.4.2. Flat Profile in Microfluidic Device

When aligning the optical path to create a flat beam profile inside a chip, there was a tendency to compensate for flow-related photo bleaching of the fluorescein as it travelled through the laser spot. To correct for this effect the laser beam was chopped at 0.5 Hz while images where taken by the CCD camera at a rate of 5 frames per second. During the time when the beam was blocked the fluorescent solution filled the microfluidic channel without exposure to the laser. The first image after modulation of the chopper showed no effects from photobleaching; however, consecutive images showed reduction of the signal at the waste side of the detection zone (Figure 3-3). This indicated that significant photobleaching occurred as the fluorescein traversed the illumination zone. The intensity profile of the beam can be intentionally adjusted to offset for the photobleaching so that an image of uniform intensity can be collected (data not shown but similar to the top trace of Figure 3-3). This effect can be used to advantage when trying to image flowing streams that are susceptible to bleaching.

In this setup the spot size in the microfluidic device is dependent on two factors, the magnification and the initial beam diameter. The magnification is given by the familiar M = f1/f2 where f1 is the distance from the optical centre of the microscope focusing objective to the image spot and f2 is the distance from the output of the Keplerian reshaper to the objective.

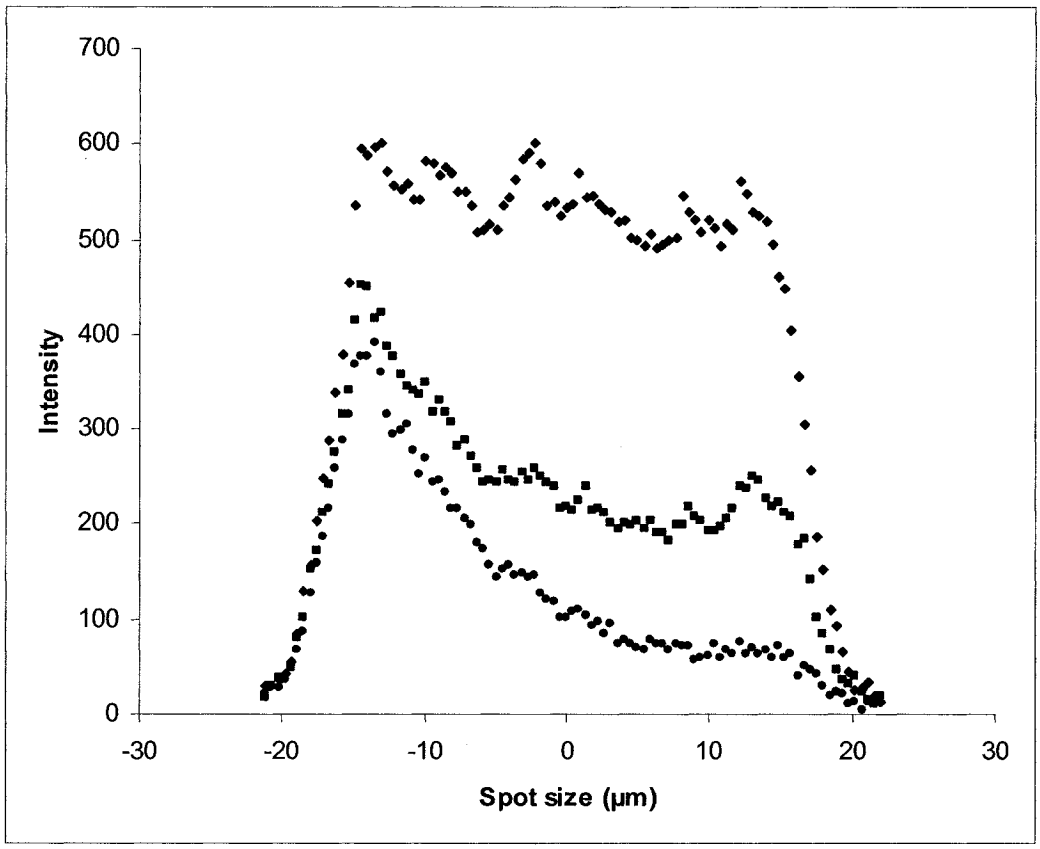

Figure 3-3: Flow related photo bleaching of fluorescein, plotted are the intensity profile of the laser spot images taken successively during continuous exposure to the laser light. Top data is first image; flow is from left to right. The fluorescence intensity is given in arbitrary units.

Given the diameter of the laser beam at the object plane which is measured at the exit of the reshaper, and the lens magnifications, the final spot size can be calculated. In the first setup we used a 40 times magnification, 0.50 NA infinity corrected focusing objective with a magnification of ≈ 1/240 times and a laser diameter of ≈ 8 mm which gave us a measured spot size of 30±2 μm and a 6.4 % RSD over the surface of the flat profile (Figure 3-4). This spot size ($1/e^2$ or 13.5 %) was measured in a chip with a channel width of 50 μm. To demonstrate that the flattop profile extends a significant distance away from the image plane a 20X, 0.45 NA infinity corrected focusing objective with a magnification of ≈ 1/120 X was used with the same input laser beam. At the focal point the image is expected to be 60 μm in diameter, we adjusted the position of the objective to approximately 40 μm "out of focus" and measured a spot size of 79±3 μm and a 6.2 % RSD over the surface of the flat profile (Figure 3-4). This spot size was measured in a chip with a channel width of 100 μm. We used the 20X objective because of the difficulty in precisely adjusting and measuring the position of the 40X objective. Figure 3-4 shows both the 30 and 79 μm intensity profiles, with the geometric centre of the intensity profile indicated by the tall cylinder while the large ring indicates the area over which the RSD was calculated. The area inside the large ring represents 90% of the total spot intensity

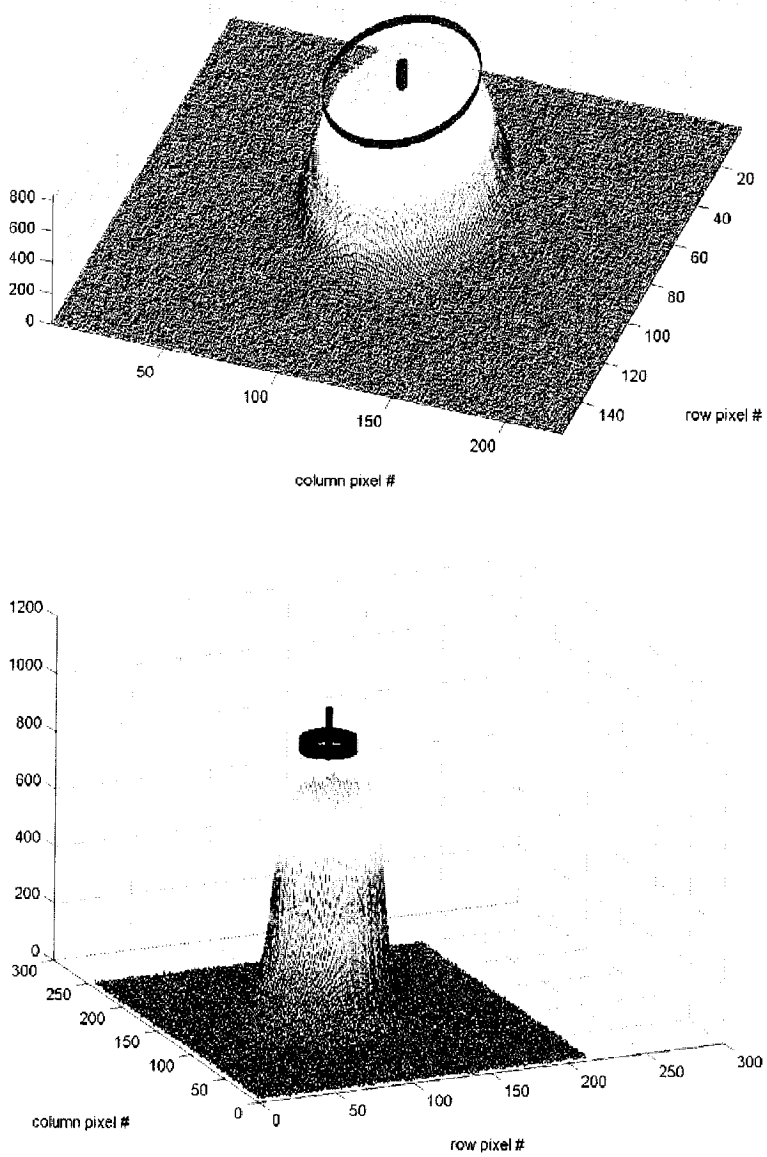

Figure 3-4: Intensity profile of a 30 (0.45 microns/pixel) and 79 μm (1.1 microns/pixel) flat top laser beam, the geometric centre of the intensity profile is indicated with the tall cylinder while the area over which the RSD was calculated is indicated by the large ring.

3.4.3. Microchip Operation

The complexes were focused into a narrow stream as they passed through the cross intersection of the chip, as shown in Figure 3-5. Focusing was established by either applying potentials or by applying vacuum to the outlet. The potentials were applied using an in-house built high-voltage power supply with four independent outputs, two of which were controlled using the 2 analog outputs from the PCI-1200 card.

For electrokinetic focusing, the side (focusing) reservoirs were set at 800 V (300V/cm), the inlet vial was set 690 V (100V/cm) and the outlet reservoir was set at -5400 V (700 V/cm). The experiments involving electrokinetic focusing were carried out in 10 mM phosphate buffer (pH 7.4). This buffer exchange was necessary due to excessive joule heating in the original buffer when using large electric fields. Alternatively, a vacuum applied to the waste reservoir, created with a water aspirator, was used to transport and focus the complexes. The vacuum induced flow from the side channels hydrodynamically focused the particles flowing from the sample reservoir into a narrow steam. In these experiments no buffer change was needed from the assay buffer, PBS with 4% BSA (w/v).

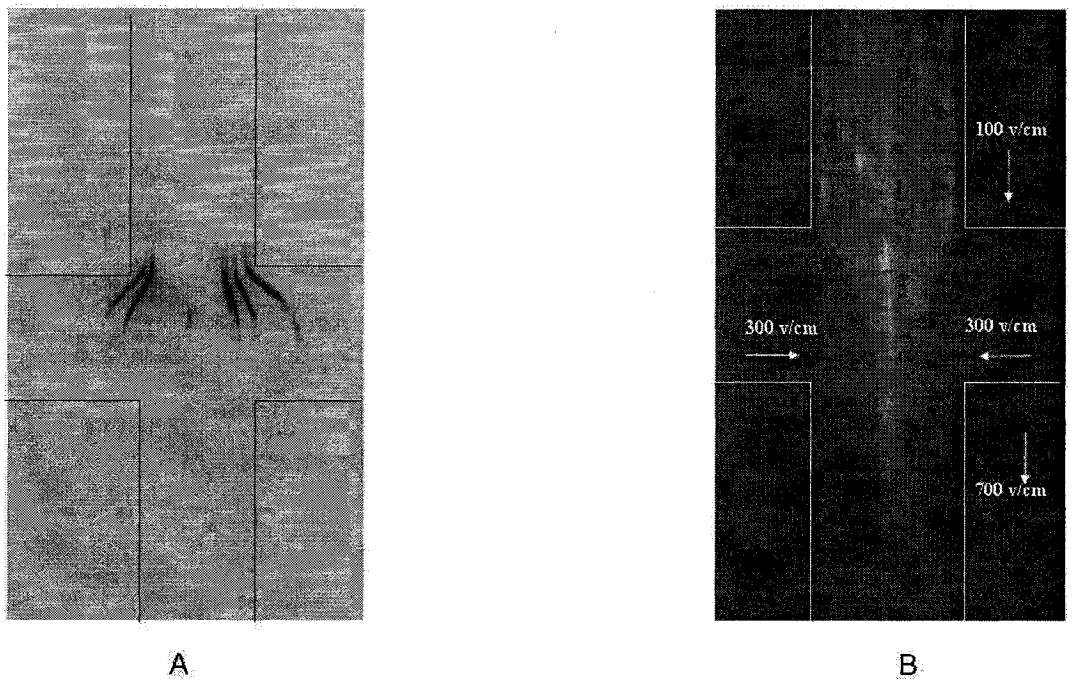

Figure 3-5: Focusing of 1μm fluorescent particles, a) without focusing voltage applied, picture is inverted for clarity and b) with focusing voltage. The exposure time was adjusted to allow the fluorescent particles to "streak" and indicates the flow path(s) in the microfluidic channel. Channel widths are 50 microns.

3.4.4. Detection of Microspheres

The concentration of the microspheres in the immunoassay sample had to be adjusted to a range in which the chance of detecting more than one microsphere event at a time was minimal. The probability that more than one microsphere is present in the detection region is dependent on the average event rate (arrival rate of microspheres) and the transit time through the detection zone[46]

$$P_{(2)} = \frac{(rt)^n e^{-(rt)}}{n!}$$ Equation 3-1

where $P_{(2)}$ represents the chance that two particles are present in the detection region (30 μm) at the same time, r is the average event rate (particles/sec), n was set at a value of two events and t is the transit time of a complex through the detection zone. At the chosen concentration of about 1 x 10^6 beads/mL typically used in this assay, the event rate was approximately 10 per second with a transit time of approximately 0.5 milliseconds. The probability of two simultaneous events at this rate is extremely low (1.2 x 10^{-5}) and only becomes significant at much higher particle concentrations.

The time the spheres spent in the detection zone was between 0.2 and 0.5 ms, requiring a collection rate of 60 ks/s per channel (data collection rate of 180 ks/s) to allow sufficient number of data point to be collected per particle (>12 points) for an accurate measurement of the intensity profile.

3.4.5. The Immunoassay

Initially, assays were carried out in 96 well microtiter plates and read on a fluorescence microtiter plate reader to verify blocking procedures and complex formation. Using a plate reader for analysis has several drawbacks, first of all, the fluorescent background of the capture beads and the PBS/BSA buffer solution raises the detection limits. Secondly, all the non-bound detection spheres had to be washed away to enable detection of the complexed ones. This was accomplished by washing the complexes three times with PBS buffer, containing 4 % BSA (w/v), for 5 minutes with constant agitation followed by magnetic separation. Thirdly, multiple analyte detection is not feasible using this type of detection because all complexes contribute simultaneously to the plate reader signal. Multiplexing becomes practical when the complexes are detected and classified individually based on size and colour combinations. Flow cytometry allowed us to address all these problems; however the final goal is to develop an integrated system where all steps are carried out sequentially. This is not easily accomplished on a flow cytometer therefore our focus has been to implement the assay on a microfluidic device. Figure 3-6 shows the calibration curve of tumour necrosis factor α (TNF-α) in a sample measured on the flow cytometer and on the microfluidic chip. Plotted is the percentage of all the complexed capture beads that flowed passed the detector. The detection limit of the assay is determined by the non-specific binding of detection beads to the capture beads, which leads to a non-zero blank. For this reason, prevention of non-specific binding is very important in this assay.

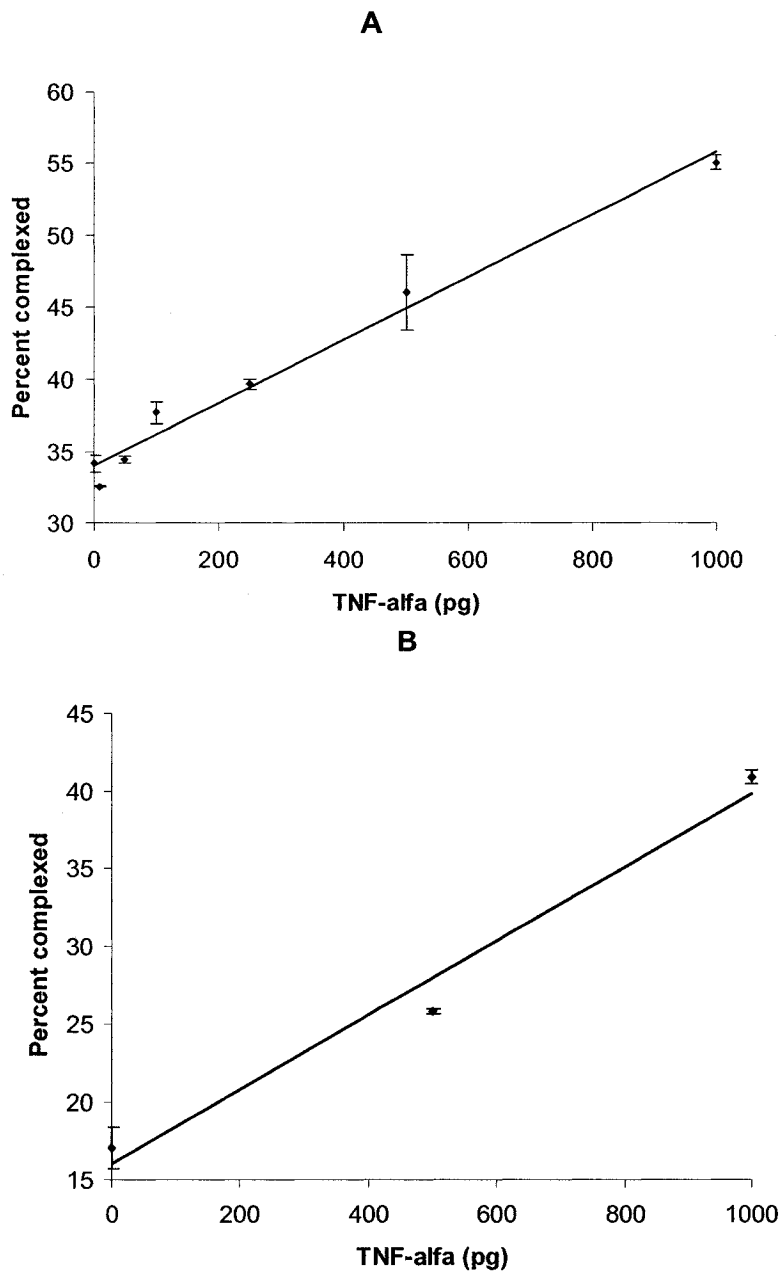

Figure 3-6: Calibration curve of TNF-α using a flow cytometer (A) and the confocal microscope and chip (B) for detection. In (A) seven concentration data points were measured in duplicate while in (B) three concentration data points were measured in duplicate.

It is clear from Figure 3-6 that the blank levels are higher using the flow cytometer for counting the duplexed spheres. This problem is mainly due to the fact that the flow cytometer used was not designed to measure the small particles and the associated fluorescence. This resulted in poor signals and difficulties in obtaining proper numbers from the collected data. The 4% BSA used for blocking is not completely effective in preventing these interactions. Improvements could be achieved with the use of additional blockers such as Triton X-100, however these additional surfactants can weaken the antibody-antigen link leading to loss of complexes. Sensitivity of the assay can be adjusted by changing the concentration of capture beads, lower concentrations can be detected using lower concentrations of capture spheres (data not shown). The reason for the increased sensitivity (slope of the calibration curve) is due to the ratio of capture beads to analyte molecules. When the number of capture beads decreases the chance that a capture bead will bind an analyte increases. Thus at low capture bead concentration a higher percentage of capture beads will bind analyte molecules, also a small increase in analyte concentration will result in a larger percentage of capture beads binding the analyte (compared to a higher concentration of capture beads). The concentration range targeted in the present assay is from 100 pg to 2 ng per mL, this is within the range of most *in vitro* applications. The next step is to show that this assay can also be performed as a multiplex assay where both analytes are measured simultaneously.

3.5 Conclusions

In conclusion, we have found that the two-bead assay has sensitivity comparable to a standard ELISA for the analytes we examined. Unlike an ELISA, this assay can be multiplexed, allowing multiple assays to be run simultaneously. The flat profile output from a Keplerian beam reshaper can be maintained when reduced to only 33 μm in size facilitating its use inside a 50 μm wide channel of a typical microfluidic device. The unique combination of the flat profile and the two-bead immunoassay permits a more accurate determination of complexes as they pass through the detection zone. To add even greater multiplex capability, replacement of the microspheres with fluorescent quantum dots (QD) would allow expansion of the possible colour and intensity combinations used for tagging the antibodies, resulting in thousands of different tags.[16,17,57]

To obtain the maximum performance from this assay, a specially designed microfluidic device where not only the detection, but also all the incubation steps are performed, would be ideal. Since on this chip all components will be in close proximity to each other the reaction time will be very short allowing for a complete assay in only minutes instead of hours as in a standard ELISA.[53]

3.6 Acknowledgements

We thank Dr. Hoffnagle, IBM Almaden Research Centre for the loan of the Keplerian beam reshaper. This was supported by the National Science and Engineering Research Counsel of Canada.

CHAPTER 4

A Fast Multiplexed Immunoassay

4.1 Abstract

We developed a multiplexed immunoassay using a two-bead system with paramagnetic capture beads as a solid support for binding of antigens and highly fluorescent detection beads for visualization of the presence of these antigens. Detection of the (capture bead)-antigen-(detection bead) complexes was performed in a microfluidic device using a confocal detector system. Two antigens relevant to immunological activation, IL-6 and TNF-α, were detected simultaneously using this system. The detection limits were dependent on the concentration of beads used in the reaction, and therefore the number of beads where chosen so that the calibration curve was in the physiological range of these peptides in amniotic fluid. A complete assay can be performed in as little as 15 minutes.

4.2 Introduction

The following chapter deals with the development of a multiplexed immunoassay in a microfluidic device. Unlike the previous chapter this chapter will perform a multiplex assay using the two beads for the detection of IL-6 and TNF-α simultaneously. In chapter 3 we were using scatter of the capture bead and fluorescence in the detection bead. Here we will use fluorescence for detection of both the capture and detection sphere.

4.2.1. Microspheres

Two antibody sandwich immunoassays as implemented in ELISA, are laborious and time consuming. Robotics can improve throughput however, the incubation steps needed for binding of antigen to antibody depend on their proximity to each other making the assay diffusion rate limited. In a microtiter plate well the antibodies are on the wall while the target is in the bulk solution. The incubation time is then dependent on the concentration of target and the size of the well. A significant decrease in incubation time can be achieved by bringing the antibodies out into free solution, reducing the diffusion distance and time. Using small particles as carriers of the antibodies, instead of the microtiter plate wall, effectively provides the advantage of having the antibodies free in solution while still being easily controlled. Since these particles are suspended in the solution, the time it takes for an antigen to find a complimentary antibody is greatly reduced. Additionally, the amount of antibody is no longer limited to the binding capacity of the titer plate wall and is easily adjusted by changing the number of beads introduced. The first attempts to use microspheres in combination with antibodies to capture antigens were made as early as 1977,[58] a patent was issued even before that in 1976 to Fulwler.[59] Since then many more assays have been described, primarily for the analysis of serum proteins[60-70] but other bead based assays have been reported for the detection of nucleic acids, drugs, enzymes, viruses and bacteria.[71,72]

Typically, most assays test only one indicator of disease, however to obtain a clear picture of a patients disease state not one but several indicators for disease must be determined. A class of these indicator molecules are cytokines, regulatory proteins that are secreted by cells of the immune system. The function of these peptides in the body is

very complex and several of the cytokines have overlapping functions. Besides cell to cell signalling as immunoregulators for hematopoiesis, inflammation, and wound healing, they also have a systemic effect resulting in fever, intravascular coagulation and shock. The production of several types of cytokines above the normal levels are indicative of a systemic immunological response. Therefore, analysis of a complete set of cytokines will be more valuable than the analysis of only a single cytokine.[73,74] Several methods for quantitating cytokine concentrations exist, such as; target cell function assay; B9 cell line depends on interleukin [IL]-6 for proliferation, enzyme linked immunosorbent assay (ELISA), antibody interactions for determining concentrations, and polymerase chain reaction (PCR), indirect determination of concentration.[75] Determining the concentration of cytokines by individual assays such as ELISA can be very time consuming and expensive and requires large volumes of sample.[75] To address this problem several multiplex single bead immunological assays have been in development in the last few years. Most prominent amongst these is the Luminex system with assay kits that include appropriate software.[76,77] These single bead assays are fast, due to the rapid association kinetics of the antibodies with the antigen, uses about 1000-5000 5.2 μm beads in the sample. With this size of beads there are enough antibodies on each sphere (1-2 $X10^6$) to have a high signal and a satisfactory calibration range.[78] A drawback to using relatively few beads with large diameters is the reduced surface area available for antibody attachment compared to that used in a microtiter plate. The analytical signal is obtained when the second antibody binds the antigen in a sandwich type assay. This second antibody is labelled with biotin allowing the binding of a fluorescently labelled streptavidin. Quantification of this fluorescence signal is performed in a flow cytometer

where the intensity of the signal per bead is measured. To enable multiplexing the set of beads, one for each type of analyte, they are impregnated with a unique ratio of red (658 nm emission) and infrared (712 nm emission) dyes that have no spectral overlap with the reporter dye. Each bead set has a unique distribution of fluorescent intensities that can be resolved by the Luminex instrument. The Luminex 100 is a flow cytometer equipped with two lasers, a 635 diode laser for exciting the red and infrared dyes and a 523 nm frequency doubled Nd-YAG laser to excite the orange reporter dye phycoerythrin (PE, 658 nm emission).[79] With the Luminex system, up to 100 different coloured beads are distinguishable, allowing multiplexing assays of 100 analytes and controls. When using a multiplex assay containing 100 beads, very large data sets are created. For example, when detecting an array of 100 sets of microspheres in a 96 well plate detecting 100 microspheres per population, 3 fluorescent signals per microspheres, a minimum of 2,880,000 signals need to be managed. The reduced number of detected events per analyte does not significantly affect the precision of these assays.

Multiplex assays for both human and mouse cytokines have been described to date measuring 15 different cytokines in each assay.[50,80] The accuracy and reproducibility of these assays are now comparable to the gold standard ELISA assay. The major drawback is the sensitivity that can be limiting for the bead based assays. As an example, the lower limit for IL-4 in the bead assay is about 40 pg/mL while the ELISA has a lower detection limit of about 0.8 pg/mL.

The Luminex bead system is a very versatile system that is capable of detecting many analytes simultaneously. However, the small number of fluorescent molecules used for detection per bead demands a very sensitive detection system, especially since

the bead passes the detector in less than a millisecond. The technical requirements for such a detection system are high, and are not easily made portable using inexpensive excitation and detection electronics/optics. Additionally, the detection limits of the system are good but not always sufficient for many biological applications. To address these shortcomings we developed a two bead assay for detecting analytes on a chip system. This system has the potential to detect lower concentrations of analytes since it uses beads for both the capture as well as for the reporting. With such a system, the requirements for the excitation and detection system are significantly relaxed and an inexpensive portable diode based system is technically possible.

Performing an assay on a microfluidic chip allows the development of a total analysis system, where not only the detection but also the mixing and incubation are carried out. Already, fast assays have been demonstrated using microfluidic devices.[81] Cheng *et al* showed that several immunoassays can be performed in just a minute when using a multichannel fluidic device.[53] The decrease in analysis time was, in part due to the close proximity of the antibody and antigen inside the channels, allowing for fast binding kinetics. In this last assay, the detection limit was approximately 600 pg/mL, which is much less sensitive than a standard ELISA and insufficient for many biological systems. In biological fluids many of the interesting regulatory peptides are present at concentrations well below the detection limit of this assay; therefore a more sensitive test is needed.

As described, our assay detects the presence of an antigen by the formation of a two bead complex, containing a large capture bead (2.8 μm) and a small detection bead (0.1-0.2 μm), each labelled with a separate fluorescent dye enabling differentiation.

Detection of the complexes is accomplished using a microfluidic device where the complexes were focused into the sensing region and detected using a confocal detection setup. Unlike the previous chapter where the assays where performed and measured separately, here the assay was performed and measured in the same sample. The multiplex assay was performed with IL-6 and TNF-α using two differently fluorescently dyed capture spheres and one fluorescein dyed detection spheres.

4.3 Materials and Methods

4.3.1. Instrumentation

The basic layout of the experimental setup is similar to what was described earlier, however some significant differences were introduced. Instead of detecting two fluorescence signals and one scatter signal, three fluorescence signals were detected (Figure 4-1) at a scan rate of 60 KHz per channel.

An argon ion laser with a 0.69 mm diameter 488 nm emission line (Model 2214-10SL, JDS Uniphase, CA) was expanded using a variable-magnification beam expander (Model 07 HBZ 001, Melles Griot, CA) to a spot size of about 8 mm. This increase is important since it reduces the beam waist to 21μm after focussing by the 20X, 0.45 NA infinity corrected focusing objective (Model 556015, Leica, CA).

A microfluidic device (Model PC-SC, Micralyne, Canada) with a simple T layout was used for all experiments.

4.3.2. Detection

In an epi-fluorescence confocal system the fluorescence signal is collected using the same set of optics as for excitation. To separate the fluorescence signal from the excitation beam, a 515 DFLP dichroic filter (Omega Optical, VT) is used. This also has the advantage of reducing the scatter and reflection signals to 5% while passing more than 95% of fluorescence signal, improving the signal to background ratio. A field lens with a focal length of 19.5 cm focused the fluorescence light onto a 100 μm pinhole for spatial discrimination of scatter signal from the channel walls in the microfluidic device. Wavelength selection by the detector is accomplished using a series of dichroic and bandpass filters in the configuration as shown in Figure 4-1. The dichroic filters are arranged to pass progressively longer wavelengths while reflecting shorter wavelengths into bandpass/PMT detectors. Thus PMT 1 senses 535 nm, PMT 2 senses 570 nm and PMT 3 senses 670 nm.

Signals from the PMT's were digitized with a 12 bit data acquisition board with a maximum collection rate of 200 ks/s (PCI-6023E National Instruments, TX). Since the time that the spheres spent in the detection zone was about 0.5 ms, a collection rate of 60 ks/s per channel was needed to be able to collect a sufficient number of points per peak for accurate integration (>12 points per peak).

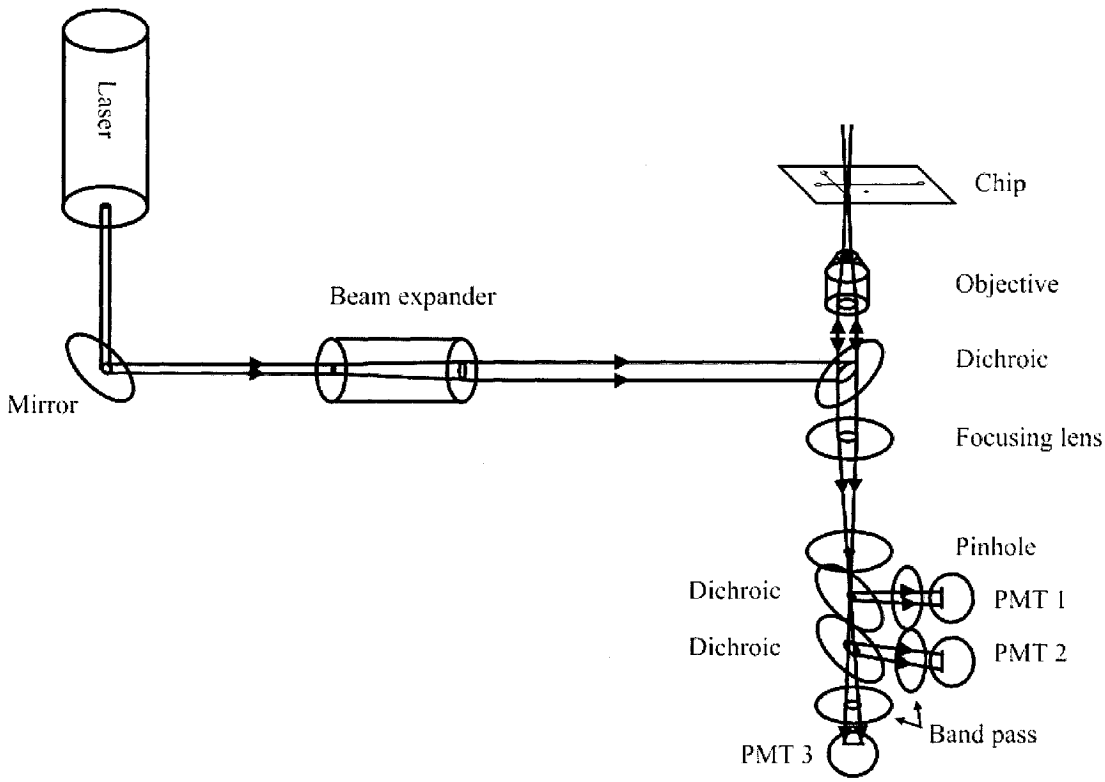

Figure 4-1: Schematic representation of the optical path used in the confocal detection system. First, if fluorescence light is emitted by a particle it will reach a dichroic mirror (565 ALP) set at 45° to the incident beam reflecting shorter wavelengths in the direction of the first PMT. In front of this first PMT a bandpass filter (535 DF 30) is placed to reduce interference from other wavelengths. The light transmitted (long wavelengths) through the 565 ALP dichroic mirror is discriminated by a second dichroic (600 FLP) also set at 45° to the incident beam. Light with wavelengths shorter than 600 nm are reflected towards the second PMT, where a band pass filter 570 DF 55 eliminates interfering wavelengths. The light transmitted by the 600 ALP dichroic mirror is discriminated by a 670DF 15 bandpass filter, and collected with a third PMT.

*4.3.3. **Data Analysis***

An Igor Pro Macro (ThreeChannelNieuwVers2.4, Appendix A) was written for detecting and extracting the microsphere signals out of the raw data. The signal from a microsphere is a relatively rare event in an essentially empty background signal (Figure 4-2). To process the data, it is more efficient to compress the data into a table of peak intensities. Peaks are detected by evaluating the signal magnitude compared to the baseline signal (and its noise) and the peak magnitudes are tabulated and processed as standard flow cytometric data. The details of the processing are: First the standard deviation (SD) of the complete string of data was calculated to determine the approximate baseline and magnitude of the baseline noise. Of course the determined SD is larger than the SD of just the baseline signal, but since only a very small fraction of the raw data contains peaks it is a good first approximation (Figure 4-2). Then, in a second pass through the data to isolate just the baseline, data points that were three SD above the average were culled from this data set as being potential peaks. A second SD was calculated on the remaining data to determine the "real" variation in the baseline. Finally, all of the peaks were detected in the original data when a signal was more than three times this "real baseline" SD. A table containing the magnitudes of the three (two capture bead, and one detection bead) data channels with all the peak maxima was compiled by the program and stored. In this assay two types of capture beads were used so the presence of signal in either of the two capture bead channels determined if an entry was made.

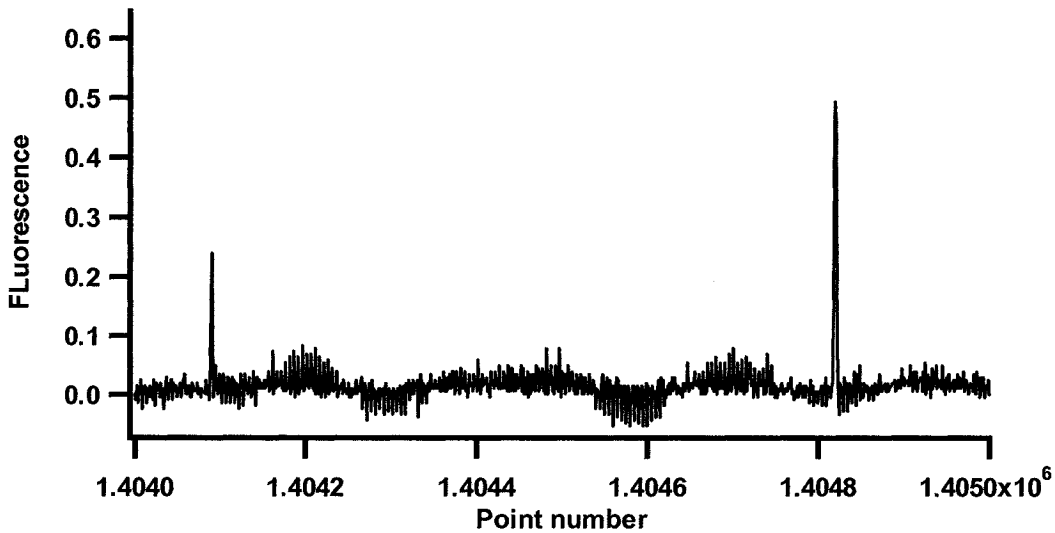

Figure 4-2 : Raw data of IL-6 capture beads. Shown are one thousand data point (about 16 ms) with two peaks indicating capture beads.

This table, in ASCII format, was converted into the standard flow cytometer data format (FCS) using the program A2FCS (ASCII to FCS) (Joseph Trotter, Scripps Research Institute) and analyzed with WinMDI flow cytometer software (Joseph Trotter, Scripps Research Institute). Data visualization and analysis were performed using standard cytometer methods. First, in a dot plot of blank signal vs. capture spheres fluorescence, a blank region was set by gating the signal region occupied by the blank. Second, the same gate was applied to a dot plot profile of a sample. Points outside the gated area are considered to be complexed (Figure 4-3).

4.3.4. Reagents

Stock solutions of PBS (phosphate buffered saline, 0.88 g NaCl in 0.01 M sodium phosphate pH7.4) with 4% (w/v) BSA (Bovine Serum Albumin) were prepared by diluting a 10% (w/v) BSA PBS (Pierce, WI) solution with PBS. The 0.2 μm NeutrAvidin-labelled yellow-green FluoSpheres (F-8774, excitation/emission: 505/515 nm, Molecular Probes,OR) and the 0.1 μm NeutrAvidin-labelled red TransFluoSpheres (T-8861, excitation/emission: 488/605 nm, Molecular Probes,OR) were diluted in PBS 4% BSA (w/v) before use. Dynabeads, tosylated superparamagnetic polystyrene beads (2.8 μm diameter) with a polyurethane coating layer (Dynal, Norway) were used as capture beads. Diamino terminated Poly(ethylene oxide) (3000 M_W), (Polymer Source Inc, QC) was dissolved in 50 mM Borate pH 9.5. This polymer was used for covering of the bead surface and as a site for labeling with a fluorescent probe.

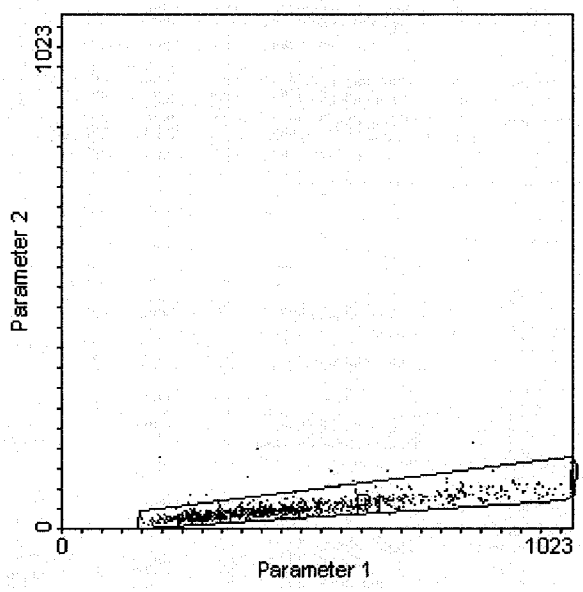

WinMDI Version 2.8 - Windows 3.95/DOS 5.0
File: A2 Sample: 0 pg/ml
Date: 12/18/04 Parameters: 3
Total Events 960
System: Log Parameter Means: Geometric
Fluorescence (1) vs Fluorescence (2)

Region	Events	%Total	%Gated
R0	960		100.00
R1	941		98.02

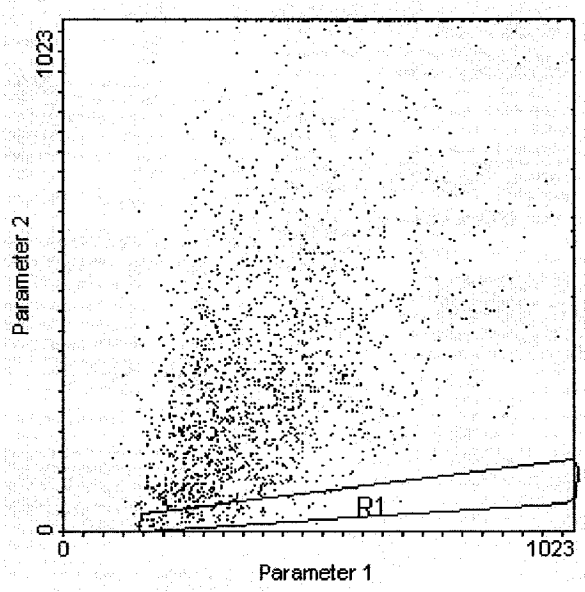

WinMDI Version 2.8 - Windows 3.95/DOS 5.0
File: H2 Sample: 1000 pg/ml
Date: 12/18/04 Parameters: 3
Total Events 2905
System: Log Parameter Means: Geometric
Fluorescence (1) vs Fluorescence (2)

Region	Events	%Total	%Gated
R0	2905		100.00
R1	123		4.23

Figure 4-3: Dotplots of 0 and 1000 pg/mL IL-6. Indicated is the gated area R1 which is used for the calculation of the percentage change in unbound beads.

Bodipy TMR-X, succinimidyl ester or Alexa Fluor® 594 carboxylic acid, succinimidyl ester (Molecular Probes, OR) was used to label the capture beads. A stock solution was prepared by dissolving 0.5 mg in 100 µl NN-dimethylformamide (Sigma-Aldrich, MO).

4.3.5. DAPEO Labeling

Diamino terminated Poly(ethylene oxide) (DAPEO) was reacted at a concentration of 3.1 mM with 2.1 mM of 5-carboxyfluorescein, succinimidyl ester (5-FAM, SE). Verification of labeling of the DAPEO was accomplished using a Beckman CE system. Separation of the labelled DAPEO and unreacted dye was performed on a bare fuse capillary (68 cm) at 440 V/cm in a 50mM borate buffer (pH 9.5) for 10 minutes.

4.3.6. Capture Bead Preparation

The Dynabeads were vortexed for approximately 1 minute. The required amount of beads (at a concentration of 2 x 10^9 beads/mL) were directly pipetted into separate 0.5 mL conical centrifuge tubes and placed near a rare-earth magnet (Catalog #99k32.13, Lee Valley Tools, Canada) for 1 min to pull the beads to the wall. All the liquid was removed using a pipette and the beads were resuspended in ample volume of 50 mM Borate (pH 9.5). After mixing for 2 minutes the washing process was repeated. After the second wash the beads were resuspended in their original volume and an equal volume of antibodies at a concentration of 1 mg/mL was added (approximately 5 µg antibody/10^7

beads). The mixture was incubated overnight at room temperature (19°C) while slowly rotating to prevent settling of the beads. After incubation the beads were washed twice in PBS (pH 7.4) with 0.1% BSA (w/v) and once with 5mg/mL Diamino terminated Poly(ethylene oxide) in 50 mM Borate (pH 9.5). Again the mixture was incubated overnight at room temperature to block all the non-reacted Tosyl sites with the polymer. After this last incubation, the beads were washed twice in 50 mM Borate (pH 9.5) and reacted with for 1 hour with the fluorescent dye 1.6 mM of Bodipy TMR-X, succinimidyl ester., or Alexa Fluor® 594 carboxylic acid, succinimidyl ester. After this last incubation, the beads were washed twice in PBS (pH 7.4) with 4% BSA (w/v) and stored at 4° C until used.

4.3.7. Detection Bead Preparation

The FluoSpheres and the TransFluoSpheres were covered with the appropriated antibody by incubation of $1x10^{11}$ beads/mL of either bead with 100 μg/mL biotin-labelled antibodies. The final volume was dependent on the need but typically between 50 and 100μL. After one hour incubation at room temperature the beads were spun down for 10 min at 14000 rpm. The supernatant was subsequently removed and the beads were resuspended in the same volume.

4.3.8. Two Bead Assay

The assays were performed in flat bottom 96 well plates (model 3591, Costar, NY) that were blocked overnight with PBS (pH 7.4) with 4% BSA (w/v). Into each well,

50 μL containing 10^6 capture beads and 50 μL of the appropriate concentration of antigen, both in PBS (pH 7.4) with 4% BSA (w/v), were added. After 5 minutes of incubation, on a slow mixing vortex, the beads were pulled to the bottom of the plate using a magnetic separator plate. This plate contained 24 0.5 rare-earth magnets, one per four wells (#99k31.03, LeeValley Tools, Canada). After removal of the liquid, the beads were washed twice with washing solution (PBS (pH 7.4) with 4% BSA (w/v)). After removal of the washing solution, the 96 well plate was removed from the magnetic separator and 100 μL containing 10^8 beads in PBS (pH 7.4) with 4% BSA (w/v) detection beads were added. Again, five minute incubation was used to allow for the formation of the complexes. Finally, two washing steps were performed to remove excess detection spheres.

4.4 Results and Discussion

4.4.1. Labelling of Capture Beads with Fluorescent Molecules

Reaction of a succinimidyl ester with a primary amine group is an often used reaction mechanism to attach dye molecules to proteins. The number of available primary amines for the succinimidyl ester to react to is limited on an antibody and might render the antibody inactive due to attachment at the active site. We therefore developed a method to attach the dye to the surface of the bead using a linker. Both the dye and the surface of the beads are amine reactive, the linker therefore needed to have two primary amine groups separated by a hydrophilic spacer to minimize non-specific binding.

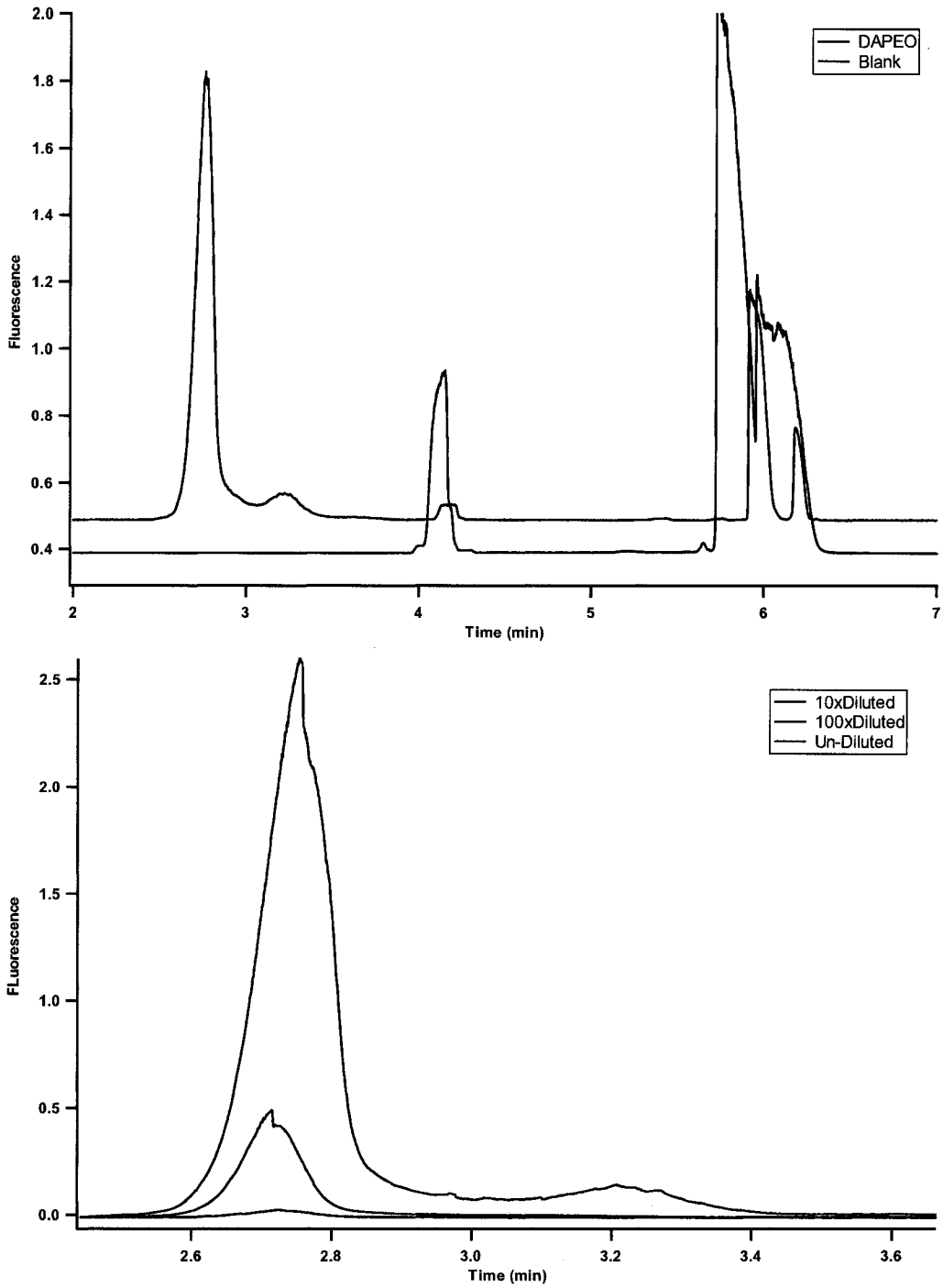

Figure 4-4: CE profiles of Diamino terminated Poly(ethylene oxide) labelled with 5-carboxyfluorescein, succinimidyl ester. Top figure shows blank and DAPEO electropherograms while the bottom figure shows the effect of dilution of the reactive dye on the labelling efficiency.

DAPEO allows for attachment at one end to the bead surface by reacting with the tosyl group while at the opposite site it can react with the succinimidyl ester of the dye. To assure reactivity of the succinimidyl ester with the amine groups from the DAPEO we first reacted 5-carboxyfluorescein, succinimidyl ester (5-FAM, SE). The mixture was run on a Beckman CE system to verify labelling of the PEO. As can be seen from Figure 4-4 the DAPEO shows two peaks, one with a single label and one doubly labelled. By reducing the concentration of dye used for labelling by 10 and 100 times, the size of the single and double labelled DAPEO peaks diminish indicating that fewer DAPEO molecules are labelled. These results indicate that it is possible to label both amine groups on the DAPEO. It is important that both amine groups can be used since one amine group has to attach to the capture bead while the other amine group has to be labelled with a dye.

The next step was to first attach the DAPEO to the capture-beads followed by the labelling step. As a control we used capture beads that were not reacted with DAPEO. Both control and DAPEO covered beads were reacted with 5-FAM, SE. After washing away the unreacted and hydrolysed dye, both control and PEO beads were run on the chip system. The control beads did not have any fluorescence signal associated with them while the DAPEO labelled beads gave very strong signals.

To validate that the labeling did not interfere with the antibody activity an assay using DAPEO labelled and TNF-α antibody coated beads demonstrated that the antibody was still capable of binding to its antigen.

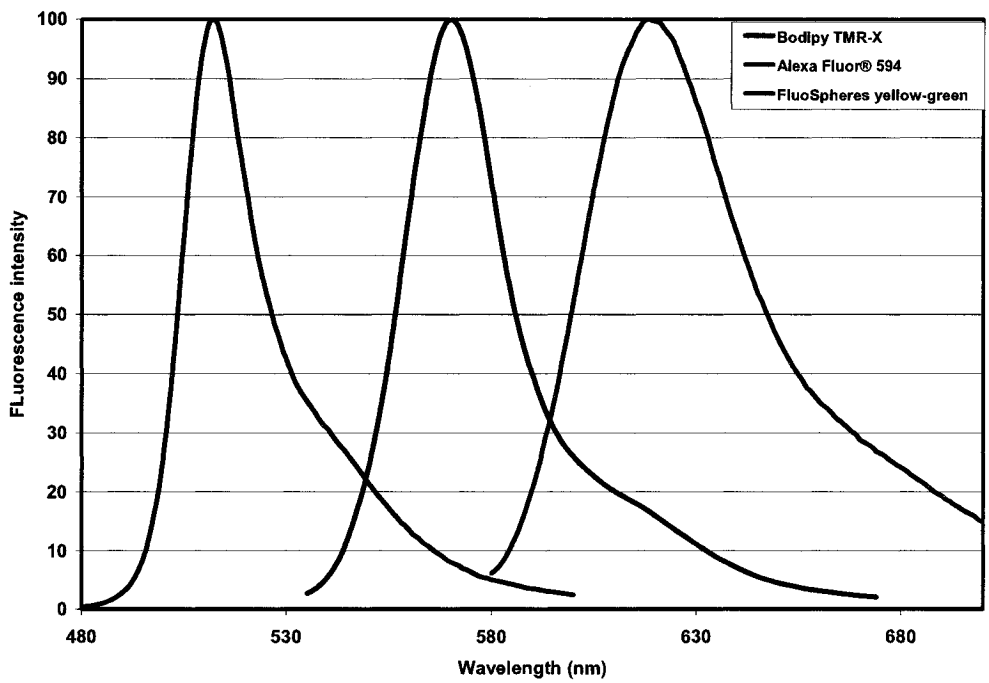

Figure 4-5: Normalized fluorescence emission spectra of the capture- and detection-beads. Bodipy and Alexa dyes were used to externally label the capture beads while the detection beads were internally labelled. Adapted from Molecular Probes web page (www.probes.com).

The percentage binding was equivalent to that observed previously with non-labelled capture beads. An added advantage was the reduction in non-specific binding of the detection to the capture-beads. This reduction was most likely due to the hydrophilic PEO polymer covering the hydrophobic surface of the capture-beads, reducing unwanted bead-bead interactions.

Two types of capture beads were made by external labelling; one with a maximum emission wavelength of 570 nm using Bodipy TMR-X SE, and one with a maximum emission wavelength of 618 nm using Alexa Fluor 594 SE. The detection bead was internally labelled and had an emission wavelength of 515 nm (Figure 4-5). The intensities of the capture beads were tuned in such a way that crosstalk between the two detection channels due to spectral overlap could not result in misinterpretation of the type of detection bead. This tuning was accomplished by reducing the number of labels per bead. Since the Bodipy TMR-X dye is more efficiently excited by the 488 nm line of the Argon ion laser than the Alexa Fluor dye, the number of molecules per bead of Bodipy needed to be much lower. To accomplish this Bodipy TMR-X SE was used at a 10 fold lower concentration than that of Alexa Fluor 594 SE.

4.4.2. Multiplex Assay

Before performing a multiplex assay, we first ran the assays separately to verify that the assays worked and it allowed us to compare the multiplexed assay results with the individually run assays. Three assays were performed, IL-6 and TNF-α in separate samples and one assay with both antigens in the same sample. From these three assays

four calibration curves were constructed. The IL-6 capture beads were labelled with Bodipy TMR-X SE while the TNF-α capture beads were labelled using Alexa Fluor 594 SE. Figure 4-6 shows the calibration curve of an assay using IL-6 (A) and TNF-α (B) run individually. The slope of the calibration curve is dependent on the number of capture beads present. Lower detection limits can be achieved by reducing the concentrations of capture beads, but this also decreases the dynamic range of the assay. Non-specific binding for TNF-α capture beads seems higher than for IL-6 capture beads (about 2.5 times). This might be partly due to the fewer number of TNF-α capture beads (loss of beads during preparation) and to the higher number of poorly excited Alexa Fluor 594 dye molecules on the surface. Additionally, these dye molecules are hydrophobic and increase the likelihood for non-specific 'sticking' of detection beads. Following these assays, the experimental procedure was modified to include blocking with BSA and the use of DAPEO on the detection beads. These blocking strategies have solved much of the non-specific binding by reducing it to about 2% of the total beads. The multiplexing assay was performed with the same colour combination of capture beads as used for the individual calibration curves. Figure 4-7 shows the calibration curves of IL-6 and TNF-α obtained with the multiplex assay. The time to perform the assay was approximately 15 min, about 10 minutes for the incubation steps and 5 minutes of washing. A time course was performed to optimize the incubation time and with this particular assay, longer incubation times did not result in a significantly better signal, shorter than 5 minutes of incubation however did reduce the signal significantly. The shape of the curves are different from the ones seen in a typical ELISA assays. The reason for this is most likely due to multiple antigens and consequently detection beads

binding to a single capture bead at the higher concentrations. These multiple bindings reduce the slope of the line since a complex is counted as a single antigen, even if there are multiple detection microspheres. As a result the shape of the calibration curve levels off gradually at higher antigen concentrations. Detection limits for the combined assay are very low, 8 and 14 pg/mL for TNF-α and IL-6 respectively. The detection limits for the TNF-α and IL-6 in the separate assay are 12 and 41pg/mL. The higher detection limits for IL-6 are mainly due to higher capture bead concentration. As mentioned in Chapter 2, the slope of the line and thus the sensitivity is dependent on the concentration of beads used. When more capture beads are used, the slope of the line decreases and the DL is increased although there is an increase in dynamic range. The opposite is also true when fewer capture beads are used and the sensitivity of the assay increases. The concentration at witch TNF-α and IL-6 are present in blood is about 11 pg/mL and 4.6 pg/mL respectively.[82] These concentrations are equivalent or slightly lower than that measured with our assay. To implement our assay in the clinical setting would require lower concentration detection limits that can easily be obtained by decreasing the concentration of capture beads.

From the results presented here we can say that the assay performs reasonably well, and provides detection limits comparable to an ELISA. However there is definitely room for improvement which is not surprising since commercial assays need many years of development carried out by a team of researchers.

Manual manipulation of the beads as currently done in the assay, is one area in need of major improvements. These manipulations are mostly responsible for the large SD and variations in the calibration curve. When the beads are washed the chance of

losing a portion of the beads is relatively large. This loss is not important after the antigens are bound since we actually count them. If the losses occur before analytes are bound to them the concentration per bead changes and variation between measurements will occur. Elimination of this problem can be achieved using a robot for the pipetting steps. When the robot is used in combination with a magnetic plate, that pulls the beads to the side of the well, instead of the bottom as currently done, even better results will be obtained.

One of the major problems with all assays, especially multiplexing assays, is the false-positive or –negative results due to erophilic antibodies, human anti-animal antibodies, rheumatoid factors (RF), soluble receptors for the analyte, etc., similar to those encountered in human serum or plasma samples in two-site assays such as ELISA.[83-87] These factors can create these false signals by preventing the binding of the analyte to the antibody, as with soluble receptors or by non-specific binding, as with RF factors.

Activity of the antibodies is dependent on their treatment during attachment to the beads and surface characteristics of these beads. Only 1 in every 250 analyte molecules forms a complex with the capture beads as we have observed in our assays. As mentioned before the inactivation of the antibody can be due to several factors. First of all the long incubation steps at elevated temperatures we used for attaching the antibody to the bead surface. Also the reaction of the tosyl groups and succinimidyl ester with primary amines can inactivate the antibody. The orientation of the antibody on the surface can add to the list of possible reasons for low binding efficiency of the antibodies.

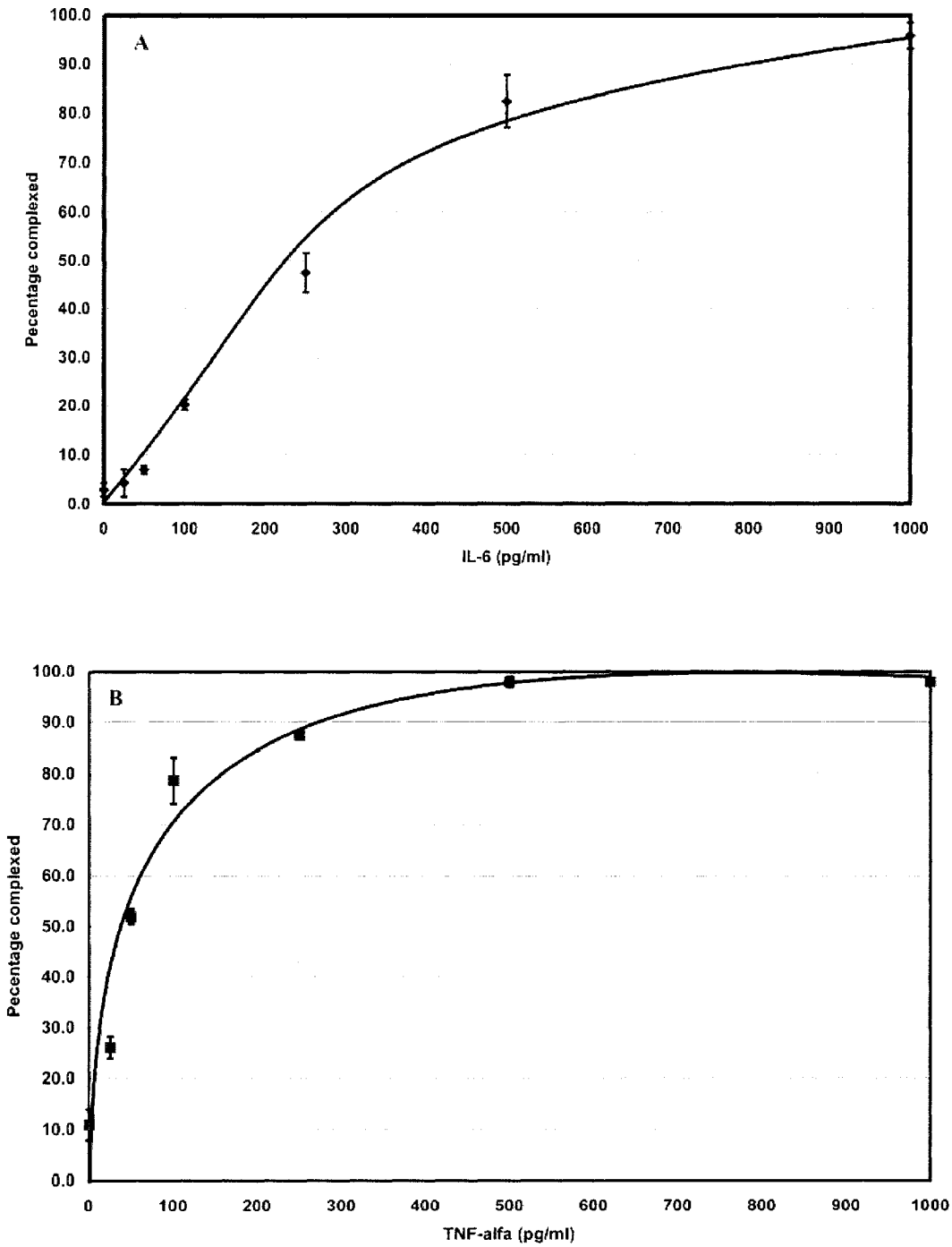

Figure 4-6: Calibration curve for IL-6 (A) and TNF-α (B) using respectively yellow and red fluorescent capture beads and green detection beads for both antigens. The complexed percentages are measured against the total number of beads available for that analyte

Better attachment schemes for connecting the antibody to the bead surface might improve this significantly. One such system could use beads with a PEG layer between the surface and the antibody, preventing the denaturation of the antibody upon contact with the surface. One other reason for low binding efficiencies can be the disruption of the two bead complex due to Brownian motion. These forces can rip apart the complexes and in this way reduce the "apparent" affinity of the antibodies. The volumes that have been analyzed using the microfluidic device are extremely small. Per sample only ~180 nL is analyzed, while 50 μL of sample was prepared. In principle only 3 X 180 nL (triplicate measurement) is needed to perform an assay on a patient. These kinds of volumes can easily be obtained using a finger prick replacing the more invasive blood sampling method. But it is not easy to manually handle these volumes, therefore you need to utilize a nano-volume fluid handling system, thus a microfluidic device for the full assay. An added advantage is that the time scale at which components are moved in a microfluidic device is perfect for a two bead immuno assay. On the other hand, ELISA and also the Luminex system need more sample and time to perform the assay, and are not as amendable to a microfluidic device.

The goal is now to combine all steps on a microfluidic device, where not only the detection takes place, but all incubation and washing steps are performed. However, microfluidic devices are still relatively expensive and are not without difficulties, but appearance of commercial fluidic devices on the market indicates that this field is maturing.

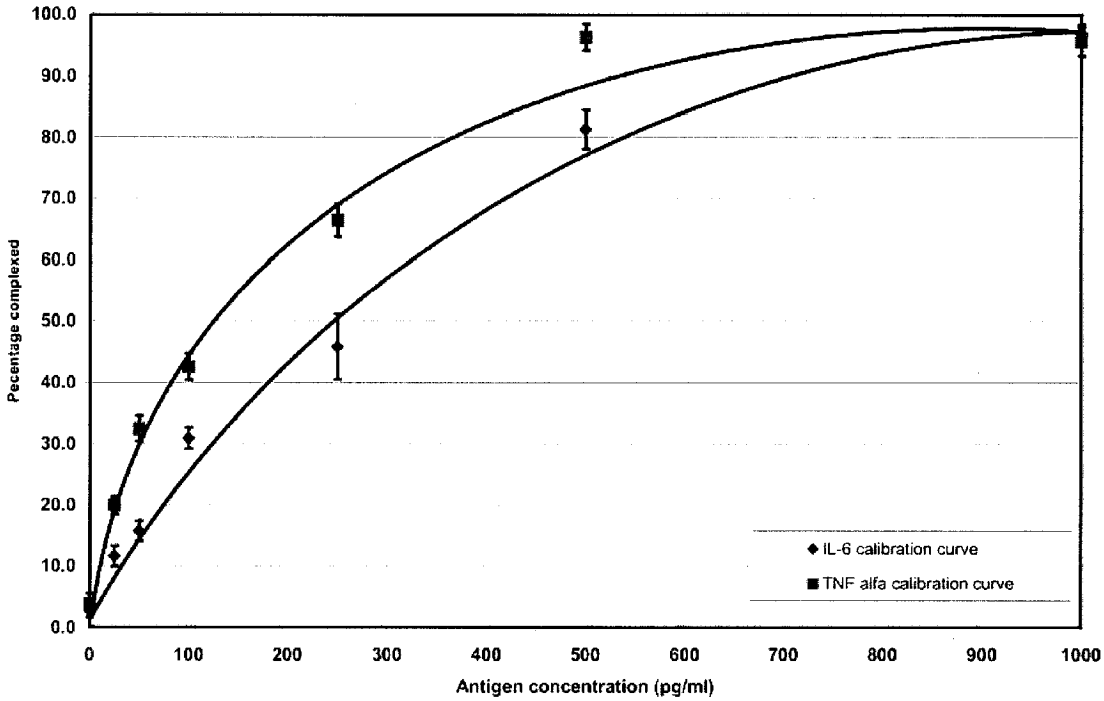

Figure 4-7:Multiplexed calibration curve of IL-6 and TNF-α using yellow and red fluorescent capture beads respectively and green detection beads for both antigens. The complexed percentages are measured against the total number of beads available for that analyte

4.5 Concluding Remarks

We have described a method for the simultaneous detection of TNF-α and IL-6 that is fast and sensitive. The use of a chip with this method not only allows for small volumes to be used but has the potential to be used for all the steps necessary in this assay: the integration of all manual handling steps on a chip is set out by the uTAS (micro-Total Analytical Systems) to reduce analysis time. This particular assay would be very suitable to be setup as a total analysis system on a chip since it requires only 2 steps. The first step is the mixing of all the components and a short incubation step, the second step would be the detection of the formed complexes.

CHAPTER 5

Conclusions and Future Work

5.1 General Conclusions

Improving the speed and throughput of immunoassays can have a significant effect in diagnostic procedures. Typically a sample is taken from the patient and sent for analysis, after a few days the result is sent back to the doctor. In recent years, faster direct analysis tests have been put on the market. A classic example is of course the pregnancy test that can, with very high accuracy, tell the person if she is pregnant in only a few minutes. The two-bead immunoassay system that we developed, just as the pregnancy test, might be performed in the doctor's office but will be able to screen several key diagnostic markers at one time. This in-office screening enhances the diagnostic capacity while cutting time and cost compared to traditional assays.

Chip based total analysis systems are slowly starting to appear as commercial products, replacing laborious analytical methods with much faster analysis. In our view, it will not be too long before these products will be able to perform several types of diagnostics in a very short time with minimal manual handling.

5.1.1. Flat Beam Profile

The use of a flat beam profile might be interesting to manufactures of instrumentation that use laser beam expansion to achieve uniform illumination. The flow cytometer is a good example of an instrument that could benefit from the use of a Keplerian beam reshaper. As shown in Chapter Three, the reshaper can be used efficiently to form a very small, uniform intensity profile (50 μm) out of a Gaussian

intensity profile with the use of simple optics. In the experimental setup described in Chapter Three, it was possible to reduce the variation in fluorescence signals from labelled beads. The reshaper does require a lot of tinkering to establish the proper profile. In our opinion, the reshaper would be best used as an attachment directly to the laser head, reducing the instrumental setup problems. As part of an instrument, such as a flow cytometer, it should be relatively straight forward to integrate it with the existing optical path.

5.1.2. Multiplex Assay

Detecting many antigens simultaneously is highly desirable since it can create a better picture of a particular disease state, conserve precious sample, and save money. In Chapter Four we demonstrated a multiplex assay capable of measuring multiple antigens using the two bead immunoassay in less than 15 minutes, with sensitivity equal or better than that of a standard ELISA (low pg/mL). The fast reaction kinetics of this assay were possible due to the use of free floating small particles, creating short diffusion distances between the antigen and antibody. Low detection limits were facilitated by using a second smaller detection bead loaded with fluorescent dye rather than a fluorescently labelled secondary antibody. The large signal from this small detection bead allowed individual antibody-antigen interactions to be visualized and is effectively a method of molecular counting. The use of a microfluidic chip for detection of the complexes eliminated the need for a more complicated cytometry sheath flow cell system.

5.2 Future Work

The two bead assay as we see it can play an important role when small volumes and fast analysis times are needed. Some samples that come to mind are rat or mouse samples or samples from neurological studies, but also when taking a larger amount of blood is not desirable as in the case of pre-mature babies. The type of analytes that can be measured as a multiplex assay are plentiful, some examples are the measurement of cytokines, growth factors, bacteria, sero typing of bacteria, viruses, drugs of abuse, etc..

Before this assay is an entirely chip-based system, several issues have to be addressed. First, a range of capture bead colours have to be created. The best approach would be the use of Quantum Dots encapsulated in polystyrene beads.[17] Of course it is possible to use a similar system used by Luminex were the ratio of two dyes allows identification of the bead,[79] however this would limit the number of different capture beads to about one hundred. Data collection has to be tailored towards the measurement of multiple fast events. Here a lock-in amplifier detection system would allow the determination and recording of only the peak events. This strategy will greatly reduce the amount of data, and allow much faster data processing.

Requirements for the bead detection system are not as stringent as that of the Luminex system. This may allow the use of ultra bright diodes for excitation of these beads replacing the large gas laser. Using diodes will not only reduce the cost of such a system (Ultra bright diode $15.00) but will make it more portable. Transportability is

key to practical implementation of this technology as a biological weapons detector, a detector for food quality and for use in hospitals and doctor's offices.

The ability to produce a network of channels in a microfluidic chip also offers the possibility to integrate the complete immunoassay by performing all incubations and separation steps on-chip. The microfluidic chip must be designed such that it allows for a predetermined incubation time of the antigen with the capture spheres followed by a controlled incubation with the detection beads. The time needed for this must be first determined before the final chip can be designed. Initially a chip with different length mixing channels should be designed to determine the optimal time to allow binding. The time needed is dependent on: concentration, diffusion distances and the affinity of the antibodies used. Therefore an adequate time is needed to allow most antibodies to bind satisfactorily to its target antigen. Once this incubation requirement is established a final chip can be designed that preferably not just runs one sample but rather a set of samples including the standards.

Making chips out of plastic such as PDMA (poly(N,N-dimethylacrylamide)) would make these devices inexpensive, costing not more than a couple of cents per device unlike its expensive glass counterpart that cost tens to hundreds of dollars (dependent on size and layout). Making a chip out of glass requires the use of expensive lithography techniques, while with PDMA, (once a design is established) a template (out of glass) can be made for easy casting of the chips.

Magnets can be used to trap the paramagnetic capture beads to allow removal of sample matrix and excess detection beads along with washings. These washing steps might be useful for lowering the background signal and thus improving the signal to

noise ratio. Electromagnetic based magnets can be used to facilitating automation of the procedure although rare earth magnets are much stronger.

An alternative method to trap the beads is by using a weir, allowing binding of antigens and removal of the matrix.[88,89] Detection beads are small enough to pass over the weir while the capture beads and complexes stay behind assisting the washing of excess detection beads. One pitfall of this method would be the formation of a packed bed before the weir. When a sample enters this bed the first beads will soak up all antigens from the solution while beads downstream will bind none since the sample will be depleted. The two-bead immunoassay does not look at how many antigens are bound on the surface of a capture bead, but rather looks at what percentage of the capture beads have at least one antigen attached to its surface. Thus having a few beads with many antigens and many beads with no antigens on the surface will distort the counting statistics making it impossible perform an accurate measurement.

In our chip, an electric field or vacuum was used to mobilize the different components, however other methods might be considered. The Gyroslab™ from Gyros AB is a microfluidic device that uses centrifugal forces to move liquid around. By making use of different surface characteristics it is possible to prevent liquids from flowing unless a larger centrifugal force is applied. In this way mixing and incubation steps can be regulated.

It is obvious that the technology described here is still in its infancy and still needs a significant amount of work before it can be used in a clinical setting. However, it is also clear that this technology is going to be very useful, as an inexpensive diagnostic

tool for quick screening of multiple indicators in a variety of settings (doctor's office, air quality screening, food quality inspection, etc.).

References List

1. R. S. Yalow and S. A. Berson, "Assay of plasma insulin in human subjects by immunological methods," *Nature* 184 (Suppl 21), 1648-9 (1959).

2. R. P. Ekins, "The estimation of thyroxine in human plasma by an electrophoretic technique," *Clinica chimica acta* **5**, 453-9 (1960).

3. C. P. Price and D. J. Newman, *Principles and Practice of Immunoassay*, (Macmillan Reference ltd., London, 1997).

4. A. K. Abbas, A. H. Lichman, and J. S. Pober, *Cellular and Molecular Immunology*, (W.B.Saunders company, 2003).

5. E. P. Diamandis and T. K. Christopoulos, "Immunoassay Configurations," *Immunoassay,* E. P. Diamandis and T. K. Christopoulos, eds., (Academic Press Limited, San Diego, 1996), 227-236.

6. L. J. Kricka, "Simultaneous Multianalyte Immunoassays," *Immunoassay,* E. P. Diamandis and T. K. Christopoulos, eds., (Academic Press, 1996), 389-404.

7. K. Spencer, J. N. Macri, R. W. Anderson, D. A. Aitken, E. Berry, J. A. Crossley, P. J. Wood, E. J. Coombes, M. Stroud, D. J. Worthington, and ., "Dual analyte immunoassay in neural tube defect and Down's syndrome screening: results of a multicentre clinical trial," *Annals of clinical biochemistry* 30 (Pt 4), 394-401 (1993).

8. Y. Y. Xu, K. Pettersson, K. Blomberg, I. Hemmila, H. Mikola, and T. Lovgren, "Simultaneous quadruple-label fluorometric immunoassay of thyroid-stimulating hormone, 17 alpha-hydroxyprogesterone, immunoreactive trypsin, and creatine kinase MM isoenzyme in dried blood spots," *Clinical Chemistry* 38, 2038-2043 (1992).

9. Sun, M. and Pfeiffer, F. R. Analytical test devices for competition assay for drugs of non-protein antigens using immunochromatographic techniques. 1993.

10. J. Singer and C. Plotz, "Slide latex fixation test; a simple screening method for the diagnosis of rheumatoid arthritis," *Journal of the American Medical Association.* 168, 180-181 (1958).

11. Bangs Laboratories, Inc. Immunological Applications. rev#001[TechNote #301]. 1999.

12. S. A. Dunbar, C. A. Vander Zee, K. G. Oliver, K. L. Karem, and J. W. Jacobson, "Quantitative, multiplexed detection of bacterial pathogens: DNA and protein

applications of the Luminex LabMAP system," *Journal of microbiological methods* 53, 245-52 (2003).

13. K. Bodelier and J. Schorr, "Preparation and Analysis of DNA," *Current Protocols in Molecular Biology,* 1998), 2.1.11-2.1.18.

14. R. L. Edelstein, C. R. Tamanaha, P. E. Sheehan, M. M. Miller, D. R. Baselt, L. J. Whitman, and R. J. Colton, "The BARC biosensor applied to the detection of biological warfare agents," *Biosensors & bioelectronics* 14, 805-813 (2000).

15. A. Lamprech, U. Schäfer, and C.-M. Lehr, "Structural Analysis of Microparticles by Confocal Laser Scanning Microscopy," *AAPS PharmSciTech.* **1**, 17 (2000).

16. W. C. Chan and S. Nie, "Quantum dot bioconjugates for ultrasensitive nonisotopic detection," *Science* 281, 2016-8 (1998).

17. M. Han, X. Gao, J. Z. Su, and S. Nie, "Quantum-dot-tagged microbeads for multiplexed optical coding of biomolecules," *Nature biotechnology* 19, 631-5 (2001).

18. J. N. Herron, Wang Hsu-Kun, Janatova Vera, Durtschi Jac, Durtschi Jacob D., Caldwell Karin, Chang I-Nan , Huang, and Shao-Chie., "Orientation and activity of immobilized antibodies," *Surfactant Science Series* 110, 115-163 (2003).

19. Hanson Kristi L., Filipponi Luisa, and Nicolau Dan V., "Biomolecules and cell on surfaces-fundamental concepts," *Microarray Technology and its Applications,* U. R. Muller and D. V. Nicolau, eds., 2005), 23-44.

20. Bangs Laboratories, Inc. Technote #205 Rev. #002. 1999.

21. B. Akerstrom and L. Bjorck, *Journal of Biological Chemistry* 261, 10240-10247 (1986).

22. Sheikh S.H. and Mulchandani A., "Continuous-flow fluoro-immunosensor for paclitaxel measurement," *Biosensors & bioelectronics* 16, 647-52 (2001).

23. J. E. Butler, "Solid Phases in Immunoassay," *Immunoassay,* E. P. Diamandis and T. K. Christopoulos, eds., (Academic Press, San Diago, 1996), 205-225.

24. P. N. Dean, "Flow Cytometery Instrumentation," *Current Protocols in Cytometry,* 1998).

25. M. F. M. Tavares and V. L. McGuffin, "Theoretical Model of Electroosmotic Flow for Capillary Zone Electrophoresis," *Analytical Chemistry* 67, 3687-3696 (1995).

26. M. S. Bello, L. Capelli, and P. G. Righetti, "Dependence of the electroosmotic mobility on the applied electric field and its reproducibility in capillary electrophoresis," *Journal of chromatography. A* 684, 311-22 (1994).

27. K. R. Williams and R. S. Muller, "Etch Rates for Micromachining Processing," *Journal of Microelectromechanical Systems.* 5, 256-269 (1996).

28. P. C. Simpson, A. T. Woolley, and R. A. Mathies, "Microfabrication Technology for the Production of Capillary Array Electrophoresis Chips," *Journal of Biomedical Microdevices* 1, 7-26 (1998).

29. D. J. Harrison, K. Fluri, K. Seiler, Z. Fan, C. S. Effenhauser, and A. Manz, "Micromachining a Miniaturized Capillary Elecrtrophoresis-Based Chemical Analysis System on a Chip," *Science* 261, 895-897 (1993).

30. Z. H. Fan and D. J. Harrison, "Micromachining of Capillary Electrophoresis Injectors and Separators on a Glass and Evaluation of Flow at Capillary Intersections," *Analytical Chemistry* 66, 177-184 (1994).

31. T. Corman, P. Enoksson, and G. Stemme, "Deep wet etching of borosilicate glass using an anodically bonded silicon substrate as mask," *Journal of Micromechanical Microengineering* 8, 84-87 (1998).

32. V. Kachel, H. Fellner-Feldegg, and E. Menke, "Hydrodyanmic Properties of Flow Cytometry Instruments," *Flow Cytometry and Sorting,* (Wiley-Liss, 1990), 27-44.

33. G.-B. Lee, C.-I. Hung, B.-J. Ke, G.-R. Huang, B.-H. Hwei, and H.-F. Lai, "Hydrodynamic Focussing for a Micromachined Flow Cytometer," *Journal of Fluids Engeneering* 123, 672-678 (2001).

34. D. Y. Chen and N. J. Dovichi, "Yoctomole detection limit by laser-induced fluorescence in capillary electrophoresis," *J Chromatogr B Biomed Appl* 657, 265-9 (1994).

35. N. Gunasekera, K. Musier-Forsyth, and E. Arriaga, "Electrophoretic behavior of individual nuclear species as determined by capillary electrophoresis with laser-induced fluorescence detection," *Electrophoresis* 23, 2110-6 (2002).

36. C. F. Duffy, A. A. McEathron, and E. A. Arriaga, "Determination of individual microsphere properties by capillary electrophoresis with laser-induced fluorescence detection," *Electrophoresis* 23, 2040-7 (2002).

37. C. F. Duffy, K. M. Fuller, M. W. Malvey, R. O'Kennedy, and E. A. Arriaga, "Determination of electrophoretic mobility distributions through the analysis of individual mitochondrial events by capillary electrophoresis with laser-induced fluorescence detection," *Analytical Chemistry* 74, 171-6 (2002).

38. D. P. Schrum, C. T. Culbertson, S. C. Jacobson, and J. M. Ramsey, "Microchip Flow Cytometry Using Electrokinetic Focusing," *Analytical Chemistry* 71, 4173-4177 (1999).

39. J. D. Ingle and S. R. Crouch, "Signal to Noise Considerations," *Spectrochemical Analysis,* (Prentice-Hall, New Jersey, 1988), 141-163.

40. H. B. Steen, "Noise, sensitivity, and resolution of flow cytometers," *Cytometry* 13, 822-830 (1992).

41. J. D. Ingle and S. R. Crouch, "Optical Components of Spectrometers," *Spectrochemical analysis,* (Prentice-Hall, 1988), 30-86.

42. A. Rüdiger, R. Schilling, L. Schnupp, W. Winkler, H. Billing, and K. Maischberger, "A Mode Selector to Suppress Fluctuations in Laser Beam Geometry," *Journal of Modern Optics* 28, 641-658 (1981).

43. Melles Griot. Gausian Beam Optics. 2005.

44. G. Ocvirk, T. Tang, and D. J. Harrison, "Optimization of confocal epifluorescence microscopy for microchip-based miniaturized total analysis systems," *The Analyst* 123, 1429-1434 (2005).

45. T. M. Jackson and R. P. Ekins, "Theoretical limitations on immunoassay sensitivity. Current practice and potential advantages of fluorescent Eu3+ chelates as non-radioisotopic tracers," *Journal of immunological methods* 87, 13-20 (1986).

46. T. Lindmo and K. Fundingsrud, "Measurements of the distribution of time intervals between cell passages in flow cytometry as a method for the evaluation of sample preparation procedures.," *Cytometry* 2, 151-4 (1981).

47. H. Kogelnik and T. Li, "Laser beams and resonators," *Applied Optics* 5, 1550-67 (1966).

48. J. Hoffnagle and C. M. Jefferson, "Design and performance of a refractive optical system that converts a Gaussian to flattop beam," *Applied Optics* 39, 5488-5499 (2000).

49. C. F. Duffy, S. Gafoor, D. P. Richards, H. Admadzadeh, R. O'Kennedy, and E. A. Arriaga, "Determination of properties of individual liposomes by capillary electrophoresis with postocolumn laser-induced fluorescence detection," *Anal Chem* 73, 1855-61 (2001).

50. R. T. Carson and D. A. Vignali, "Simultaneous quantitation of 15 cytokines using a multiplexed flow cytometric assay," *Journal of immunological methods* 227, 41-52 (1999).

51. M. Hall, I. Kazakova, and Y. M. Yao, "High sensitivity immunoassays using particulate fluorescent labels," *Analytical biochemistry.* 272, 165-70 (1999).

52. D. A. Vignali, "Multiplexed particle-based flow cytometric assays," *Journal of immunological methods* 243, 243-55 (2000).

53. S. B. Cheng, C. D. Skinner, J. Taylor, S. Attiya, W. E. Lee, G. Picelli, and D. J. Harrison, "Development of a multichannel microfluidic analysis system employing affinity capillary electrophoresis for immunoassay," *Analytical Chemistry* 73, 1472-9 (2001).

54. P. C. Li and D. J. Harrison, "Transport, manipulation, and reaction of biological cells on-chip using electrokinetic effects," *Analytical Chemistry* 69, 1564-8 (1997).

55. S. Fiedler, S. G. Shirley, T. Schnelle, and G. Fuhr, "Dielectrophoretic sorting of particles and cells in a microsystem," *Analytical Chemistry* 70, 1909-15 (1998).

56. S. C. Jacobson and J. M. Ramsey, "Electrokinetic Focusing in Microfabricated Channel Structures," *Analytical Chemistry* 69, 3212-3217 (1997).

57. S. J. Rosenthal, "Bar-coding biomolecules with fluorescent nanocrystals," *Nature biotechnology* 19, 621-2 (2001).

58. P. K. Horan and L. L. Wheeless, Jr., "Quantitative single cell analysis and sorting," *Science* 198, 149-57 (1977).

59. Fulwyler, M. J. Method for detecting and separating antigens and antibodies in blood and other samples. [1561042]. 1976. UK. 1976.

60. P. J. Lisi, C. W. Huang, R. A. Hoffman, and J. W. Teipel, "A fluorescence immunoassay for soluble antigens employing flow cytometric detection," *Clinica chimica acta* 120, 171-9 (1982).

61. G. C. Saunders, J. H. Jett, and J. C. Martin, "Amplified flow-cytometric separation-free fluorescence immunoassays," *Clinical Chemistry* 31, 2020-3 (1985).

62. T. M. McHugh, D. P. Stites, M. P. Busch, J. F. Krowka, R. B. Stricker, and H. Hollander, "Relation of circulating levels of human immunodeficiency virus (HIV) antigen, antibody to p24, and HIV-containing immune complexes in HIV-infected patients," *The journal of infectious diseases* 158, 1088-91 (1988).

63. T. M. McHugh, R. C. Miner, L. H. Logan, and D. P. Stites, "Simultaneous detection of antibodies to cytomegalovirus and herpes simplex virus by using flow cytometry and a microsphere-based fluorescence immunoassay," *Journal of clinical microbiology.* 26, 1957-61 (1988).

64. M. R. Wilson, S. P. Mulligan, and R. L. Raison, "A new microsphere-based immunofluorescence assay for antibodies to membrane-associated antigens," *Journal of immunological methods* 107, 231-7 (1988).

65. M. R. Wilson and J. S. Wotherspoon, "A new microsphere-based immunofluorescence assay using flow cytometry," *Journal of immunological methods* 107, 225-30 (1988).

66. G. Presani, S. Perticarari, and M. A. Mangiarotti, "Flow cytometric detection of anti-gliadin antibodies," *Journal of immunological methods* 119, 197-202 (1989).

67. J. J. Scillian, T. M. McHugh, M. P. Busch, M. Tam, M. J. Fulwyler, D. Y. Chien, and G. N. Vyas, "Early detection of antibodies against rDNA-produced HIV proteins with a flow cytometric assay," *Blood* 73, 2041-8 (1989).

68. T. M. McHugh, Y. J. Wang, H. O. Chong, L. L. Blackwood, and D. P. Stites, "Development of a microsphere-based fluorescent immunoassay and its comparison to an enzyme immunoassay for the detection of antibodies to three antigen preparations from Candida albicans," *J Immunol Methods* 116, 213-9 (1989).

69. V. L. Lim, M. Gumbert, and M. R. Garovoy, "A flow cytometric method for the detection of the development of antibody to Orthoclone OKT3," *Journal of immunological methods* 121, 197-201 (1989).

70. T. Lindmo, O. Bormer, J. Ugelstad, and K. Nustad, "Immunometric assay by flow cytometry using mixtures of two particle types of different affinity," *Journal of immunological methods* 126, 183-9 (1990).

71. R. E. Biagini, D. L. Sammons, J. P. Smith, B. A. MacKenzie, C. A. Striley, V. Semenova, E. Steward-Clark, K. Stamey, A. E. Freeman, C. P. Quinn, and J. E. Snawder, "Comparison of a Multiplexed Fluorescent Covalent Microsphere Immunoassay and an Enzyme-Linked Immunosorbent Assay for Measurement of Human Immunoglobulin G Antibodies to Anthrax Toxins," *Clin Diagn Lab Immunol* 11, 50-55 (2004).

72. R. E. Biagini, S. A. Schlottmann, D. L. Sammons, J. P. Smith, J. C. Snawder, C. A. Striley, B. A. MacKenzie, and D. N. Weissman, "Method for simultaneous measurement of antibodies to 23 pneumococcal capsular polysaccharides," *Clin Diagn Lab Immunol* 10, 744-50 (2003).

73. D. R. Lucey, M. Clerici, and G. M. Shearer, "Type 1 and type 2 cytokine dysregulation in human infectious, neoplastic, and inflammatory diseases," *Clinical Microbiology Reviews* 9, 532-62 (1996).

74. T. L. Whiteside, "Cytokine measurements and interpretation of cytokine assays in human disease," *Journal of clinical immunology.* 14, 327-39 (1994).

75. K. L. Kellar, R. R. Kalwar, K. A. Dubois, D. Crouse, W. D. Chafin, and B. E. Kane, "Multiplexed fluorescent bead-based immunoassays for quantitation of human cytokines in serum and culture supernatants," *Cytometry* 45, 27-36 (2001).

76. T. M. McHugh, "Flow microsphere immunoassay for the quantitative and simultaneous detection of multiple soluble analytes," *Methods in cell biology* 42, 575-95 (1994).

77. T. M. McHugh, "Application of bead-based assays for flow cytometry analysis," *Clinical Immunology Newsletter* 11, 60-64 (1991).

78. J. R. Kettman, T. Davies, D. Chandler, K. G. Oliver, and R. J. Fulton, "Classification and properties of 64 multiplexed microsphere sets," *Cytometry* **33**, 234-43 (1998).

79. M. C. Earley, R. F. Vogt, Jr., H. M. Shapiro, F. F. Mandy, K. L. Kellar, R. Bellisario, K. A. Pass, G. E. Marti, C. C. Stewart, and W. H. Hannon, "Report from a workshop on multianalyte microsphere assays," *Cytometry* 50, 239-42 (2002).

80. W. de Jager, H. te Velthuis, B. J. Prakken, W. Kuis, and G. T. Rijkers, "Simultaneous detection of 15 human cytokines in a single sample of stimulated peripheral blood mononuclear cells," *Clin Diagn Lab Immunol* 10, 133-9 (2003).

81. N. H. Chiem and D. J. Harrison, "Microchip systems for immunoassay: an integrated immunoreactor with electrophoretic separation for serum theophylline determination," *Clinical Chemistry* 44, 591-598 (1998).

82. J. Juvonen, H. M. Surcel, J. Satta, A. M. Teppo, A. Bloigu, H. Syrjala, J. Airaksinen, M. Leinonen, P. Saikku, and T. Juvonen, "Elevated Circulating Levels of Inflammatory Cytokines in Patients With Abdominal Aortic Aneurysm," *Arterioscler Thromb Vasc Biol* 17, 2843-2847 (1997).

83. L. M. Boscato and M. C. Stuart, "Heterophilic antibodies: a problem for all immunoassays," *Clin Chem* 34, 27-33 (1988).

84. J. Frengen, B. Kierulf, R. Schmid, T. Lindmo, and K. Nustad, "Demonstration and minimization of serum interference in flow cytometric two-site immunoassays," *Clin Chem* 40, 420-5 (1994).

85. I. V. Kaplan and S. S. Levinson, "When is a heterophile antibody not a heterophile antibody? When it is an antibody against a specific immunogen," *Clinical Chemistry* 45, 616-8 (1999).

86. C. Hennig, L. Rink, U. Fagin, W. J. Jabs, and H. Kirchner, "The influence of naturally occurring heterophilic anti-immunoglobulin antibodies on direct measurement of serum proteins using sandwich ELISAs," *J Immunol Methods* 235, 71-80 (2000).

87. L. J. Kricka, "Interferences in immunoassay--still a threat," *Clinical Chemistry* 46, 1037-8 (2000).

88. R. D. Oleschuk, L. L. Shultz-Lockyear, Y. Ning, and D. J. Harrison, "Trapping of bead-based reagents within microfluidic systems: on-chip solid-phase extraction and electrochromatography," *Analytical Chemistry* 72, 585-590 (2000).

89. A. B. Jemere, R. D. Oleschuk, and D. J. Harrison, "Microchip-based capillary electrochromatography using packed beds," *Electrophoresis* 24, 3018-3025 (2003).

Appendix A

Igor Pro program that takes the raw date and extract the peaks intensities of both capture and detection bead and tabulates them for further analysis.

```
Macro FlowCytometerNew(fluorescent1,fluorescent2,fluorescent3,threshold)
        String fluorescent1
        String fluorescent2
        String fluorescent3
        Variable threshold
        Prompt fluorescent1, "Input data 535 nm:",popup WaveList("*",";","")
        Prompt fluorescent2, "Input data 595 nm:",popup WaveList("*",";","")
        Prompt fluorescent3, "Input data 675 nm:",popup WaveList("*",";","")
        Prompt threshold, "Number of standart deviations above the average for cut
                off:"



        Execute "Duplicate " + fluorescent1+ " s1"
        Execute "Duplicate " + fluorescent2 + " s2"
        Execute "Duplicate " + fluorescent3 + " s3"
        KillWaves  wave0,wave1,wave2
        variable firstpass = 2

Wavestat(s1,s2,s3)

        Duplicate s1 cx1
        Duplicate s2 cx2
        Duplicate s3 cx3

WaveSubstract(cx1,cx2,cx3,firstpass)        | Zeros everything below the (average plus X
        times the stdev) from the data

        Duplicate s1 c1
        Duplicate s2 c2
        Duplicate s3 c3

Deletepeaks(cx1,cx2,cx3,c1,c2,c3)           | Delete all peaks higher than (Average plus
        X times the stdev) from the data
```

```
        KillWaves cx1,cx2,cx3

Wavestat(c1,c2,c3)                          | determines the New stdev and average
        without the large peaks present
        KillWaves c1,c2,c3
        Duplicate s2 sx2


WaveSubstract(s1,s2,s3,threshold)

Make /O /N= 100000
        PeakmaxiumF1,PeakmaxiumF2,PeakmaxiumF3,PeakmaxiumF4,peak_start1,
        peak_end1,PeakArea1, peak_start2,
        peak_end2,PeakArea2,PeaklocationF1,PeaklocationF3,LocF1,PeakM1,PeakM2,P
        eakM3,PeakM1, PeakM2, PeakM3,Red,RedGreen,Yellow,YellowGreen

Findthatpeak(s1,s2,s3,PeakmaxiumF1,PeakmaxiumF2,PeakmaxiumF3,PeakmaxiumF4,
        peak_start1, peak_end1,PeakArea1, peak_start2,
        peak_end2,PeakArea2,PeaklocationF1,PeaklocationF3)
        KillWaves s1,s2,s3

SortingofData(PeakmaxiumF1,PeakmaxiumF2,PeakmaxiumF3,PeakmaxiumF4,Peaklocat
        ionF1,PeaklocationF3,LocF1,PeakM1,PeakM2,PeakM3,sx2)
        KillWaves
        PeakmaxiumF1,PeakmaxiumF2,PeakmaxiumF3,PeakmaxiumF4,PeaklocationF1,
        PeaklocationF3,sx2

Categorize(PeakM1, PeakM2, PeakM3,Red,RedGreen,Yellow,YellowGreen)
        KillWaves PeakM1, PeakM2, PeakM3

ConvertData (Red,RedGreen,Yellow,YellowGreen)
        KillWaves/A/Z
End




Function Wavestat(s1,s2,s3)

        Wave s1
        Wave s2
        Wave s3
```

```
	Variable /G VnpntsFL1 = 0, V_avgFL1 = 0, V_sdevFL1 = 0
	Variable /G VnpntsFL2 = 0, V_avgFL2 = 0, V_sdevFL2 = 0
	Variable /G VnpntsFL3 = 0, V_avgFL3 = 0, V_sdevFL3 = 0

	WaveStats /Q s1
	VnpntsFL1  = V_npnts
	V_avgFL1   = V_avg
	V_sdevFL1  = V_sdev


	WaveStats /Q s2
	VnpntsFL2  = V_npnts
	V_avgFL2   = V_avg
	V_sdevFL2  = V_sdev


	WaveStats /Q s3
	VnpntsFL3  = V_npnts
	V_avgFL3   = V_avg
	V_sdevFL3  = V_sdev

End

Function WaveSubstract(cx1,cx2,cx3,Error) | set baseline to zero


	Wave cx1,cx2,cx3
	variable Error
	Variable numPionts = numpnts(cx1)
	Variable p=0

	Do
		if (cx1[p] < (V_avgFL1+Error*V_sdevFL1))
			cx1[p] = 0
		endif
		p+=1
	While (p < numPionts)

	p=0
	Do
		if (cx2[p] < (V_avgFL2+Error*V_sdevFL2))
			cx2[p] = 0
		endif
		p+=1
	While (p < numPionts)
```

```
p=0
Do
        if (cx3[p] < (V_avgFL3+Error*V_sdevFL3))
                cx3[p] = 0
        endif
        p+=1
While (p < numPionts)


End

Function Deletepeaks(cx1,cx2,cx3,c1,c2,c3) | finds a value larger than zero in (cx) and
        delete these peaks in (c)

        Wave cx1,cx2,cx3
        Wave c1,c2,c3
        variable  p_start=0 , p=0
        Variable numPionts = numpnts(cx1)
        Do
                if (cx1[p] !=  0)
                  p_start = p
                  Do
                        p +=1
                  While (cx1[p] != 0)
                  DeletePoints p_start, p, c1
                  p = p_start
                  endif
                 p+=1
        While (p < numPionts)

         p_start=0
         p=0

        Do
                if (cx2[p] !=  0)
                  p_start = p
                  Do
                        p +=1
                  While (cx2[p] != 0)
                  DeletePoints p_start, p, c2
                  p = p_start
                  endif
                 p+=1
        While (p < numPionts)

        p_start=0
```

```
p=0

Do
        if (cx3[p] !=  0)
          p_start = p
          Do
                p +=1
          While (cx3[p] != 0)
          DeletePoints p_start, p, c3
          p = p_start
          endif
         p+=1
While (p < numPionts)

End


Function
        Findthatpeak(s1,s2,s3,PeakmaxiumF1,PeakmaxiumF2,PeakmaxiumF3,Peakmaxiu
        mF4,          peak_start1,          peak_end1,PeakArea1,          peak_start2,
        peak_end2,PeakArea2,PeaklocationF1,PeaklocationF3)

        Wave s1,s2,s3,PeakmaxiumF1,PeakmaxiumF2,PeakmaxiumF3,PeakmaxiumF4
        Wave          peak_start1,          peak_end1,PeakArea1,peak_start2,
        peak_end2,PeakArea2,PeaklocationF1,PeaklocationF3
        variable  p_start=0 , p=0, z=0, Peakmax=0,y=0,temp1=0, temp2=0,t=0,nmpntF2
        Variable numPionts = numpnts(s1)
        print numPionts
        Do
                if (s1[p] !=  0)
                        peak_start1[z] = p
                        p_start=p
                                Do
                                        p +=1

                                While (s1[p] != 0)
                        peak_end1[z] = p

                        PeakArea1[z]=  Abs(area(s1,  peak_end1[z],peak_start1[z]))  |Why
        is this needed??
                        if (PeakArea1[z] > (2*V_sdevFL1* 25))
                                WaveStats/R=(peak_start1[z],peak_end1[z]) s1
                                PeakmaxiumF1[z]= V_max
                                PeaklocationF1[z]= V_maxloc                  | Peak location
                                z+=1
                         endif
```

```
            endif
            p+=1
        While (p < numPionts)


        Do
            WaveStats/R= (peak_start1[y],peak_end1[y]) s2
            temp1=V_max

                if (temp1 != 0)
                    PeakmaxiumF2[y]= temp1
                else
                    PeakmaxiumF2[y] = V_avgFL2
                endif
            y+=1
        While (peak_start1[y] !=0)

nmpntF2=y
 p_start=0 ;p=0; z=0; Peakmax=0;y=0;temp1=0; temp2=0;t=0


Do
            if (s3[p] !=  0)
                peak_start2[z] = p
                p_start=p
                    Do
                        p +=1

                    While (s1[p] != 0)
                peak_end2[z] = p

                PeakArea2[z]=  Abs(area(s3,  peak_end2[z],peak_start2[z]))  |Why
        is this needed??
                if (PeakArea2[z] > (2*V_sdevFL3* 25))
                    WaveStats/R=(peak_start2[z],peak_end2[z]) s3
                    PeakmaxiumF3[z]= V_max
                    PeaklocationF3[z]= V_maxloc | Peak location
                    z+=1
                 endif
             endif
            p+=1
        While (p < numPionts)


        Do
            WaveStats/R= (peak_start2[y],peak_end2[y]) s2
```

```
            temp1=V_max

                    if (temp1 != 0)
                            PeakmaxiumF4[y]= temp1
                    else
                            PeakmaxiumF4[y] = V_avgFL2
                    endif
            y+=1
        While (peak_start2[y] !=0)


        Redimension/N = (nmpntF2) PeakmaxiumF1
        Redimension/N = (nmpntF2) PeakmaxiumF2
        Redimension/N = (y) PeakmaxiumF3
      Redimension/N = (y) PeakmaxiumF4
        Redimension/N = (nmpntF2) peak_start1
        Redimension/N = (nmpntF2) peak_end1
        Redimension/N = (nmpntF2) PeakArea1
        Redimension/N = (y) peak_start2
        Redimension/N = (y) peak_end2
        Redimension/N = (y) PeakArea2
        Redimension/N = (nmpntF2) PeaklocationF1
        Redimension/N = (y) PeaklocationF3


End



Function ConvertData (Red,RedGreen,Yellow,YellowGreen)
        wave Red,RedGreen,Yellow,YellowGreen

        Red=Red*102.3
        RedGreen=RedGreen*102.3
        Yellow=Yellow*102.3
        YellowGreen=YellowGreen*102.3
        Save/J/M="\r\n"/W Red,RedGreen,Yellow,YellowGreen as "name"

End

Function
        SortingofData(PeakmaxiumF1,PeakmaxiumF2,PeakmaxiumF3,PeakmaxiumF4,P
        eaklocationF1,PeaklocationF3,LocF1,PeakM1,PeakM2,PeakM3,sx2)
```

```
Wave
PeakmaxiumF1,PeakmaxiumF2,PeakmaxiumF3,PeakmaxiumF4,PeaklocationF1,
PeaklocationF3,LocF1,PeakM1,PeakM2,PeakM3,sx2
Variable a=0, b=0, x=0, p=0,q=0
Variable numPointsF1 = numpnts(PeaklocationF1)
Variable numPointsF3 = numpnts(PeaklocationF3)



If (numPointsF1<numPointsF3)
        p=numPointsF3
else
        p=numPointsF1
endif

Do
        If(Abs(PeaklocationF1[a]-PeaklocationF3[b])>4)
                If(PeaklocationF1[a]<PeaklocationF3[b])
                        LocF1[x]=PeaklocationF1[a]

                        PeakM1[x]=PeakmaxiumF1[a]
                        PeakM2[x]=sx2[LocF1[x]]
                        PeakM3[x]=V_avgFL3

                        a+=1
                else
                        LocF1[x]=PeaklocationF3[b]

                        PeakM1[x]=V_avgFL1
                        PeakM2[x]=sx2[LocF1[x]]
                        PeakM3[x]=PeakmaxiumF3[b]


                        b+=1
                endif
        else
                LocF1[x]=PeaklocationF1[a]

                PeakM1[x]=PeakmaxiumF1[a]
                PeakM2[x]=sx2[LocF1[x]]
                PeakM3[x]=PeakmaxiumF3[a]

                a+=1
                b+=1
        endif
```

```
        x+=1
    While(x<=(p*2))

    Do
        q+=1
    while(LocF1[q] != 0)
    print q
    Redimension/N = (q) LocF1
    Redimension/N = (q) PeakM1
    Redimension/N = (q) PeakM2
    Redimension/N = (q) PeakM3
End

Function Categorize(PeakM1, PeakM2, PeakM3,Red,RedGreen,Yellow,YellowGreen)

    Wave PeakM1, PeakM2, PeakM3,Red,RedGreen,Yellow,YellowGreen
    Variable numPionts = numpnts(PeakM1)
    Variable a = 0,x=0,y=0,q=0,p=0
    Do
        if(PeakM1[a]/PeakM3[a] >1)
            Red[x]=PeakM1[a]
            RedGreen[x]=PeakM2[a]
            x+=1
        else
            Yellow[y]=PeakM3[a]
            YellowGreen[y]=PeakM2[a]
            y+=1
        endif

        a+=1

    While(a<=numPionts)
    Do
        q+=1
    while(Red[q] != 0)
    Do
        p+=1
    while(Yellow[p] != 0)

    Redimension/N = (q) Red
    Redimension/N = (q) RedGreen
    Redimension/N = (p) Yellow
    Redimension/N = (p) YellowGreen

End
```

Appendix B

Three Matlab programs, Loader loads the data in Matlab, Vector determines the x and y position of the center of mass of the beam, and Intg1 determents the RSD in the flat part of the beam.

Loader.m

```
maxnum=5
for i=1:maxnum
  file=strcat('flowdye',num2str(i,1),'.png');
  X1=imread(file);
  X1=double(X1);
  if i>1
    Average_img=Average_img+X1;
  else
    Average_img=X1;
  end

end
X1=Average_img/5;
clear Average_img
clear i
clear file
```

Vector.m

```
ED=0;
Mass_X=0;
Mass_Y=0;
A=size(X1);
for i=1:A(1)
  for j=1:A(2)
    if X1(i,j)>150
      ED(i,j)=X1(i,j);
    else
      ED(i,j)=0;
      end
```

```
  end
end
Mass_Y=sum(ED);
Mass_X=sum(transpose(ED));
Total_Y=sum(Mass_Y);
Total_X=sum(Mass_X);
temp=0;
for i=1:A(1)
  temp=temp+Mass_X(i);
  if temp <= 0.5*Total_X
    Center_X=i;
  end
end
temp=0;
for j=1:A(2)
  temp=temp+Mass_Y(j);
  if temp <= 0.5*Total_Y
    Center_Y=j;
  end
end
Center_X
Center_Y
```

Intg1.m

```
hold off;
clear Radius;
clear How_mny;
clear Test_img;
clear X2;


X2=X1;
% use this if Gaussian test pk
%  X2=zeros(200,200);
%  max_A=100;
%  sigma=90;



A=size(X2);
Thresh=0.3*max(max(X2));

% This is the expected data center of mass
```

```
Colcntr=Center_X
Rowcntr=Center_Y

% Threshold routine

for Col=1:A(1)
  for Row=1:A(2)
% use this to generate G pk
%     X2(Col,Row)=(max_A*(exp(-(Col-Colcntr)^2/sigma))*max_A*(exp(-(Row-
Rowcntr)^2/sigma)));
    if X2(Col,Row)<Thresh
      X2(Col,Row)=0;
    end
  end
end



% find the edges of the minimal box that encopases the spot

Garb(1)=A(1)-Colcntr;
Garb(2)=Colcntr;
Garb(3)=A(2)-Rowcntr;
Garb(4)=Rowcntr;
Colmin=min(Garb(1:2));
Rowmin=min(Garb(3:4));

% find the max radius from center
Hypo=sqrt(Colmin^2+Rowmin^2);
% set a arbitrary number of divisions

no_steps=100;
Step=Hypo/no_steps;
How_mny=zeros(no_steps,1);
Radius=zeros(no_steps,1);

%clear Garb,A;

Test_img=X2;
figure
image(X2);
hold on;

for Col=Colcntr-Colmin+1:Colcntr+Colmin-1  %for the columns to the left to the right
  for Row=Rowcntr-Rowmin+1:Rowcntr+Rowmin-1 % for the rows above to below
center
```

```
    r_dist=sqrt((Col-Colcntr)^2+(Row-Rowcntr)^2); %what is the radial distnce
    r_pix=round(r_dist/Step); %round it to a value
    temp(Row,Col)=r_dist;
    if r_pix>0 %at center things go bad
      Radius(r_pix)=Radius(r_pix)+X2(Col,Row); %Sum all intensities at this radius
      How_mny(r_pix)=How_mny(r_pix)+1; %count the number of pixels at this dist
%       Test_img(Col,Row)=100; %make sure we are getting the correct area
    end
end
end

for i=1:no_steps
  if How_mny(i)>0
    Radius(i)=Radius(i)/How_mny(i);  %calc the mean intensity at this radius
  end

end

%assign any zero values in Radius the neighbouring value so we can threshhold

for i=1:no_steps-1
  if Radius(i)==0
    j=i;
    while Radius(j)==0  %look forward to non-zero value
      j=j+1;
      if j==no_steps
        break
      end
    end
    Radius(i)=Radius(j);
  end
end


clear r_pix
clear r_dist

  %now we know the intensity profile as a funct of r
  Cuttoff=0.45

  Cuttoff=Cuttoff*max(Radius);
  i=no_steps;
  while Radius(i)<Cuttoff %search for cutoff threshhold
    i=i-1;
  end
  %cut off radius is=i
```

```
%this radius refers to the Radius vector and not hte original image
%each element in this vector is actually Step units long on the image

cuttoff_r=i*Step
%summ the peak within the cut off radius
%best done by transfering the data to a vector then easy to calc mean and std dev
i=1;
cuttoff_r=round(cuttoff_r);
for Col=Colcntr-cuttoff_r:Colcntr+cuttoff_r
  for Row=Rowcntr-cuttoff_r:Rowcntr+cuttoff_r
    r_dist=sqrt((Col-Colcntr)^2+(Row-Rowcntr)^2); %what is the radial distnce
    if r_dist<=cuttoff_r  %ie inside of the cuttoff radius
      All_pix(i)=X2(Col,Row);
      i=i+1;
    end
  end
end
rsd=std(All_pix)/mean(All_pix)



[A,B,C]=cylinder(cuttoff_r,100);
A=A+Rowcntr;
B=B+Colcntr;
i=1.05*max(max(X1));
C=C*50+i;
surf(X1);
hold on;
surf(A,B,C);
[A,B,C]=cylinder(2,10);
A=A+Rowcntr;
B=B+Colcntr;
C=C*150+i;
surf(A,B,C);
v=axis;
p=max(v(2),v(4));
v(2)=p;
v(4)=p;
axis(v);
view(90,90);
ylabel('column pixel #');
xlabel('row pixel #');
hold off
```